Heterogeneity of the STV in the CAVB dog model for Torsade de Pointes

Marlies Gillis

Supervisor: Nele Vandersickel

Master's dissertation submitted in order to obtain the academic degree of
Master of Science in Biomedical Engineering

Vakgroep Fysica en Sterrenkunde
Chair: Prof. dr. Dirk Ryckbosch
Faculty of Engineering and Architecture
Academic year 2017-2018

GHENT
UNIVERSITY

Heterogeneity of the STV in the CAVB dog model for Torsade de Pointes

Marlies Gillis

Supervisor: Nele Vandersickel

Master's dissertation submitted in order to obtain the academic degree of
Master of Science in Biomedical Engineering

Vakgroep Fysica en Sterrenkunde
Chair: Prof. dr. Dirk Ryckbosch
Faculty of Engineering and Architecture
Academic year 2017-2018

GHENT
UNIVERSITY

Acknowledgements

A huge 'thank you!' goes to Nele Vandersickel. She is one of the best supervisors I've ever met. Her coaching power lies in the fact that she's able to focus on all the positive aspects of someone's work. Her positive mindset kept me motivated the whole year long. As a student supervised by Nele, I felt like my work had a purpose and that my opinion was appreciated. Nele is a very enthusiastic and passionate person whereby she affected me with her enthusiasm and passion for research. Thanks to Nele I learnt more about myself. During the timespan of my final year, I learnt a lot about how I cope with stress, how I deal with team work, ... Nele is an empathic person which is, according to me, a very important characteristic of a good mentor.

I would like to thank Agnieszka Smoczynska for evaluating the signals to determine the short-term variability (STV). Her medical knowledge gave me more insight in the signals and results.

Wout, thank you for being the shoulder to cry on. Every research is characterized by ups and downs. I am thankful that I could celebrate every up with you and vent off my frustrations with every down I experienced.

This master's dissertation is not only a final product of my last master year but actually a product of my whole academic route. Therefore I would like to thank Hannah Notebaert, Lize Linclau, Fien De Coster, Marlies Leysen, Mathilde Vantyghem and Tosca Meylemans for being there for me. I truly hope I was able to give the same support to all of you as I got from you. I am grateful to Anne-Camille Bettens who took the time to correct my master's dissertation with her linguistic talent.

Last but not least, I would like to thank my parents for giving me the opportunity of studying what and where I want. Their believe in me means a great deal. During whole my academic route, they have never stopped supporting me. Thank you!

Abstract

Heterogeneity of the STV in the CAVB dog model for Torsade de Pointes

Marlies Gillis

Introduction - This master's dissertation focusses on the polymorphic ventricular tachyarrhythmia Torsade de Pointes (TdP). To investigate this arrhythmia, unipolar electrogram (UEG) data, obtained from the chronic atrioventricular block (CAVB) dog model, was used to answer 2 research questions. (1) Is STV of the activation repolarization interval (ARI) determined in local UEG data also a good biomarker for the prediction of TdP? In literature it is stated that the STV in intracardiac electrogram (EGM) and monophasic action potential (MAP) data increases just before the offset of the first ectopic beat. This master's dissertation focusses on whether the same trend is visible in UEG data. (2) Are the origins of the focal beats homogeneously or heterogeneously distributed over the heart? Since this has never been experimentally verified, it would gain more insight in the focal mechanism of TdP which is a subject of controversy.

Methods - The recordings of detailed UEG mapping experiments of the heart of 5 chronic atrioventricular block (CAVB) dogs were received from UMC Utrecht. The recordings consisted of a baseline recording and a recording during the administration of dofetilide to induce TdP. (1) To determine the STV increase, the STV of the baseline recording and of the recording during dofetilide administration was calculated. (2) To determine the origin of each ectopic beat, the first activated channel was determined via earliest local time of excitation. This was done for every ectopic beat during the dofetilide recording.

Results - Due to limited time, only the recordings of 1 dog were analysed. (1) No clear increase in STV is seen before and after the dofetilide administration. The average STV difference was equal to -0.446 ms which implies that the average STV during the baseline recording was higher than the STV in the dofetilide recording. (2) The distribution of the origins of ectopic beats is highly heterogeneous.

Conclusion - Since only one dog was analysed, no general conclusion for Torsade de Pointes can be drawn. From the results of this one dog, it was seen that the UEG data obtained via needles did not show the trend of a STV increase just before the offset of the first ectopic beat. Therefore it was concluded that STV could not be used as a biomarker for the prediction of Torsade de Pointes in UEG data. The distribution of origins of the ectopic beats is heterogeneous. Therefore it was concluded that the ectopic beats origin in preferable locations. It is presumed that the theory of Vandersickel, Boer, Vos, and Panfilov (2016) is more likely.

Keywords: Arrhythmia, Torsade de Pointes, Short term variability, Focal mechanism

Heterogeneity of the STV in the CAVB dog model for Torsade de Pointes

Marlies Gillis[1]
Supervisor: Nele Vandersickel[2]

Abstract— **Torsade de Pointes (TdP) is a possible lethal cardiac arrhythmia. To investigate this arrhythmia, local unipolar electrogram (UEG) data, obtained from the chronic AV-block (CAVB) dog model, was used to answer 2 research questions. (1) Is short term variability (STV) of the activation recovery interval (ARI) determined in UEG data also a good biomarker for the prediction of TdP? In literature it is stated that the STV increases just before the offset of the first ectopic beat in intracardiac electrogram (EGM) and monophasic action potential (MAP) data. This study focusses on whether the same trend is visible in UEG data. (2) Are the origins of the ectopic beats homogeneously or heterogeneously distributed over the heart? Since this has never been experimentally verified, it would gain more insight in the focal mechanism of TdP.**

***Methods* - The recordings of detailed mapping experiments via UEG data of the heart of 5 CAVB dogs was received from UMC Utrecht. The recordings consisted of a baseline recording and a recording during the administration of dofetilide to induce TdP. (1) To determine the STV increase, the STV was calculated of the baseline recording and of the recording during dofetilide administration. (2) To determine the origin of each ectopic beat, the first activated channel was determined via earliest local time of excitation. This was done for every ectopic beat during the dofetilide recording.**

***Results* - Due to limited time, only the recordings of 1 dog were analysed. (1) No clear increase in STV is seen before and after the dofetilide administration. The average STV difference was equal to -0.446 ms which implies that the average STV during the baseline recording was higher than the STV in the dofetilide recording. (2) The distribution of the origins of ectopic beats is highly heterogeneous.**

***Conclusion* - Since only one dog was analysed, no general conclusion for Torsade de Pointes can be drawn. From the results of this one dog, it was seen that the UEG data obtained via needles did not show the trend of a STV increase just before the offset of the first ectopic beat. Therefore it was concluded that STV could not be used as a biomarker for the prediction of Torsade de Pointes in UEG data. The distribution of origins of the ectopic beats is heterogeneous. Therefore it was concluded that the ectopic beats origin in preferable locations. It is presumed that the theory of Vandersickel, Boer, Vos and Panfilove (2016) [1] is more likely.**

I. INTRODUCTION

Torsade de Pointes (TdP) is a polymorphic ventricular tachycardia with a typical twisting pattern on the electrocardiogram (ECG). The name 'Torsade de Pointes', French for 'twisting of points', is directly derived from this pattern since the QRS-complexes are twisting around the ECG baseline [2]. In case of sudden cardiac death (SCD), TdP could only be identified when an ECG is obtained. Since this is often not the case, the incidence of death by TdP is difficult to estimate [3]. The prevalence in Belgian hospitals is estimated onto 173 possible lethal cases of TdP each year [4].

Torsade de Pointes is initiated by an early afterdepolarization (EAD). This is commonly accepted in scientific literature, however the perpetuation of TdP is still a subject of controversy [1]. Different theories are suggested in order to explain the mechanism of TdP. There are theories which suggest that the mechanism of TdP is maintained via focal activity. Other theories are based on re-entrant activity or even a combination of focal activity and re-entrant activity. Different theories try to explain the phenomenon of perpetuation by focal activity. (1) A first theory hypothesizes that the focal activity is caused by shifting focal focuses triggered by a cluster of synchronized EADs [5]. (2) Another theory states that a focal episode of TdP is maintained by focal beats arising from fixed heterogeneities in the heart tissue [1]. These theories have never been experimentally verified. In this study, the origins of the ectopic beats are determined to gain more insight in the focal mechanism.

Another challenge is to find a biomarker for the prediction of TdP. Previous literature stated that short term variability (STV) might be a successful biomarker for monitoring the the arrhythmic risk in intracardiac electrogram (EGM) and monophasic action potential duration (MAPD) data. A trend was seen that the STV increases just before the offset of an ectopic beat [6]. However the mentioned articles gave no insight in how the STV increase is distributed over the heart. The distribution of the STV increase over the heart would be of clinical importance to determine the optimal electrode location of the implantable cardiac defibrillator (ICD). In case of a homogeneous STV increase, the location of the ICD electrode is not of importance. When this STV increase is heterogeneous, the optimal location of the ICD electrode is of course the location where the increase is most prominent. The optimal position of the electrode would allow a faster detection of a coming episode of Torsade de Pointes and thus a faster application of the shock which might even increase the survival rate.

This study aims to verify whether a STV increase before the offset of the first ectopic beat is seen in local unipolar electrogram (UEG) data. In case the STV increase would be seen, it would be interesting to see how the STV increase is distributed over the heart and whether there is a correlation with the origins of the ectopic beats.

[1]Faculty of Engineering and Architecture, Ghent University, Ghent, Belgium
[2]Department of Physics and Astronomy, Ghent University, Ghent, Belgium

II. MATERIAL & METHODS

A. Detailed mapping experiments

For this study, no animal experiment is performed. Data of previous animal experiments were received from UMC Utrecht. These experiments happened with consent of the Committee for Experiments on Animals of Utrecht University which is in agreement with the European Directive for the Protection of Vertebrate Animals used for Experimental and Other Scientific Purposes (86/609/CEE) and the Dutch Law on animal experimentation.

This data contained recordings of mapping experiments of the heart of 5 chronic AV-block (CAVB) dogs. A recording consisted of a baseline recording and a recording during the administration of dofetilide, a drug which induces TdP. During this mapping experiment, UEG data was gathered via needles which contained 4 electrode terminals or channels. In total 56 needle electrodes were inserted in the canine heart, whereby 48 needles in the ventricular myocardium and 8 in the septal wall. A more detailed description of the mapping experiment is described by Dunnink, Stams, Bossu, Meijbor, Beekman, Wijers, De Bakker and Vos (2017) [7].

B. Determination of the STV

The short term variability (STV) is a measure for the variability of the activation recovery interval (ARI). The ARI is related to the action potential duration [8]. The STV is determined as:

$$STV = \frac{\sum_1^N |D_{n+1} - D_n|}{(N-1) \times \sqrt{2}}$$

where D represents the duration of the ARI and N the amount of beats -1. To determine the STV minimum 31 consecutive beats without ectopic activity must be incorporated in the analysis [9].

The ARI is calculated as the time difference between the local time of excitation and local time of repolarization. The local time of excitation is the time of most rapid decrease in the QRS-complex which corresponds with the maximal negative derivative of the UEG signal (dV/dt min). In a similar way the local time of repolarization is calculated, namely the maximal positive derivative near the peak of the T-wave (dV/dt max). This method is called the 'Wyatt method' for ARI determination [8].

First, different time periods of 31 consecutive beats were selected for the baseline recording as the dofetilide recording. The time period for the baseline recording was taken at the end of the baseline measurement to avoid influence of other effects as ectopic activity due to the insertion of the needles. For the recording during dofetilide administration this time period was taken in the beginning of the recording just before the first ectopic beat. Via a dedicated algorithm, all the local times of excitation and local times of repolarization were determined within this time period.

Since biological data was used, a high variability between the UEG signals was seen. Due to this high variability in the signals, writing an algorithm which works for all the signals is challenging. The written algorithms performed well however not perfect. Therefore all the determined local times of excitation and local times of repolarization had to be visually inspected and corrected if necessary. To ease this process, a graphical user interface (GUI) was written. However the usage of the GUI has also a clear disadvantage: the correction of a local time of excitation or local time of repolarization allows misplacement and makes the analysis more subjective.

C. Determination of the origins of ectopic beats

The recording was separated into different episodes. A timespan of a paced beat followed by one ectopic beat or multiple ectopic beats was denoted as 'episode'. Per episode the local times of excitation were determined for all the beats in the episode over all the different channels. Then a comparison was made per ectopic beat over all the channels to find the earliest local time of excitation. The channel containing the earliest local time of excitation was labelled as the first activated channel.

The local times of excitation of the beats in the episode were determined via a dedicated algorithm. However due to the high variability, the algorithm could have determined these time points incorrectly. Therefore the result of the algorithm was visually inspected for all the channels via a GUI.

III. RESULTS

Due to limited time only one dog, namely dog 901016, could be evaluated. Therefore only results of the analysis of dog 901016 are shown in this section.

A. STV increase

Different heat maps were made representing the STV values for each channel. This was done for the STV values during the baseline recording and during the dofetilide recording. These heat maps are represented in respectively the figures 1 & 2. The difference between the STV value of the baseline recording and dofetilide recording was calculated for every channel and represented in figure 3. Remark that the differences were calculated only of channels which were of good quality in the baseline recording as well as in the dofetilide recording.

Fig. 1. An overview of the calculated STV values for each channel during the baseline recording presented on a electrode map for dog 901016.

On the figures 1 & 2 is seen that the STV values are heterogeneously distributed over the heart. The STV values during the baseline recording varied between 1.2 and 10.2. For the dofetilide recording, these STV values varied between 1.0

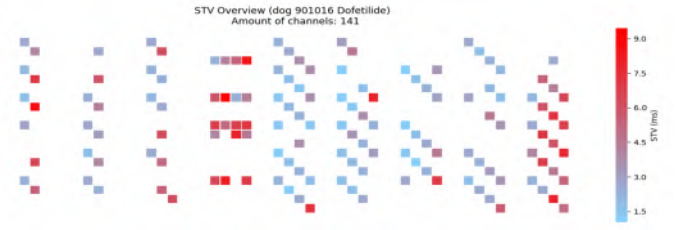

Fig. 2. An overview of the calculated STV values for each channel during the dofetilide recording presented on a electrode map for dog 901016.

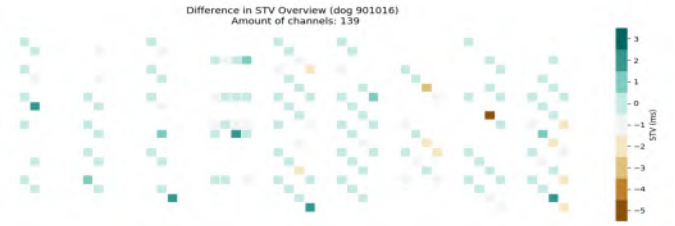

Fig. 3. An overview of the difference in STV values for each channel presented on a electrode map for dog 901016.

and 9.4. When looking at figure 3, no clear increase or decrease in STV is seen. The average STV difference was equal to -0.446ms.

B. Distribution of the origins of ectopic beats

The heat map containing the origins of all ectopic activity is shown in figure 4. In figure 5 an overview is given of the origins of the first ectopic beat over all the different episodes. The origins of the ectopic beats in episodes with only 1 ectopic beat is represented in figure 6. The origins of the first ectopic beat in re-entrant and non-terminating episodes are depicted on figure 7. Figure 8 shows an overview of the origins of the ectopic beats in episodes with at least 2 ectopic beats.

As seen in figure 4 there are 3 preferable origins for the ectopic activity. These locations are (1) epicardial in the middle between the base and apex posterior to the septum in the left ventricle, (2) endocardial near the apex anterior to the left ventricle and (3) endocardial near the apex posterior to the septum in the left ventricle. A total amount of 229 ectopic beats were evaluated. Notice that the same trend is visible in figure 5.

In figure 6 is seen that the dominant location to initiate individual ectopic beats is situated endocardial near the apex anterior to the left ventricle. Notice that the other locations as seen in figure 4 are minor preferable locations. The same locations initiate the first ectopic beat in re-entrant and non-terminating episodes as seen in figure 7. Remark that this result is based on only 6 ectopic beats.

Figure 8 shows that for episode with multiple ectopic beats, at least 2 ectopic beats, the dominant location shifts towards the epicardial location in the middle between the base and apex posterior to the septum in the left ventricle. The location endocardial near the apex anterior to the left ventricle initiate only 1 ectopic beat.

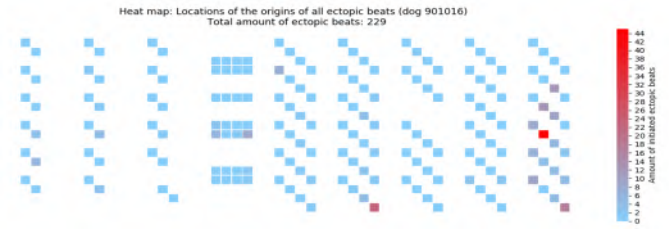

Fig. 4. An overview of the origins of all the ectopic activity presented on a electrode map for dog 901016.

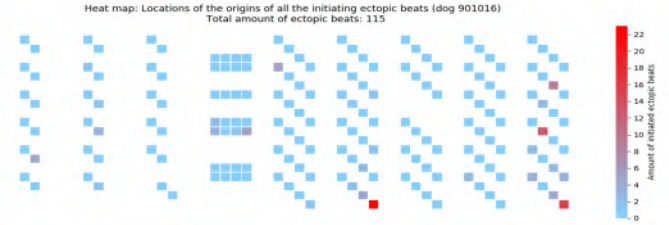

Fig. 5. An overview of the origins of the first ectopic beat of all the ectopic activity presented on a electrode map for dog 901016.

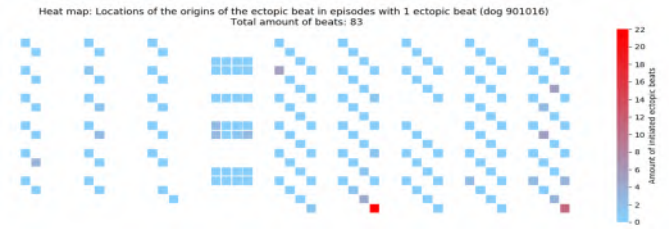

Fig. 6. An overview of the origins of the ectopic beats in episodes with only 1 ectopic beat presented on a electrode map for dog 901016.

Fig. 7. An overview of the origins of the ectopic beats of each episodes classifies as re-entry or non-terminating presented on a electrode map for dog 901016.

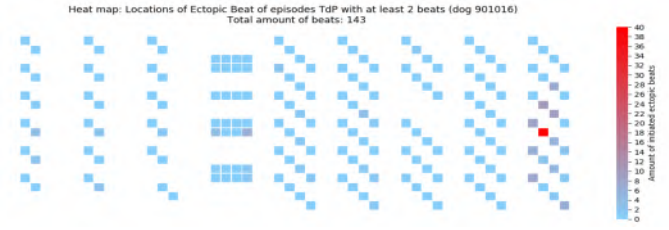

Fig. 8. An overview of the origins of all the ectopic beats in episodes with at least 2 ectopic beats presented on a electrode map for dog 901016.

IV. DISCUSSION

A. STV increase

The STV values varied over different regions in the heart. When figures 1 & 2 are compared, it is seen that the STV values behave similarly. The region of the septum as the region posterior to the septum in the left ventricle showed elevated values of STV in both the baseline and the dofetilide recording.

In figure 3 no distinct increase in STV value is seen. This implies that the trend of a STV increase just before the offset of an ectopic beat was not seen in the UEG data of dog 901016. This could be due to different possible explanations. (1) Destructive interference between the different cells influenced the morphology of the T-wave which caused the T-wave to smooth. This would increase the uncertainty on the determination of the local time of repolarization and would thus directly affect the value of the STV. (2) The insertion of the needles damages a significant amount of cells causing a variable behaviour of repolarization. This has an impact on the distribution of the STV values. (3) The repolarization is too sensitive to noise to determine the local time of repolarization. (4) The GUI makes the determination of the local time of repolarization too subjective. (5) It might be that in dog 901016 the dominant effect of the STV increase is the remodelling of the heart. This is derived from the baseline recording which contained a significant amount of ectopic activity. The administration of dofetilide causes a minor effect which is not detectable in the analysis. However this hypothesis contradicts previous findings in literature [6].

Since the slope of the QRS-complex is very steep, the determination of the local time of excitation is rather certain. It is presumed that uncertainty is introduced via the determination of the local time of repolarization. This is explained via the increase of the T-wave which increases over a broad time span and is characterized by smaller increase in magnitude. Hereby more uncertainty is introduced in the determination of the local time of repolarization than the determination of the local time of excitation. A wrong placement of a few milliseconds influences the STV of the channel directly.

B. Distribution of the origins of ectopic beats

From figure 4 it is seen that the origins of ectopic beats are heterogeneously distributed over the heart. Thereby it is presumed that the theory of Vandersickel et al. (2016) [1] is more likely than the theory of de Lange, Xie and Qu (2012) [5]. The theory of de Lange et al. (2012) [5] is less feasible since it assumes a regionally synchronized EAD which propagates through the tissue. In that case the origins of the ectopic beats would be more homogeneously distributed over the heart.

Comparing the figures 6 & 8, it is observed that depending on amount of beats in the episode, the preferable location to initiate the ectopic beats changes. This shift might be due to a difference in local characteristics of the tissue.

V. CONCLUSIONS

Only one dog, namely dog 901016, was analysed which does not allow to draw a general conclusion for Torsade de Pointes.

From the analysis of dog 901016, it is concluded that the UEG data obtained via needles did not show the trend of a STV increase just before the offset of the first ectopic beat. Therefore it was concluded that the STV could not be used as a biomarker for the prediction of Torsade de Pointes. The STV values were highly heterogeneously distributed over the heart. Presumably the determination of STV was highly dependent of the morphology of the T-wave.

For dog 901016, the distribution of origins of the ectopic beats was heterogeneous. Therefore it was concluded that the ectopic beat origins in preferable locations. It is presumed that the theory of Vandersickel et al. (2016) [1] is more likely.

VI. LIMITATIONS

No general conclusion can be draw since only one dog was analysed. No statistical analysis has been done therefore the statements as 'there is no increase in STV' or 'distribution of origins of the ectopic beats is heterogeneous' should be carefully interpret.

VII. ACKNOWLEDGEMENTS

Gratitude goes to UMC Utrecht for sharing the data of the different mapping experiments.

REFERENCES

[1] N. Vandersickel, T. P. Boer, M. A. Vos, and A. V. Panfilov, "Perpetuation of torsade de pointes in heterogeneous hearts: competing foci or re-entry?," *The Journal of physiology*, vol. 594, no. 23, pp. 6865–6878, 2016.

[2] R. Hu, W. G. Stevenson, and L. S. Lilly, "Clinical aspects of cardiac arrhythmias," in *Pathophysiology of heart disease: a collaborative project of medical students and faculty* (L. S. Lilly, ed.), ch. 12, pp. 279–300, Boston: Lippincott Williams & Wilkins, 2012.

[3] P. J. Schwartz and R. L. Woosley, "Predicting the unpredictable: drug-induced qt prolongation and torsades de pointes," *Journal of the American College of Cardiology*, vol. 67, no. 13, pp. 1639–1650, 2016.

[4] E. Vandael, B. Vandenberk, J. Vandenberghe, H. Pincé, R. Willems, and V. Foulon, "Incidence of torsade de pointes in a tertiary hospital population," *International Journal of Cardiology*, 2017.

[5] E. de Lange, Y. Xie, and Z. Qu, "Synchronization of early afterdepolarizations and arrhythmogenesis in heterogeneous cardiac tissue models," *Biophysical journal*, vol. 103, no. 2, pp. 365–373, 2012.

[6] S. C. Wijers, D. J. Sprenkeler, A. Bossu, A. Dunnink, J. D. Beekman, R. Varkevisser, A. A. Hernández, M. Meine, and M. A. Vos, "Beat-to-beat variations in activation-recovery interval derived from the right ventricular electrogram can monitor arrhythmic risk under anesthetic and awake conditions in the canine chronic atrioventricular block model," *Heart rhythm*, 2017.

[7] A. Dunnink, T. R. Stams, A. Bossu, V. M. Meijborg, J. D. Beekman, S. C. Wijers, J. M. De Bakker, and M. A. Vos, "Torsade de pointes arrhythmias arise at the site of maximal heterogeneity of repolarization in the chronic complete atrioventricular block dog," *EP Europace*, vol. 19, no. 5, pp. 858–865, 2017.

[8] C. W. Haws and R. L. Lux, "Correlation between in vivo transmembrane action potential durations and activation-recovery intervals from electrograms. effects of interventions that alter repolarization time.," *Circulation*, vol. 81, no. 1, pp. 281–288, 1990.

[9] S. C. Wijers, H. Ritsema van Eck, P. F. Doevendans, M. Meine, and M. A. Vos, "Fiducial segment averaging for accurate determination of the inflection points on the 12-lead surface ecg and semi automatic measurement of qt variability.,"

Table of Contents

List of Figures

List of Tables

Acronyms

APD	action potential duration.
ARI	activation repolarization interval.
AV	atrioventricular.
CAVB	chronic atrioventricular block.
CO	cardiac output.
DAD	delayed afterdepolarization.
EAD	early afterdepolarization.
ECG	electrocardiogram.
EGM	intracardiac electrogram.
GUI	graphical user interface.
HR	heart rate.
HW/BW	ratio heart weight/body weight.
ICD	implantable cardiac defibrillator.
latent pacemaker	other structures which are capable of firing an action potential, also called ectopic pacemaker.
LQTS	long QT syndrome.
LV dP/dt	maximal rise in left ventricular pressure.
MAP	monophasic action potential.
native pacemaker	pacemaker cells in the sinoatrial (SA)-node which dominate the heart rhythm.

QTc	corrected QT.
SA	sinoatrial.
SCD	sudden cardiac deaths.
STV	short-term variability.
TdP	Torsade de Pointes.
UEG	unipolar electrogram.

Symbols

Ca^{2+}	Calcium ion.
$\langle g_K \rangle$	K^+ conductance.
$\langle g_{Ca} \rangle$	Ca^{2+} conductance.
σ_{gCa}	standard deviation of Gaussian distribution of Ca^{2+} conductance.
K^+	Potassium ion.
Na^+	Sodium ion.

Chapter 1

Background Research

1.1 Introduction to the heart

1.1.1 Heart chambers

The heart is divided into 4 chambers: 2 atria and 2 ventricles. The septum separates the right side of the heart from the left side, whereas each side contains one atrium and one ventricle. There are 4 valves present in the heart structure. The atrioventricular valves which are the valves which separate the atrium from the ventricle in the right and left side of the heart, respectively the atrioventricular and mitral valve. The valves between the ventricles and their outlet are called the semilunar valves and prevent backflow in the right and left ventricle. These valves are the pulmonary and aortic valve. An overview of the different valves is given in figure 1.1 (Marieb & Hoehn, 2016, Chapter 18).

Blood enters in the atria, depending on whether the left or right atrium is considered oxygenated or deoxygenated blood is received. The left atrium is supplied of oxygenated blood by the pulmonary veins while the right atrium is supplied with deoxygenated blood by multiple veins, namely the superior vena cava, inferior vena cava and the coronary sinus. When the atria contract, the blood is pushed towards the ventricles. The ventricles are responsible for propelling the blood away from the heart. The difference between the right and left ventricle is the destination of the propelled blood. The left ventricle pushes the blood into the aorta towards the tissues while the right ventricle ejects into the pulmonary artery towards the lungs (Marieb & Hoehn, 2016, Chapter 18).

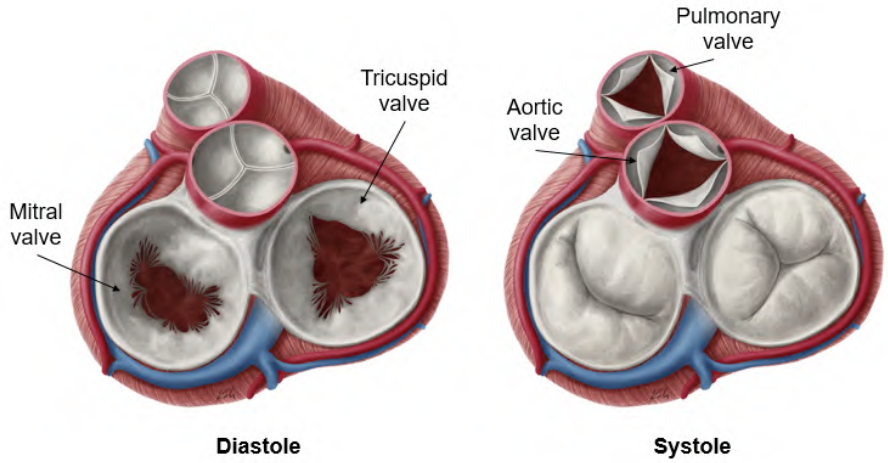

Figure 1.1: An overview of the different heart valves adapted from Sieroslawska, Alexandra (2017).

1.1.2 Layers of the heart

When discussing the heart wall, different layers can be identified: the pericardium, the epicardium, the myocardium and the endocardium. An overview of these different heart layers is given in figure 1.2. This complex structure is guaranteed and anchored by the cardiac skeleton (Marieb & Hoehn, 2016, Chapter 18).

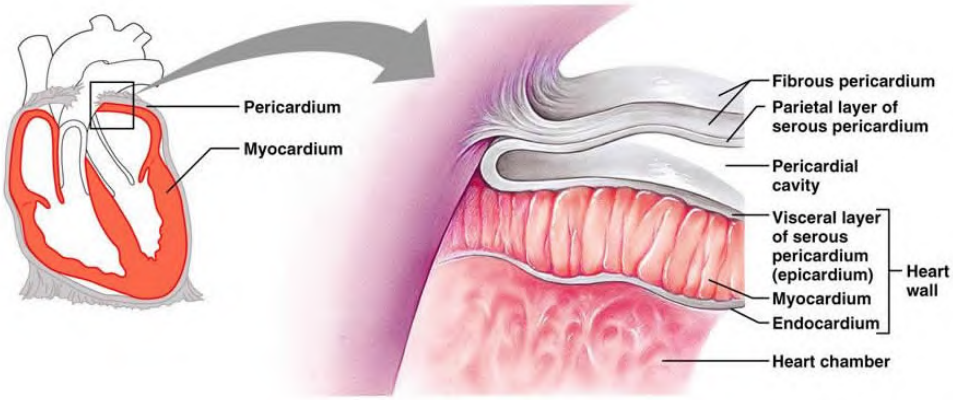

Figure 1.2: An overview of the different heart layers adapted from Marieb and Hoehn (2016).

Pericardium and epicardium

The heart is covered by the pericardium, a double-walled structure which encloses the heart. It exists out of 2 layers: (1) the fibrous pericardium and (2) the serous pericardium. (1) The fibrous pericardium consists of dense connective tissue which surrounds the heart rather loosely. It has 3 important functions: (a) protection of the heart, (b) anchoring of the heart and

(c) prevention of overfilling of the heart. (2) The serous pericardium consists of 2 separated layers: the parietal layer and the visceral layer. The outer surface of the parietal layer connects to the inner surface of the fibrous pericardium. Over the external surface of the heart, the visceral layer is connected. This layer is also called the epicardium. The space in between the 2 layers of the serous pericardium is called the pericardial cavity. The surfaces aligning this cavity are lubricated by a fluid, which is an important characteristic to allow friction-free movement of the heart (Marieb & Hoehn, 2016, Chapter 18).

Myocardium

More inward in the heart structure, a muscular layer is found. This layer is called the myocardium and contains heart muscle cells which are responsible for the contraction of the heart (Marieb & Hoehn, 2016, Chapter 18).

The myocardium is the thickest layer of the heart which significantly differs depending on the considered chamber. The thickness of myocardium in the atria is smaller compared to the myocardium in the ventricles. This is explained by the difference in work load. The atria have to push the blood over a small distance into the ventricle, while the ventricles have to propel the blood over a large distance towards the tissues (Marieb & Hoehn, 2016, Chapter 18). Also a difference in thickness of myocardium is seen when the right and left ventricle are compared. The wall of the left ventricle is roughly 3 times bigger than the wall of the right ventricle. This is again explained by the difference in workload between the ventricles (Lin, Edelmand, Strichartz, & Lilly, 2012).

Endocardium and cardiac skeleton

The most inward heart layer is the endocardium. This is a layer with endothelial cells and connective tissue which surrounds the different heart chambers and encloses the skeleton of the valves.

The cardiac skeleton consists out of collagen and elastic fibres forming a dense structure to maintain the heart structure and to provide support. Without this cardiac skeleton, certain heart structures might become stretched which would decrease the efficiency of the heart. Another important feature of the cardiac skeleton is that it separates the atria from the ventricles. Since the skeleton consists out of electrically non-excitable tissue, it acts as an insulator between the atria and ventricles (Marieb & Hoehn, 2016, Chapter 18).

1.1.3 The pulmonary and systemic circulation

The right side of the heart receives deoxygenated blood from the tissues in the right atrium and propels this blood towards the lungs via the pulmonary artery. In the lungs, the blood becomes oxygenated. This oxygenated blood then enters in the left atrium via the pulmonary veins. The circulation of blood from the right side of the heart over the lungs towards the left side of the heart is called the pulmonary circulation (Marieb & Hoehn, 2016, Chapter 18).

The oxygenated blood in the left side of the heart is pushed via the aorta towards the tissue in order to supply oxygen and nutrients. In the tissues, the blood exchanges oxygen, nutrients and wastes with the tissue cells. The deoxygenated blood enters an artery and is brought towards the right atrium. The circulation from the left side of the heart over the tissue and back towards the right heart is called the systemic circulation. The heart acts thus as a pump of either the pulmonary and systemic circulation (Marieb & Hoehn, 2016, Chapter 18).

1.2 Electric activity in the heart at cell level

A feature of cardiac cells is their capability of electrical excitation. There are 3 types of electrical excitable cells in the heart: (1) the pacemaker cells, (2) the specialized rapidly conducting tissues and (3) cardiac muscle cells, also called cardiomyocytes. These cells have a specific cell membrane which is roughly impermeable to ions. The passage for ions over the cell membrane occurs via dedicated cell membrane proteins. This impermeability is crucial to allow an imbalance of ions between the inside and outside of the cell. The most important ions in the cell are: potassium K^+, sodium Na^+ and calcium Ca^{2+} (Lin et al., 2012).

The membrane potential of the cell is defined as electrical potential difference over the membrane created by a different amount of charge inside and outside the cell. An increase or decrease of this membrane potential is caused by ions entering or leaving the cell. A negative membrane potential implies that the intracellular environment is more negatively charged compared to the extracellular environment (Lin et al., 2012).

The movement of ions across the cell membrane is determined by 2 factors:

- *Energetic factors: the concentration gradient and the membrane potential*
  The concentration gradient determines the driving force by diffusion which implies the movement of ions from high concentration to low concentration. The membrane potential determines the electric driving force on the ions. Since ions are attracted to the opposite charge, the ions experience a force towards the oppositely charged environment causing it to leave or enter the intracellular environment (Lin et al., 2012).

- *Ion permeability of the cell membrane*
  As mentioned above the cell membrane is rather impermeable to ions. This implies that dedicated membrane proteins determine the passage of the ions. These proteins are called 'ion channels'. The more ion channels are open, the more ions are able to enter or leave the cell. In heart cells, these channels are voltage-gated which implies that the opening or closing of the channel is determined by a threshold voltage (Lin et al., 2012).

The membrane potential at resting state of the cell, called the resting membrane potential, is determined by the equilibrium between the gradients across the membrane and the amount of open ion channels. The resting membrane potential of a cardiomyocyte is -90mV. Only the K^+ channels are open during this resting state which implies that only K^+ ions are able to travel across the membrane. The concentration gradient determines the movement of the K^+ ions: since the concentration of K^+ inside the cell is higher than outside the cell, the positively charged K^+ tends to leave the cell. However this causes the intracellular environment to be more negatively charged relative to the outside of the cell, causing the K^+ ions from the extracellular environment to move into the cell. When the driving force by diffusion and electrical driving force are in equilibrium, the resting state is established (Lin et al., 2012).

An important concept to understand the electrical behaviour of heart cells is 'action potential'. An action potential is a fast increase of the membrane potential, called depolarization, followed by a decrease, called repolarization. The differences in action potential pattern between pacemaker cells and cardiac muscle cells are discussed in the sections below. Both cells are important for the contraction of the heart. Without pacemaker cells the heart loses its dependency of the brain, while without contractile cardiac muscle cells the heart would not be able to fulfil its pumping activity (Marieb & Hoehn, 2016, Chapter 18). Since the action potential in the specialized rapidly conducting tissues have similar characteristics as the action potential of cardiomyocytes (Lin et al., 2012), their characteristics are not discussed in this master's dissertation.

1.2.1 Action potential in pacemaker cells

Cardiac pacemaker cells are unique since they do not have a stable resting membrane potential. The action potential of pacemaker cells is divided in 3 steps: (1) pacemaker potential, (2) depolarization and (3) repolarization (Lin et al., 2012).

The pacemaker potential is a gradual increase in membrane potential due to an inward current of Na^+, called the pacemaker current. This implies that there is no stable resting membrane potential since there is no equilibrium between the efflux of K^+, influx of Na^+ and the working of a dedicated membrane protein, namely the Na^+-K^+-pump. A membrane potential of -60 mV is above the threshold of the Na^+ channels which implies that these channels remain continuously activated allowing the inward current of Na^+. The membrane potential rises gradually from -60 mV to -40 mV (Lin et al., 2012). When the membrane potential reaches

-40 mV, the threshold for opening up the voltage-gated Ca^{2+} channels is reached. Due to the increase in membrane permeability to Ca^{2+} after opening up these channels, a high influx of Ca^{2+} occurs and a fast depolarization to +10 mV is noticed. At +10 mV another threshold is reached, namely the threshold of the voltage-gated K^{+} channels. These channels cause an efflux of K^{+} out of the cell which decrease the membrane potential up to -60 mV. The ionic balances are restored by specialized ion-pumps and the cycle repeats itself (Marieb & Hoehn, 2016, Chapter 18). The evolution of the membrane potential is represented in figure 1.3.

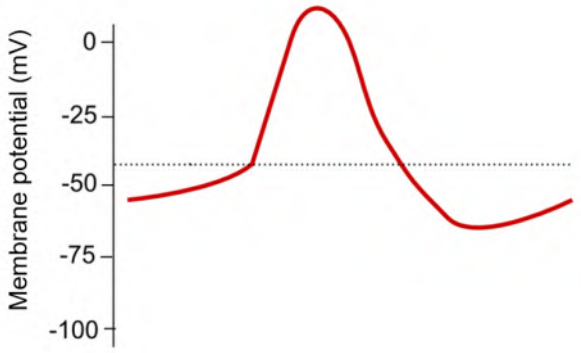

Figure 1.3: The membrane potential during a pacemaker potential adapted from Clarkson (n.d.).

The firing rate of action potential by the pacemaker cell is determined by following factors. In figure 1.4 the impact of each factor is graphically represented.

- The rate of spontaneous depolarization: the higher the pacemaker current, the higher the spontaneous depolarization rate, the faster the Ca^{2+} threshold is reached to fire the action potential and the higher the firing rate of the action potentials.
- The maximum negative diastolic potential: the more negative the maximum negative membrane potential, the longer it takes to reach the Ca^{2+} threshold and thus the lower the firing rate of the action potentials.
- The threshold potential: the lower the Ca^{2+} threshold, the higher the firing rate of the action potentials.

Pacemaker activity is present in all the structures of the electrical conduction pathway in the heart: in the sinoatrial (SA)-node but as well in the atrioventricular (AV)-node, His-bundle as the Purkinje fibres (Hu, Stevenson, Strichartz, & Lilly, 2012). All the structures of the electrical conduction pathway are explained in section 1.3. The pacemaker cells in the SA-node depolarize around 75 times per minute which is faster than the depolarization rate of pacemaker cells in the other structures, which explains why the SA-node dominates the heart rhythm and

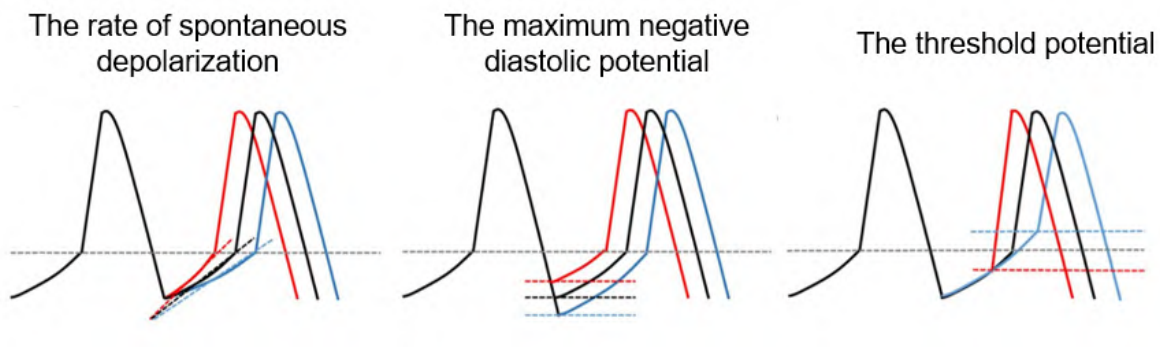

Figure 1.4: The influence of the rate of spontaneous depolarization, the maximum negative diastolic potential and the threshold potential on the firing rate adapted from Vornanen (2016). Notice that the situation in case of an increased firing rate is represented in red while the situation of a decreased firing rate is shown in blue.

is therefore called the native pacemaker (Marieb & Hoehn, 2016, Chapter 18). The other structures of the conduction pathware are capable of firing an action potential if necessary and are therefore called the latent pacemakers or ectopic pacemakers (Hu, Stevenson, Strichartz, & Lilly, 2012).

1.2.2 Action potential in cardiomyocytes

The majority of cells in the atria and ventricles are contractile muscle cells, also called cardiomyocytes. Cardiomyocytes are muscle cells which are connected with each other via gap junctions. These junctions allow ions to pass from one cell to another. The cardiomyocytes are thus electrically dependent, enabling the transmission of an electrical signal such as the development of an action potential. Compared to the pacemaker cells, these contractile cells have a resting membrane potential around -90mV (Marieb & Hoehn, 2016, Chapter 18).

An action potential in a atrial or ventricular cardiomyocyte is triggered by depolarization of their neighbouring cells. Gap junctions between the cardiomyocytes allow ions to enter from the neighbouring cell, which depolarizes the cardiomyocyte and triggers the formation of an action potential by fast opening of the voltage-gated Na^+ channels (Lin et al., 2012). This very fast increase in the intracellular Na^+ concentration causes the membrane potential to increase very fast from -90mV to +30mV. After this increase, the Na^+ channels are closed and the fast increase in membrane potential stops and a slight decrease in membrane potential is seen (Marieb & Hoehn, 2016, Chapter 18). This decrease is caused by the efflux of K^+, which is subjected to a high driving force from the concentration gradient as well as the electrical driving force (Lin et al., 2012).

The Ca^{2+} channels open up slowly and allow Ca^{2+} to enter the cell, enabling contraction of the muscle cell. The concept 'excitation-contraction coupling' denotes the ability of Ca^{2+} to regulate whether contraction occurs or not. The entrance of Ca^{2+} down its concentration gradient and efflux of K^{+} causes the plateau stage in the membrane potential pattern. The entering of the Ca^{2+} prolongs the depolarization and thus increases the tension of contraction of the cell. The plateau stage assures this way that the chamber fully contracts and all the blood is ejected out of the atrium or ventricle. This plateau stage is highly visible in an action potential in the ventricles while this stage is more subtle in an action potential in the atria. In the atria the effect of the leakage of K^{+} is more prominent compared to the influx of Ca^{2+} which causes a decrease in the membrane potential (Lin et al., 2012).

After the plateau-stage, a fast repolarization is noticed so the membrane potential returns back to its resting state. This is due to the inactivation of the Ca^{2+} channels and the opening of the voltage-gated K^{+} channels. The large efflux of K^{+} causes a decrease in membrane potential to resting membrane potential, namely -90mV (Marieb & Hoehn, 2016, Chapter 18). After the action potential, the cell contains a higher amount of Ca^{2+} and Na^{+} and a small amount of K^{+}. In order to restore the original state of the cell, dedicated membrane proteins, such as specific ion pumps and ion exchangers, recover the initial ion balance often with energy consumption (Lin et al., 2012). In figure 1.5, the action potential of the atrial and ventricular muscle is represented.

During the plateau stage and beginning of the repolarization, the cell is in a refractory state which implies that the cell can not be depolarized again. However in case of a strong stimulus the cell can be depolarized again during the repolorization. This refraction period is necessary to allow the ventricle or atria to empty their content and refill in time for the next contraction (Marieb & Hoehn, 2016, Chapter 18).

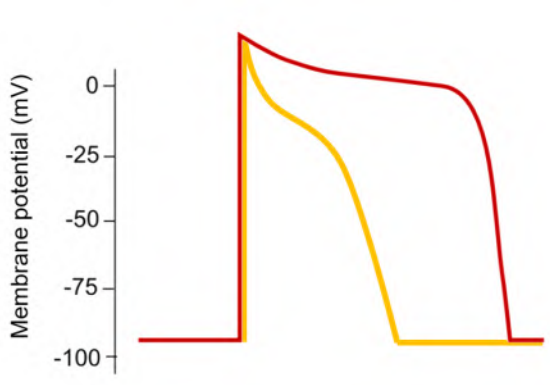

Figure 1.5: The membrane potential during the action potential of an atrial or ventricular cardiomyocyte adapted from Clarkson (n.d.). The red line represents the action potential in a ventricular muscle cell and the yellow line the action potential in an atrial muscle cell.

The difference between a cardiac muscle cell and specialized rapidly conducting tissues, such as the Purkinje fibres, is subtle. The conducting tissue is capable of reacting much faster than the muscle cells since the conducting tissues have a higher number of Na^+ channels. A higher number of Na^+ channels allows a faster depolarization and thus a faster reaction (Lin et al., 2012). An overview of all the different action potential in the heart is represented in figure 1.6.

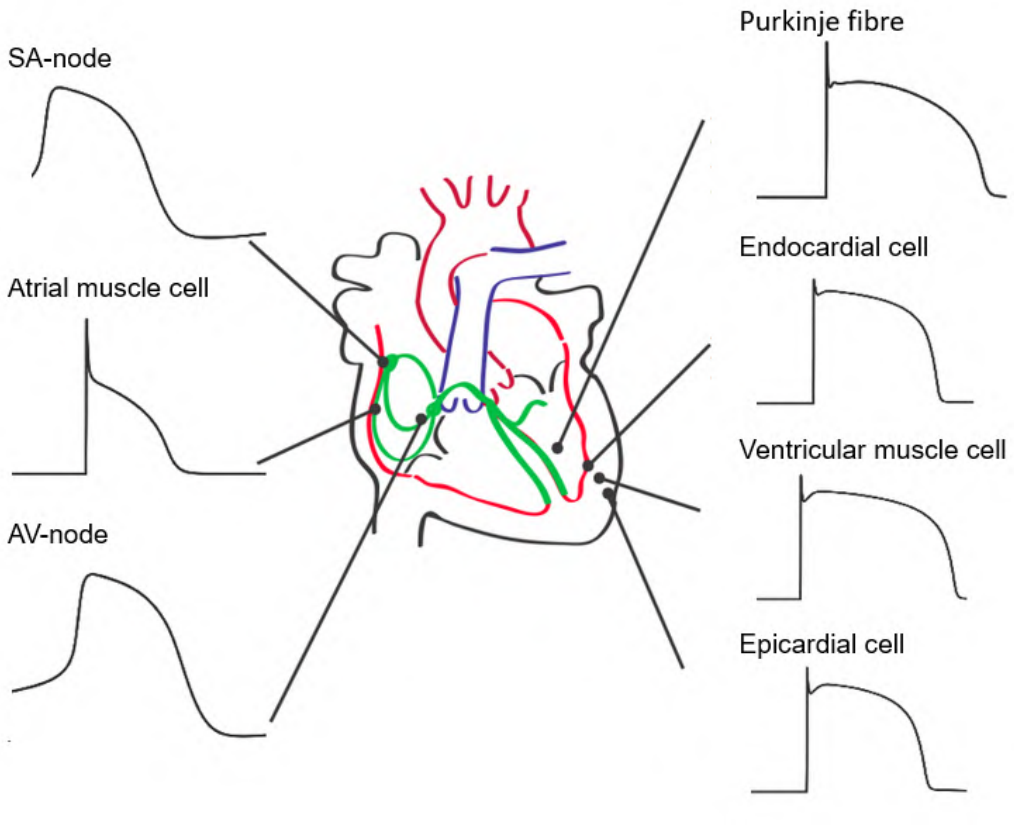

Figure 1.6: Different action potential in the heart adapted from *Cardiac action potentials in different areas of the heart* (2009).

1.3 Electrical conduction pathway

Contraction of the heart is initiated by self-excitable cells, namely pacemaker cells. Theoretically heart contraction could be fully autonomous from the brain, which is called intrinsic contraction. However during exercise or stressful situations for example, the heart rate is altered via nerve stimulation. In those situations the vagus nerve influences the pacemaker activity of the SA-node (Marieb & Hoehn, 2016, Chapter 18).

The electrical signal given from one cell to another is the development of an action potential. The signal starts in the sinoatrial node. From this node, the signal spreads via a depolarization wave over the right and left atrium and ends in the atrioventricular node. This node passes the signal towards the ventricles after the atria contracted. Via the bundle of His and the Purkinje

fibres the signal is conducted towards the ventricular cells. These ventricular cells can be excited directly by the Purkinje fibres, however most of the signal conduction happens through the gap junctions (Marieb & Hoehn, 2016, Chapter 18). A representation of the electrical conduction pathway is represented in figure 1.7.

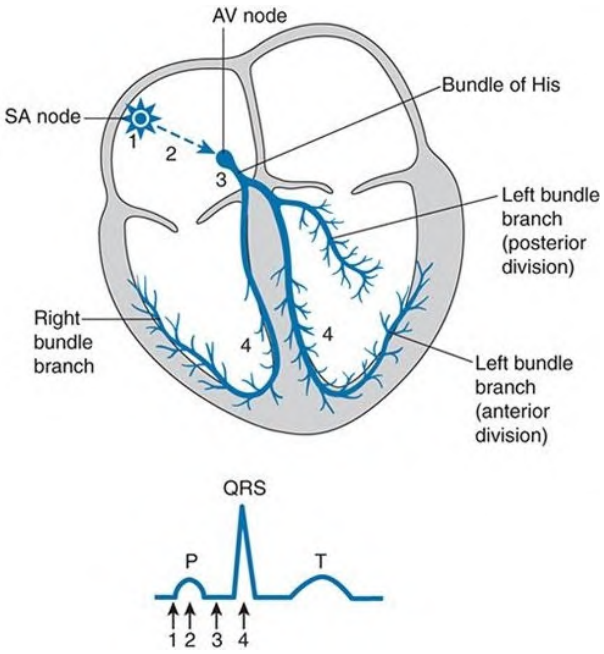

Figure 1.7: The electrical conduction pathway of the heart adapted from Romedli and Lilly (2012).

1.3.1 Sinoatrial node

The sinoatrial node, also called the SA-node, is situated in the muscle wall of the right atrium and exists of a bunch of cells with pacemaker activity. In a healthy heart, the SA-node initiates the heart contraction as explained in section 1.2.1 (Marieb & Hoehn, 2016, Chapter 18).

1.3.2 Atrioventricular node

The atrioventricular node, also called AV-node, is located in the left down corner of the right atrium near the septum. When the SA-node depolarizes, a depolarization wave is spread over the right and left atrial myocardiocytes. Eventually the depolarization arrives at the AV-node. At the AV-node the depolarization is delayed for 0.1 second caused by 2 effects. (1) A first effect causing the delay is the diminished amount of gap junctions in the AV-node. This way the depolarization of those cells develops slower. (2) Another effect is the transmission of the signal onto small diameter fibres. As a result of this delay the atria are able to contract completely before the ventricles contract (Marieb & Hoehn, 2016, Chapter 18).

1.3.3 Bundle of His

The bundle of His or atrioventricular bundle (AV-bundle), is the collective noun for the fibres starting at the AV-node. Since the myocardiocytes of the atria and ventricles are separated from each other via the cardiac skeleton, the fibres form the only electrical connection between the atria and ventricles. These dedicated conduction fibres assure a fast transmission of the electrical signal (Marieb & Hoehn, 2016, Chapter 18).

1.3.4 Bundle branches and Purkinje fibers

The bundle of His branches in two after entering the septum. Both branches run towards the apex of the heart and then split: one to the right side while the other branch goes towards the left side of the heart. These branches separate further forming a network, called the subendocardial conduction network or Purkinje fibres. This network is present in the whole ventricular wall. Some ventricular cardiomyocytes are excited by the bundle branch, but the majority of these cells depend on electrical conduction via gap junctions (Marieb & Hoehn, 2016, Chapter 18).

1.4 The electrocardiogram

An electrocardiogram (ECG) is a visualization of the electric activity of the heart. In order to understand the measured activity on the ECG, the electrical activity of an individual cell must be understood. This is explained via the single-cell model. When this model is fully understood, the model is translated to the whole heart.

1.4.1 The single-cell model

As mentioned in 1.2.2, a cardiomyocyte has a negative resting membrane potential. The intracellular environment of the cardiac heart cell is thus more negative compared to the extracellular environment. In the extracellular environment the charge is equally distributed so no gradient is seen. When the electrical activity of the cardiac muscle cell in resting state is recorded with a voltmeter, no signal is measured since there is no gradient present in the extracellular environment. This resting situation is represented in the first representation of figure 1.8 (Romedli & Lilly, 2012).

When the cell depolarizes (depicted with the lightning arrow in situation 1 of figure 1.8), the extracellular environment becomes more negative compared to the intracellular environment. The depolarization happens gradually over the cell. This implies that the charge in the extracellular environment over the cardiac muscle cell is not homogeneously distributed and a

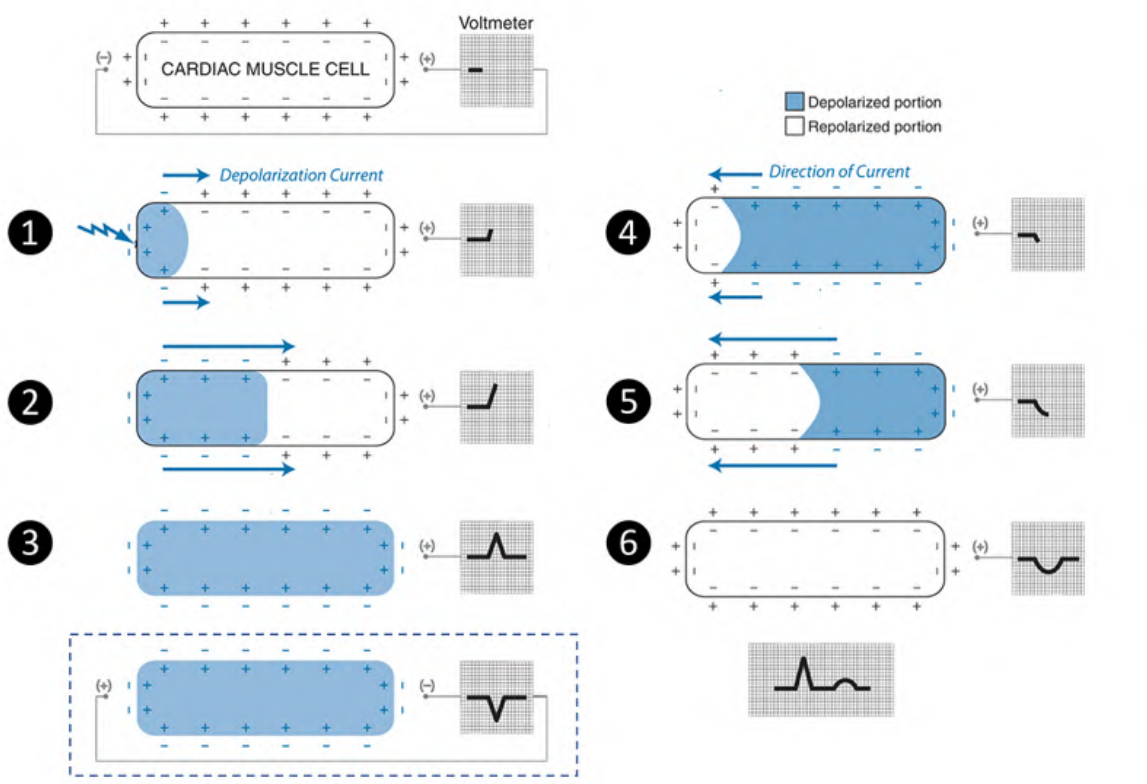

Figure 1.8: A graphical representation of depolarization and repolarization in the single cell model. Figure adapted from Romedli and Lilly (2012).

gradient is observed. This gradient causes a current from the more negative region towards the more positive extracellular region, called the depolarization current. This is registered by the voltmeter as a positive current since current flows from the negative towards the positive electrode. The magnitude of the current is determined by the magnitude of the gradient. The larger the gradient, the larger the depolarization current.

In situation 1 the gradient is present but rather small which causes a rather small, positive depolarization current. As the depolarization spreads, the gradient increases and thus the depolarization current keeps increasing until a maximum. This is represented in situation 2. After situation 2, the gradient over the cell decreases again, which still causes a positive current but with a smaller magnitude. When the cell is fully depolarized, the charge is homogeneously distributed over the cell so no signal is recorded by the voltmeter. The depolarization of the single cell is represented by situation 1, 2 & 3 in figure 1.8 (Romedli & Lilly, 2012).

Notice that when the electrodes of the voltmeter are reversed, current would flow from the positive electrode towards the negative electrode which implies a negative current. This situation is represented in the dashed box of figure 1.8 (Romedli & Lilly, 2012).

After the depolarization, the repolarization occurs to return to the resting state. The initiation of the repolarization and the depolarization is assumed to be the same in this single-cell model. During the repolarization also a gradient is noticed over the cardiac muscle cell but in the reversed direction compared to the depolarization. This implies a negative current. The waveform of the repolarization is rounded, wider and lower in amplitude since the time for the repolarization is longer compared to the time of depolarization. This is also seen in figure 1.5 where the steepness of the depolarization is higher than the steepness of the repolarization. After the repolarization the charge in the extracellular environment is again homogeneously distributed and no signal is registered by the voltmeter. This is represented by situation 4, 5 & 6 in figure 1.8 (Romedli & Lilly, 2012).

In the last representation in figure 1.8, a more realistic recording of the electrical signal in the cell is given during depolarization and repolarization. In this figure, the repolarization wave is reversed compared to the repolarization wave in the single cell model, namely positive instead of negative (Romedli & Lilly, 2012). This is explained by the fact that depolarization and repolarization are not initiated on the same spot but on the opposite side of the cell due to interaction with surrounding cells.

1.4.2 Single-cell model translated to the whole heart

Since a cell passes its depolarization onto its neighbouring cells, a certain wave-pattern is established called the depolarization wave. The muscle cells nearest to the nodes or the specialized rapidly conducting tissues, the cardiomyocytes near the endocardium, are excited first. The depolarization wave than travels through the myocardium towards the epicardium. When all the cells of the atria or the ventricles are depolarized, a repolarization wave occurs which travels in the opposite direction since the action potential duration of the cells at the epicardium is shorter than the action potential duration of cells at the endocardium. This action potential difference is schematically presented in figure 1.9. A schematic overview of the depolarization and repolarization wave together with the corresponding ECG-signal is represented in figure 1.10 (Romedli & Lilly, 2012).

Since the electrodes are placed on the skin's surface, the measured signal is a summation of all the different action potentials of the heart and even some interfering signals. An overview of this summation is given in figure 1.11. A signal on the ECG of a healthy heart is divided in different waves: a P-wave, the QRS-complex and the T-wave. The P-wave results from the depolarization wave coming from the SA-node towards the rest of the atria. The QRS-complex is the result of the depolarization of the ventricular cells which implies contraction of the ventricles and the repolarization of the atria. The shape of the QRS-complex is complex since the depolarization wave spreads in different orientations. During the T-wave the ventricular cells repolarize and the contraction of the ventricles ends (Marieb & Hoehn, 2016, Chapter 18).

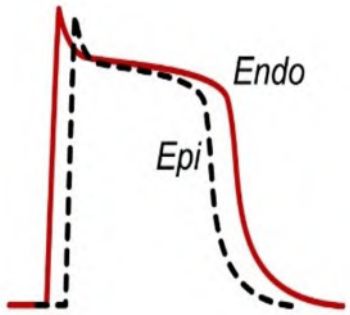

Figure 1.9: The action potential in the endocardium and epicardium of the ventricular wall adapted from Klabunde, Richard E. (2016).

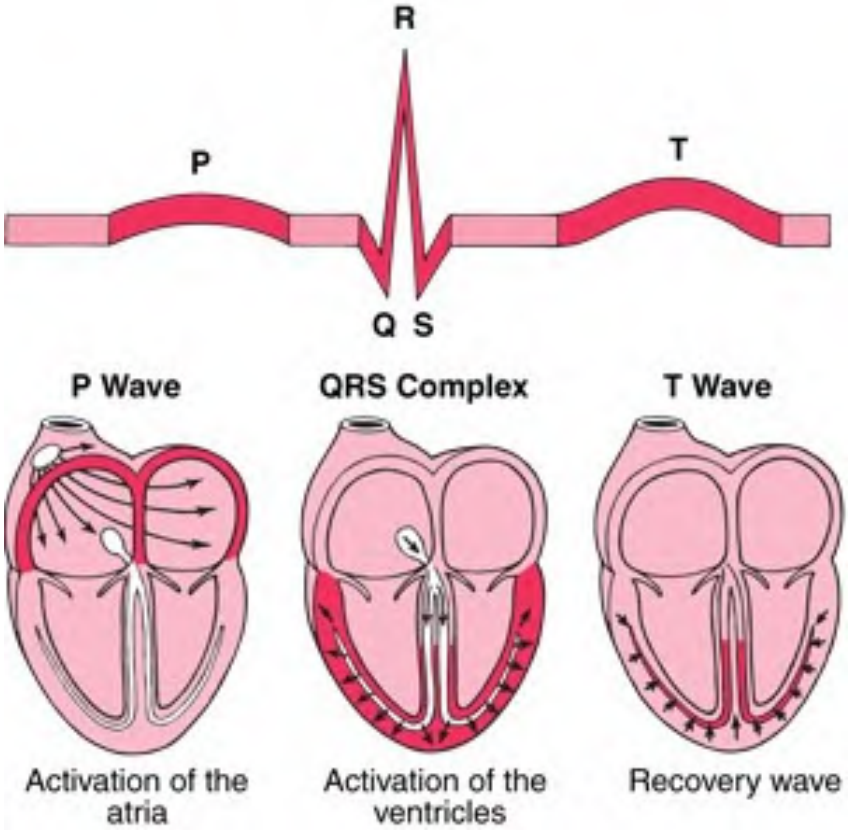

Figure 1.10: Heart contraction at its corresponding ECG-signal adapted from Webdicine, Smarter Medical Care (2011).

1.4.3 Abnormalities in ECG

Depending on the amount of nutrients, oxygen and ions available to the heart cell, it is possible that the ECG-pattern changes. A persisting abnormality in ECG-trace often implies a malfunctioning heart. In this section some ECG abnormalities relevant for this master's dissertation are discussed.

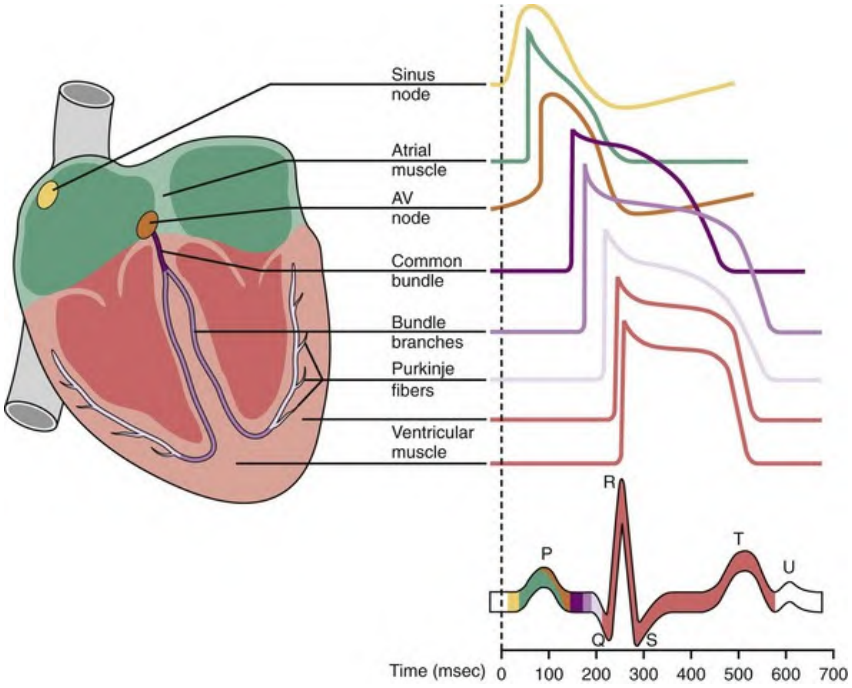

Figure 1.11: The representation of the ECG waveform resulting from the different action potentials in the heart. Figure adapted from Kay et al. (2011).

Elevated ST-interval

An elevated ST-interval is often an acute factor seen during a epicardial or transmural myocardial infarction due to restricted oxygen supply. The term 'transmural' indicates that the infarction involved the whole thickness of the heart wall. An overview of different dispersions of myocardial infarction is represented in figure 1.12. In the acute phase of a myocardial infarction, the heart cells are ischemic which means the cells are still viable but in lack of oxygen. If the cells are not perfused again, the cells eventually become necrotic. The elevation often disappears some days after the infarction. When the ST-interval elevation does not return to baseline, it indicates scar tissue formation on the site of infarction (Romedli & Lilly, 2012).

It is not clear how the ST-interval elevation occurs. Different hypotheses try to explain this phenomenon. Both hypothesis are based on injured myocardial cells.

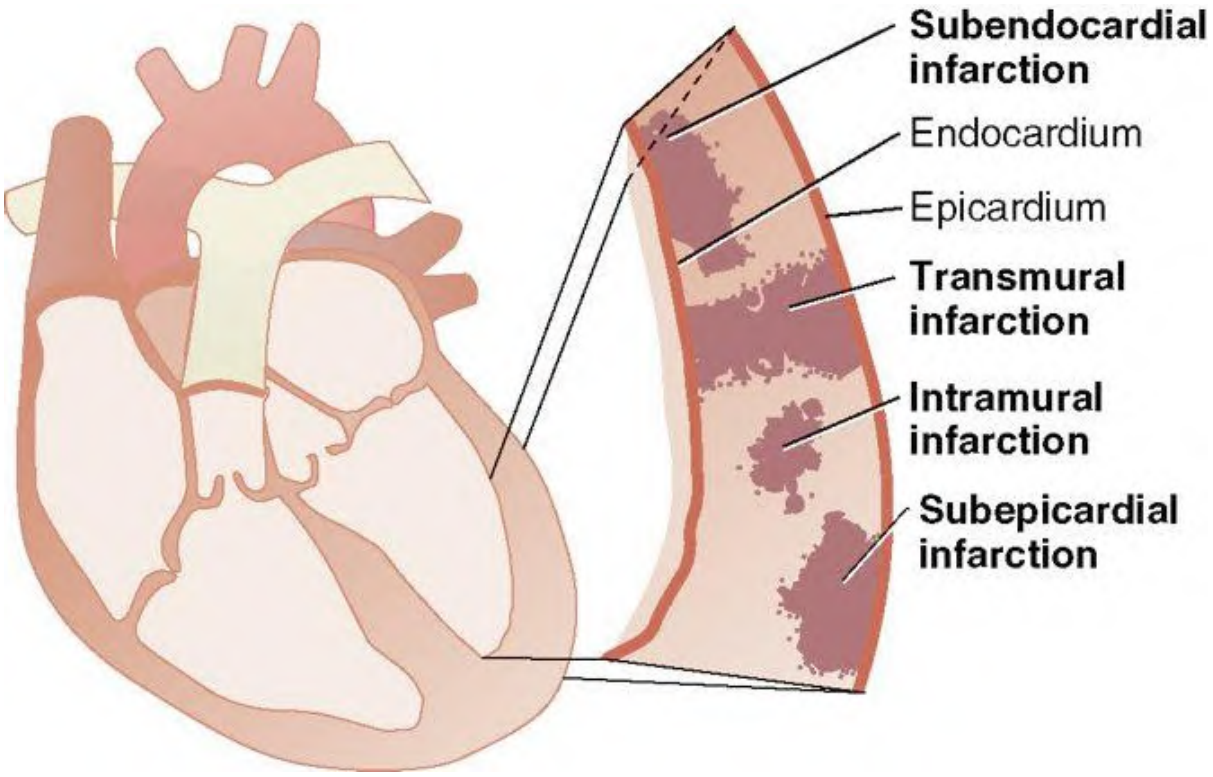

Figure 1.12: An overview of the different sites of possible infarctions adapted from Black and Hawks (2009).

1. Diastolic current theory
   This theory is focussed on the phenomenon during the resting state of the cardiomyocyte, also called the diastole or TQ-interval. The theory assumes that the injured myocardial cells are extremely leaky. Due to this leaky characteristic, ionic flow over the membrane is possible implying that the injured cell is not capable to fully repolarize. The injured heart region is thus partially depolarized which implies that intracellular environment is more positively charged compared to the rest of the heart cells during the diastole. The extracellular environment of the injured region is thus more negatively charged. This causes a gradient and a current from the injured region towards the rest of the heart. Since the current flows away from the electrode, a negative deflection is measured in the ECG which causes a downward shifted baseline and makes the ST-interval appear elevated compared to the baseline. The diastolic current theory is represented in figure 1.13 (Romedli & Lilly, 2012).

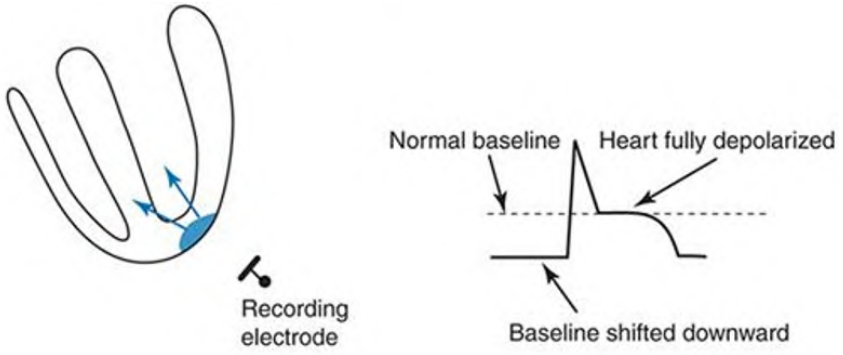

Figure 1.13: A graphical representation of the diastolic current theory adapted from Romedli and Lilly (2012).

2. Systolic current theory
   This theory is focussed on the period of systole or the QT-interval. The theory assumes that the ischemic cell is characterized by an increased resting membrane potential and a shorter duration of the action potential. This implies that the injured myocardial cells repolarize faster than normal cardiac cells. When repolarization occurs in the heart, the intracellular infarct zone is thus more negatively charged compared to the healthy heart tissue. This implies a reversed effect in the extracellular environment: a more positive charged extracellular environment near the injured cells while a more negatively charged extracellular environment near the healthy tissue. This causes a gradient and thus a current from the healthy heart tissue towards the injured region. Since the current flows towards the electrode, a positive deflection is measured with the ECG causing an elevation of the ST-interval. The systolic current theory is represented in figure 1.14 (Romedli & Lilly, 2012).

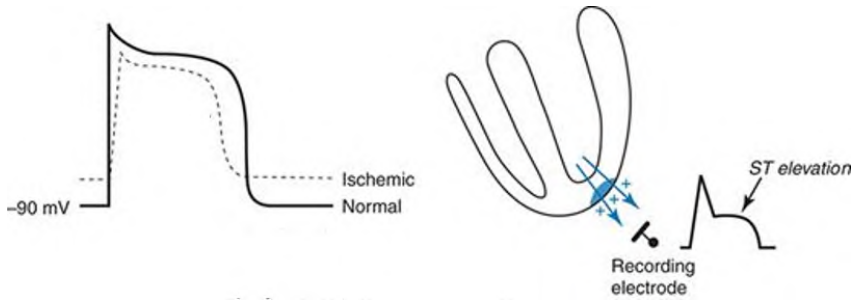

Figure 1.14: A graphical representation of the systolic current theory adapted from Romedli and Lilly (2012).

Notice that the figures 1.13 & 1.14 are causing a ST-elevation since the infarction zone is subepicardial. The same result is seen when the infarction is transmural. When the infarction happens near the endocardium, a subendocardial infarction, the opposite result is seen, namely a declined ST-interval since the direction of the current is opposite (Romedli & Lilly, 2012).

Prolonged QT-interval

Prolonged QT-intervals are induced by electrolyte disturbances and certain drugs which block the K^+ currents. These electrolyte disturbance could be caused by myocardial ischemia, a narrowed coronary artery or due to other factors such as hypocalcemia. Prolongation of the QT-interval can also be due to a genetic disorder such as long QT syndrome (LQTS) (Romedli & Lilly, 2012).

A prolongation of the QT-interval in ECG is a used biomarker for arrhytmias and increases the risk for sudden death (Schwartz & Woosley, 2016).

1.4.4 Alternative methods to measure electrical activity of the heart

When the electrical activity of the heart is measured on the inner surface of the heart, it is called an intracardiac electrogram (EGM). It is a very local measurement which determines the electrical activity of a patch of cardiac cells underneath the electrode (Goldberger & Ng, 2010). Such an EGM is often taken via a specific medical procedure with a dedicated catheter. The catheter tip contains different electrodes to measure the electrical activity on the endocardial surface. An EGM can also be recorded via the electrode of an implantable cardiac defibrillator (ICD) (Swerdlow et al., 2011). Notice that only a limited area is measured at once due to the limited amount of electrodes on the tip of the catheter (Goldberger & Ng, 2010).

Another method to determine the electrical activity is taking an electrogram via needles. Dedicated needles containing multiple electrodes are inserted over the area of interest in the heart (Dunnink et al., 2017). This way a very detailed view of the electrical activity of the heart can be given: the transmural as regional dispersion of the electrical activity is mapped. Logically this type of electrogram in the heart only has research purposes since the heart is severely damaged after the procedure.

For the measurement of an EGM different types of electrodes are available: (1) bipolar electrodes and (2) unipolar electrodes. An electrogram represents a voltage difference between 2 electrodes. When unipolar electrodes are used the difference in voltage is taken between an electrode near the tissue and an indifferent electrode which does not contain electrical activity of the heart. In case bipolar electrodes are used, the voltage different is taken between 2 electrodes near the tissue (Stevenson & Soejima, 2005).

In this master's dissertation, needle unipolar electrogram (UEG) data is used, therefore a more detailed introduction is given to this type of electrodes. When a unipolar electrogram is taken, the electrode near the tissue is by convention a positive electrode. When the depolarization wave is travelling towards the electrode, a positive deflection is seen. A negative deflection is seen when this depolarization wave is travelling away from the electrode. Therefore the maximal negative derivative of the downward slope represents the moment that the depolarization wave reaches the electrode (Stevenson & Soejima, 2005).

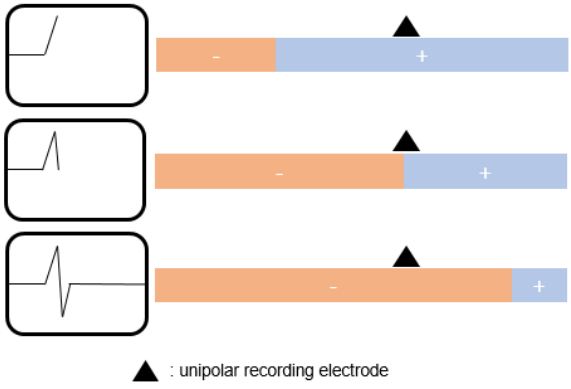

Figure 1.15: Representation of the recording of a UEG. The orange color represents the depolarization wave which corresponds to a negative charge in the extracellular environment. Figure adapted from Stevenson and Soejima (2005).

Another alternative method for measuring the electrical activity of the heart is recording the duration of a monophasic action potential (MAP). These MAP are measured via dedicated contact catheter electrodes which aim to measure the cellular properties very locally. From these recordings the action potential duration (APD) is estimated (Kadish, 2004).

(a) A representation of an EGM. Figure adapted from *EP PRINCIPLES: Catheter Positioning* (2016).

(b) Electrogram measured via needles. Figure adapted from Dunnink et al. (2017).

Figure 1.16: A graphical representation of EGM and electrogram via needles.

1.5 Introduction to arrhythmias

Arrhythmias are characterized by an abnormal activity of the heart rhythm. When discussing arrhythmias 2 different types are observed: (1) bradyarrhythmia and (2) tachyarrhythmia. Bradyarrhythmias are characterized by an abnormally slow electric rhythm of the heart in opposition to tachyarrhythmias where the heart rhythm is significantly increased. The tachyarrhythmias are divided once more in supraventricular and ventricular tachyarrhythmias depending on the origin of the arrhythmia (Hu, Stevenson, Strichartz, & Lilly, 2012). Also a distinction is made based on how the beats arise. An increased regular heart rate is denoted as tachycardias while very chaotic beat initiation is called fibrillation. An overview of the different types of arrhythmias is given in figure 1.17.

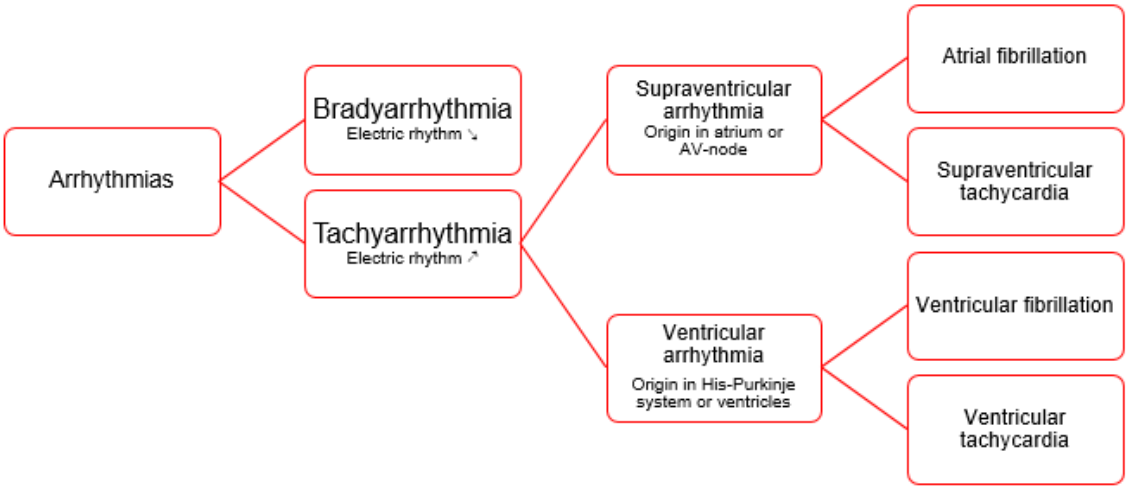

Figure 1.17: A diagram of the different types of arrhythmias.

The formation of a arrhythmias is caused different factors: (1) altered impulse formation, (2) altered impulse conduction or (3) a combination of both. In the following section altered impulse formation and altered impulse conduction are discussed. In order to properly understand how arrhythmias arise, the concept of repolarization reserve is explained first.

1.5.1 Repolarization Reserve

An important concept is 'repolarization reserve', introduced by Roden (1998), which expresses the ability of the heart to repolarize. In a healthy heart the repolarization reserve is large due to the different K^+ channels. When the K^+ currents are diminished, the repolarization reserve is decreased. Notice that the lower the repolarization reserve, the higher the probability for prolonged QT-interval.

1.5.2 Altered impulse formation

An altered impulse formation occurs when the formation of a heartbeat is altered. This is caused by abnormalities such as:

- *Altered impulse initiation*
  Due to certain medication the influence of the vagus nerve is enhanced, altered or inhibited. This can have different effects, namely the formation of escape beats or ectopic beats. An escape beat is a beat which is initiated by a latent pacemaker, as explained in section 1.2.1, when the SA-node has slowed down significantly. Escape beats are likely to occur when the pacing activity of the SA-node has significantly decreased. An ectopic beat is a beat which is initiated by a latent pacemaker in between the normal rhythm determined by the SA-node. Ectopic beats are induced by a lot of different factors, for example hypoxemia, ischemia, electrolyte disturbaces, ... The difference between an escape beat and an ectopic beat is the time of initiation: an escape beat is late compared to the normal rhythm while an ectopic beat is premature compared to the normal rhythm (Hu, Stevenson, Strichartz, & Lilly, 2012).
- *Abnormal impulse initiation*
  Abnormal impulse initiation occurs when the beat is initiated by cells other than native or latent pacemaker cells. Normally a myocardial cell has very few to no pacemaker activity. However when the cell becomes injured, the cell becomes leaky and makes the resting membrane potential less negative which might introduce spontaneous depolarization. An injured cell has an enhanced pacemaker activity which might initiate a beat in between the normal heart rhythm. Beats initiated in this particular way are called abnormal ectopic beats (Hu, Stevenson, Strichartz, & Lilly, 2012).
- *Triggered activity*
  Triggered activity describes abnormal activity stimulated by previous action potentials. These triggers are called afterdepolarization. There are 2 types: (1) early afterdepolarization (EAD) and (2) delayed afterdepolarization (DAD) (Hu, Stevenson, Strichartz, & Lilly, 2012).

An EAD occurs at (1) the end of the plateau-phase or (2) during the repolarization of the cell. EAD are caused by respectively (1) reactivation of certain Ca^{2+} channels or (2) spontaneous release of Ca^{2+} by the sarcoplasmic reticulum, a dedicated cell organelle. Notice that this release of Ca^{2+} activates a membrane pump which exchanges 1 Ca^{2+} -ion for 3 Na^{+} -ions, causing a depolarization of the cell (Tse, 2016). Another factor which influences the development of an EAD is the repolarization reserve which determines the ability to repolarize. The lower the repolarization reserve, the higher the probability of the development of an EAD (Hu, Stevenson, Strichartz, & Lilly, 2012).

A DAD occurs after a completed repolarization. It is hypothesized that delayed afterdepolarizations are more likely to develop when the intracellular Ca^{2+} concentration is high. Notice that the mechanism of the formation of such a DAD is similar as the development of an EAD during the repolarization due to the spontaneous release of Ca^{2+} (Tse, 2016). Notice that both EAD and DAD can evoke a new action potential (Hu, Stevenson, Strichartz, & Lilly, 2012).

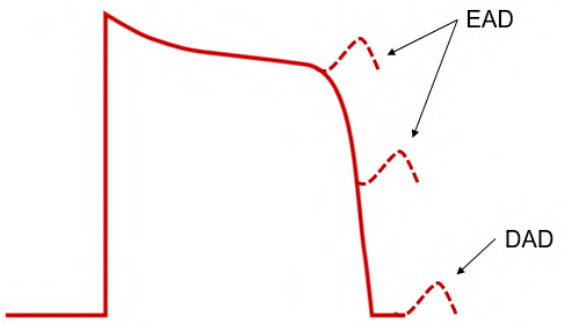

Figure 1.18: The difference between an EAD and a DAD. Figure adapted from Tse (2016).

1.5.3 Altered impulse conduction

When altered impulse conduction is discussed, 2 phenomenons should be explained: (1) conduction block and (2) re-entry. In most of the cases a conduction block causes a bradyarrhythmia while re-entry causes a tachyarrhythmia (Hu, Stevenson, Strichartz, & Lilly, 2012).

Conduction block

When a conduction block occurs, the electrical signal, such as a depolarization wave, is inhibited by a region in the heart which is not electrically excitable. Conduction blocks are characterized by the direction the block manifests, namely (1) unidirectional or (2) bidirectional. In case of a unidirectional conduction block, the electrical signal is blocked in one direction while the signal is not inhibited in the opposite direction. When the signal is blocked in both directions,

the conduction block is bidirectional. Another characteristic of a conduction block is the mechanism of the blockage which can be (1) functional or (2) fixed. A functional conduction block occurs when the electrical signal is inhibited by cardiac cells which are still in their refractory period and are thus not capable to depolarize. A fixed conduction block, also called anatomical block, is caused by non-excitable tissue other than cardiac cells, such as scar tissue. Often a conduction block causes the formation of escape beats since a latent pacemaker takes over the pacemaker activity (Hu, Stevenson, Strichartz, & Lilly, 2012).

Re-entry

In case of re-entry, a looping of the depolarization wave occurs around a functional or anatomical block. Before explaining re-entry, more detailed information about the depolarization wave is given.

When a cell depolarizes, it starts firing an action potential. After the firing state, the cell experiences a refractory state where it is not capable of firing another action potential. This is followed by a resting state in which the cell is capable of creating an action potential. The depolarization wave front is determined by all the cells in the firing state. Since all the cells are connected via gap junction this is denoted as 'conduction'. Logically after the depolarization wave passed, the cells are in a refractory state (Tse, 2016). A planar projection of a depolarization wave is represented in figure 1.19.

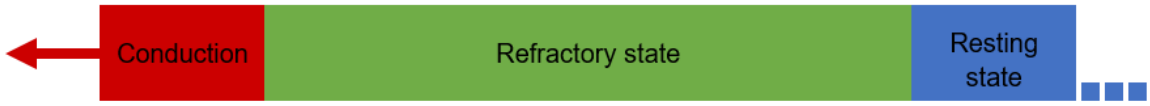

Figure 1.19: Planar projection of the different stages in a plane depolarization wave.

Re-entrant activity circulates around a functional or anatomical block. Logically the core of the circus pathway is respectively formed by a functional or fixed conduction block. Important parameters to determine whether a re-entrant circuit could occur are (1) the conduction velocity and (2) the refractory period. The conduction velocity determines at which speed the depolarization wave travels. The refractory period determines how long the cells are in a refractory state and cannot be depolarized again (Tse, 2016). A rule of thumb to determine whether the re-entrant circuit is successful is:

$$L > RF \cdot CV,$$

where $L =$ length of the circular circuit,

$RF =$ duration of the refractory period,

$CV =$ conduction velocity

Notice that the right part of the equation is the length of the depolarization wave (Tse, 2016).

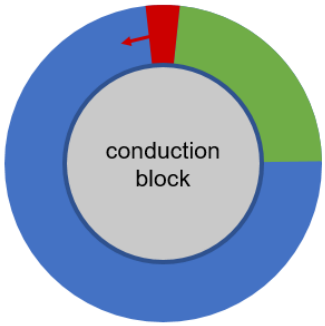

Figure 1.20: Circus type re-entry around a conduction block. Figure adapted from Tse (2016)

This circulating re-entrant activity can cause a spiral wave, often when the length of the circular circuit is close to the length of the depolarization wave. A spiral wave is considered in 2 dimensions, the equivalent considered in 3 dimensions is called the scroll wave. The core of a spiral wave caused by functional re-entry is termed as rotor. A specific type of functional re-entry is a meandering spiral wave which can drift through the tissue (Tse, 2016).

There are 2 different types of re-entry conditions visible on the ECG: (1) monomorphic tachyarrhythmia and (2) polymorphic tachyarrhythmia. In case of monomorphic tachyarrhythmia, the re-entry loop stays the same over the whole episode of the arrhythmia. This implies that the ECG of a monomorphic tachyarrhythmia consists of an abnormality which is repeated represented in figure 1.21. The polymorphic tachyarrhythmia is caused by either abnormalities in the conduction pathway. Such an abnormality might be diseased myocardium. In this case the re-entry loop is not stable and might circulate between excitable tissue and poorly excitable tissue. This results in an ECG pattern which varies heavily over time, visible in figure 1.21(Hu, Stevenson, Strichartz, & Lilly, 2012). Notice that in case the spiral wave breaks up in multiple spirals, ventricular fibrillation occurs.

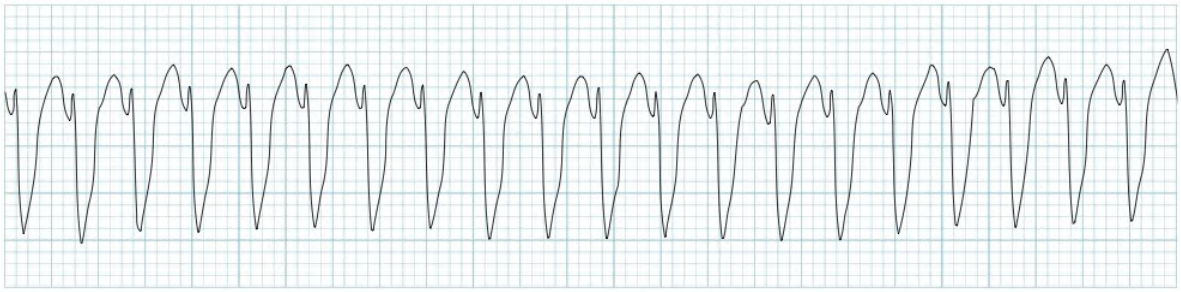

Figure 1.21: The ECG of a monomorphic tachycardia adapted from Burns, Edward (2017b).

Figure 1.22: The ECG of Torsade de Pointes, a polymorphic tachycardia, adapted from Burns, Edward (2017a).

1.6 Introduction to Torsade de Pointes

In this master's dissertation the focus lies on the arrhythmia Torsade de Pointes (TdP). Torsade de Pointes (TdP) is a polymorphic ventricular tachycardia with a typical twisting pattern on the ECG, visible in figure 1.22. The name 'Torsade de Pointes', French for 'twisting of points', is directly derived from the ECG since the QRS-complexes are twisting around the baseline of the ECG (Hu, Stevenson, & Lilly, 2012).

Sudden cardiac deaths (SCD) are estimated to be caused in 67% by ventricular arrhythmias (Huikuri, Castellanos, & Myerburg, 2001). In case of a SCD, TdP could only be identified when an ECG is obtained. Since this is often not the case, the incidence of death by TdP is difficult to estimate (Schwartz & Woosley, 2016). This is also concluded in a recent database research of Belgian cases. Only 31 cases of TdP were reported over 15 years. This research stated that a lack of awareness and knowledge might explain these low numbers (Vandael, Vandenberk, Vandenberghe, Willems, & Foulon, 2017). The same research group identified the incidence of TdP in the university hospitals of Leuven and found that 0.16% of the hospital population is diagnosed with a prolonged QT-interval each year. According to the study, this equals to 173 possible lethal cases of TdP each year in Belgian hospitals (Vandael, Vandenberk, Vandenberghe, Pincé, et al., 2017).

Different risks are identified to cause TdP such as drug-usage, individual factors, electrolyte abnormalities, ... The risk of having TdP is doubled for women. Also patients with an age above 65 have an increased risk of developing TdP (Drew et al., 2010). Since the development of TdP is multi-factorial, patient-specific prediction of a TdP is still a challenge (Schwartz & Woosley, 2016).

Depending on the cause of the TdP, the patient is treated differently. Some examples:

- Drug-induced TdP is often treated with intravenous magnesium which shortens the QT-interval or even the implantation of an artificial pacemaker.
- Congenital TdP, caused by genetic disorders as LQTS, is treated with dedicated drugs which alter the influence of the vagus nerve or the implantation of a cardiac defibrillator.

TdP is a lethal arrhythmia since the ventricles contract very fast without any coordination. Due to these fast contractions, the ventricles are not properly filled causing to decrease the efficiency of the pumping activity of the heart. The longer the duration of the episode of TdP, the more life-threatening it becomes (Hu, Stevenson, & Lilly, 2012).

1.7 Mechanism of Torsade de Pointes

Torsade de Pointes is initiated by an EAD, explained in section 1.5.2. This is commonly accepted in scientific literature, however the perpetuation of TdP is still a subject of controversy.

Different theories are suggested in order to explain the mechanism of TdP. A first theory suggests that the mechanism of TdP is maintained due to focal activity. Other theories are based on re-entrant activity or even a combination of focal activity and re-entrant activity. In the following subsections, the different theories are accentuated by articles based on animal experiments and based on experimental data. It should be stressed that only a few of many articles are accentuated in this master's dissertation.

The study 'Taking the "idio" out of "idiosyncratic": predicting torsades de pointes' by Roden (1998) hypothesized that a reduced repolarization reserve increases the risk of TdP-development. According to the study by Vandersickel et al. (2016) the repolarization reserve plays an important role in the development of either a focal or re-entrant driven TdP episode.

1.7.1 Perpetuation of TdP due to focal activity

Focal activity denotes the mechanism to develop an ectopic beat by an EAD as explained in section 1.5.2. These beats are also called focal beats. Notice that the term ectopic beat is a collective noun for beats caused by focal activity as re-entrant activity.

According to the article 'Drug-induced Torsade de Pointes Arrhythmias in the Chronic AV-Block Dog Are Perpetuated by Focal Activity', written by Boulaksil et al. (2011), the majority of episodes of Torsade de Pointes in chronic AV-block dogs are driven by focal activity. In these animal experiments the researchers examined all the self-terminating episodes with a detailed 3D mapping of all the different beats. It was concluded that the dominant mechanism of perpetuation of TdP is focal activity since the re-entrant mechanism was only sporadically observed (Boulaksil et al., 2011).

Most studies agree with the statement that an episode of TdP maintained by focal activity is more likely in heterogeneous tissue. However, the mechanism of a focal episode of Torsade de Pointes is still unknown. In this section, 2 different theories for the perpetuation of TdP by focal activity are explained. (1) A first theory hypothesizes that the focal activity is caused by shifting focal focuses triggered by a cluster of synchronized EADs (de Lange, Xie, & Qu, 2012). (2) Another theory which states that a focal episode of TdP is maintained by focal beats arising from fixed heterogeneities in the heart tissue (Vandersickel et al., 2016).

The article 'Synchronization of Early Afterdepolarizations and Arrhythmogenesis in Heterogeneous Cardiac Tissue Models' written by de Lange et al. (2012) states that the perpetuation is caused by shifting focal focuses triggered by EAD. The research started by saying that a real heart is not composed out of homogeneous tissue: the proneness of the development of an EAD varies from cell-to-cell. A computer model was based onto a rabbit ventricular myocyte model. Only 2 parameters were varied over the different simulations. (1) A first parameter which varied over different simulations was the strength of the Ca^{2+} flux across the membrane of the cell, represented by the Ca^{2+} conductance $\langle g_{Ca} \rangle$. This parameter was randomly varied over the different cells according to a Gaussian distribution, represented by σ_{gCa}. This variation of the Ca^{2+} conductance represented the heterogeneity of the heart tissue. (2) The second parameter was a parameter to determine the gap junction coupling strength.

From a one-dimensional cable model it was concluded that the higher $\langle g_{Ca} \rangle$ and the higher σ_{gCa}, the higher the probability to develop a focal beat. This was as expected since $\langle g_{Ca} \rangle$ is positively correlated with the development of an EAD. When σ_{gCa} increased, the variation among the cell increased which implies that cell-to-cell fluctuations was increased which led to a higher chance to develop a focal beat. Also the gap junction coupling strength had a significant impact on the probability of developing a focal beat. When the cells were coupled strongly a sink-source effect was seen. This implies a damping phenomenon: cells which do develop an EAD damp out over cells which do not develop an EAD. The higher the coupling strength, the more dominant the source-sink effect is and thus the smaller the probability of developing a focal beat (de Lange et al., 2012).

After the one-dimensional model a two-dimensional tissue model was simulated also. The results for a small $\langle g_{Ca} \rangle$ as large $\langle g_{Ca} \rangle$ were as expected. When $\langle g_{Ca} \rangle$ is small, the majority of the cells do not develop an EAD. The chance of developing a focal beat is thus minimal. When $\langle g_{Ca} \rangle$ is large, the cells are prone to develop an EAD and the probability of the occurrence of a focal beat increases. The source-sink effect is overcome since the majority of cells develop an EAD. An interesting phenomenon was observed at intermediate levels of $\langle g_{Ca} \rangle$, namely different sites of the heart showed a regionally synchronized EAD which propagated through the tissue giving rise to focal beats. This implies that heterogeneity in cell properties promote the formation of EAD. Depending on the spatio-temporal factors of the different sites, the phenomenon could either terminate spontaneously or degrade into re-entrant activity. More details on how this phenomenon establishes and perpetuates remain still unknown (de Lange et al., 2012).

Another theory about how focal activity drives an episode of TdP is given by the article 'Perpetuation of Torsade de Pointes in heterogeneous hearts: competing foci or re-entry?' written by Vandersickel et al. (2016). In this study 2D and whole heart stimulations were based onto a model for a human ventricular cell. Patchy locations of heterogeneities were randomly introduced over the model. A heterogeneity was defined as a location with a reduced repolarization reserve compared to the surrounding tissue. As in the paper written by de Lange et al. (2012), the reduced repolarization reserve was implemented by increasing $\langle g_{Ca} \rangle$. The effect of the dofetilide administration was modelled as reducing and blocking of the repolarizing K^+ current by reducing $\langle g_K \rangle$. Notice that the the whole simulation was characterized by a reduced repolarization reserve and the heterogeneous patches had an even lower repolarization reserve. From the simulations was derived that large heterogeneities are able to perpetuate an episode of TdP purely on focal activity. Different focal beats would arise from the different heterogeneities (Vandersickel et al., 2016).

1.7.2 Perpetuation of TdP due to re-entrant activity

The article 'Electrophysiological Mechanism of Enhanced susceptibility of Hypertrophied Heart to Acquired Torsade de Pointes Arrhythmias', written by Kozhevnikov, Yamamoto, Robotis, Restivo, and El-Sherif (2002), performed also animal experiments onto chronic AV-block dogs. However unlike the article written by Boulaksil et al. (2011), this article stated that the perpetuation of TdP was due to re-entrant excitation. In an episode of TdP a certain pattern was detected: initially a few focal beats arise from subendocardial sites resulting in re-entrant excitation. The initial focal activity had an impact on the dispersion of repolarization which results in a functional conduction block and forms the origin of re-entrant activity (Boulaksil et al., 2011).

Different theories try to explain the typical twisting ECG pattern of TdP caused by re-entrant activity. (1) A first theory given by Schmitt, Cabo, Costeas, Coromilas, and Wit (2001) states that this pattern manifests due to slight drifting and changing re-entrant activity. (2) Another theory by El-Sherif, Chinushi, Caref, and Restivo (1997) describes this pattern due to 'meandering' of the re-entrant activity.

The article 'Mechanisms for Spontaneous Changes in QRS Morphology Sometimes Resembling TdP During Reentrant Ventricular Tachycardia in a Canine Infarct Model' written by Schmitt et al. (2001) states that this twisting phenomenon is caused by a change in exit route of re-entrant activity around a function or anatomical conduction block. This changing of exit route is caused by a slight change in conduction velocity or in location of the re-entrant activity or a combination of both (Schmitt et al., 2001).

According to the article 'Electrophysiological Mechanism of the Characteristic Electrocardiographic Morphology of Torsade de Pointes Tachyarrhythmias in the Long-QT Syndrome' written by El-Sherif et al. (1997), the re-entrant activity is characterized by a heavily varying location and orientation, denoted as the 'meandering' phenomenon of the re-entrant activity (El-Sherif et al., 1997).

1.7.3 Perpetuation of TdP due to a combination of focal and re-entrant activity

Other studies like 'Perpetuation of Torsade de Pointes in Heterogeneous Hearts: Competing foci or Re-entry' written by Vandersickel et al. (2016) state that a combination of focal activity and re-entrant activity is also a possibility for the perpetuation of Torsade de Pointes. Depending on the size of the heterogeneity and the decrease in repolarization reserve, either focal activity or re-entrant activity occurs. Another hypothesis stated by the article is that the different locations of focal activity can interact and degrade into re-entrant activity (Vandersickel et al., 2016).

The article 'Short-Lasting Episodes of Torsade de Pointes in the Chronic Atrioventricular Block Dog Model Have a Focal Mechanism, While Longer-Lasting Episodes Are Maintained by Re-Entry' written by Vandersickel et al. (2017) compared the episodes of TdP based on the perpetuation and concluded that there is a correlation with the duration of the episode of TdP. Longer episodes are more often perpetuated by re-entrant activity, especially the non-self-terminating episodes of TdP, episodes driven by focal activity are generally shorter (Vandersickel et al., 2017).

1.7.4 Important Considerations

In the article by Vandersickel et al. (2017) an important aspect of the perpetuation debate is considered, namely the different definitions of TdP used in scientific literature. It is commonly accepted that TdP is characterized by this typical twisting pattern of the ECG. But what if an episode is too short to show this ECG pattern, can it be concluded that the arrhythmia is not TdP? Where to draw the line between TdP and Polyventricular Tachycardia (Vandersickel et al., 2017)?

Another important question to be asked is whether how the data is collected over different experiments influences the appearance of TdP. Different animal models as well as different drugs were used to induce the arrhythmia. Questions should be asked as: What is the best animal model? Is there a difference between the drugs to induce the arrhythmia? Which episodes to incorporate in the analysis, self-terminating or not (Vandersickel et al., 2017)?

From these considerations it is concluded that there is a need to have one clear definition which characterizes TdP. However, is this possible? A good definition would be a great support to the research in order to fully understand the mechanism of TdP.

Chapter 2

Background of the Experiment

The data used for this master's dissertation is obtained via experiments with dogs as animal model. In the following sections, an introduction is given to the usage of a dog as animal model and the set-up of the experiment.

2.1 Dog as Animal Model

The goal of a study on an animal model is to gain a better understanding of the processes and mechanisms in the human body. To enable this, the physiological processes, functionality and anatomy of the animal model must be closely related to the human processes. Experiments on animal models aim to improve clinical therapies and interventions (Dixon & Spinale, 2009).

A lot of animal experiments, often for molecular and cellular processes, use small animal models, such as mice, rats and rabbits. When the cardiac function is considered, significant differences are noticed between rodent animals and humans. The main differences are heart rate, oxygen consumption, the influence of the vagus nerve and response to loss of regulatory proteins. Also the phenomenon of excitation-contraction coupling in rodent animals differs significantly from the human contraction process (Dixon & Spinale, 2009). Thereby, it is concluded that rodent animals are not the best animal model to study human cardiac dysfunctions.

Larger animal models are better for understanding of cardiac dysfunction since their physiology, functionality and anatomy are closely related to humans. The usage of animal models enable to study the ventricular function and volume more accurate compared. Large animal models are based upon pigs, dogs, sheep, cats...

In this master's dissertation the cardiac data of dogs is collected. Dogs are frequently used as cardiac animal model. The canine myocardium is similar to the human myocardium due to their comparable β-myosin heavy-chain dominance and excitation-contraction coupling process (Colucci, 2008). Disadvantages of dogs as animal models are their high cost, housing requirements and ethical objections (Hasenfuss, 1998).

2.2 Set-up of the Experiment

For this master's dissertation, no animal experiment is performed. However, data of previous animal experiments were received from Utrecht University. The data were used for different studies such as the study 'Torsade de pointes arrhythmias arise at the site of maximal heterogeneity of repolarization in the chronic complete atrioventricular block dog' by Dunnink et al. (2017). This section is based on method-section of the mentioned article.

For the experiment 5 adult purpose-bred mongrel dogs were used. Before the actual mapping experiment took place, the dogs underwent a surgical intervention to ablate the atrioventricular (AV)-node. Via radio-frequency ablation the electrical conduction from the sinoatrial (SA)-node towards the ventricles is inhibited. In order to keep the dog alive, a pacemaker was placed during the intervention. The pacemaker lead was located near the endocardium of the right ventricular apex (Dunnink et al., 2017). After this intervention, the dog is called a chronic atrioventricular block (CAVB) dog. Due to this intervention, the ventricles remodel and become more prone to the development of Torsade de Pointes (TdP) (Dunnink, 2016).

After the canine heart remodelling, differences are seen in heart rate (HR), cardiac output (CO), maximal rise in left ventricular pressure (LV dP/dt), corrected QT (QTc), ratio heart weight/body weight (HW/BW) and the rate of dofetilide-inducted TdP arrythmia inducibility. These changes are induced due to neurohumoral activation, structural and electrical remodelling. This electrical remodelling is characterized by decreased potassium currents and altered functioning of the calcium channels. Notice that this electrical remodelling decreases the repolarization reserve. An overview of these changes is shown in figure 2.1. Images of the canine heart before and after the remodelling is shown in figure 2.2 (Dunnink et al., 2017).

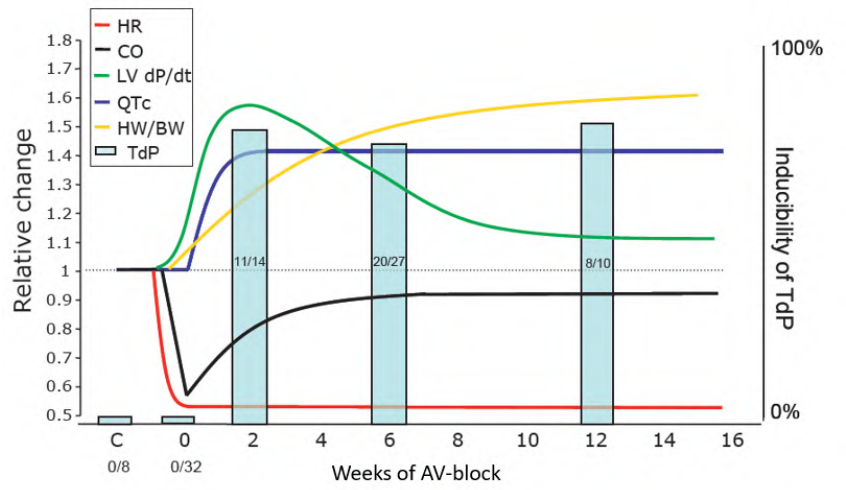

Figure 2.1: An overview of changes over weeks in the canine heart after an AV-block intervention. Figure adapted from Dunnink (2016).

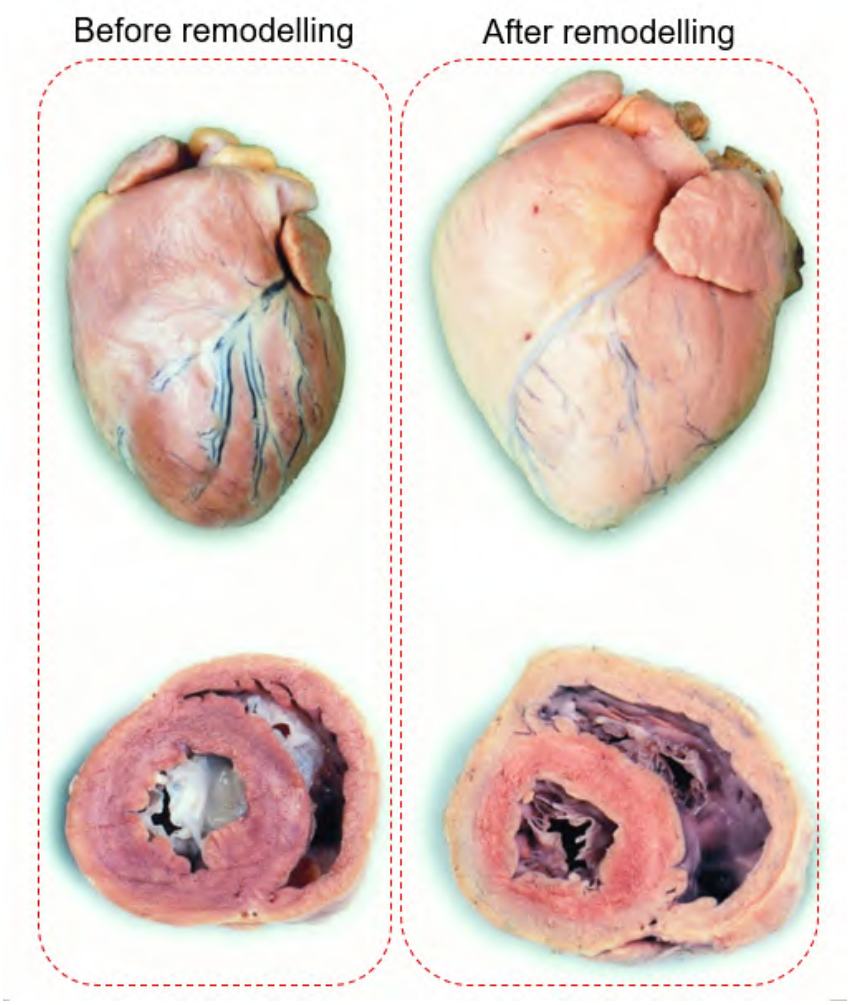

Figure 2.2: A visualization of the changes due to remodelling over weeks in the canine heart after an AV-block intervention. Figure adapted from Vos et al. (1998).

After 100 days, the mapping experiment was performed. In order to open the chest and to gain optimal access to the canine heart, a left-sided thoracotomy was performed and a partial resection of the 4th rib. The data of the mapping experiment was gathered via unipolar electrogram (UEG). In total 56 needle electrodes were inserted in the canine heart, whereby 48 needles in the ventricular myocardium and 8 in the septal wall. Each needle contained 4 electrode terminals, also called channels, with an inter-electrode distance of 4mm. Thus in total 224 electrode signals are recorded. The orientation of the needles in the ventricular myocardium are perpendicular compared to the ventricular wall. Unfortunately the orientation of the needles in the septal wall was not consistent. These needles were positioned carefully over 6 planes from base to apex, 5 evenly distributed needles in each plane in the left ventricle and 3 in the right ventricle. An overview of the different needle positions is given in figure 2.3 (Dunnink et al., 2017).

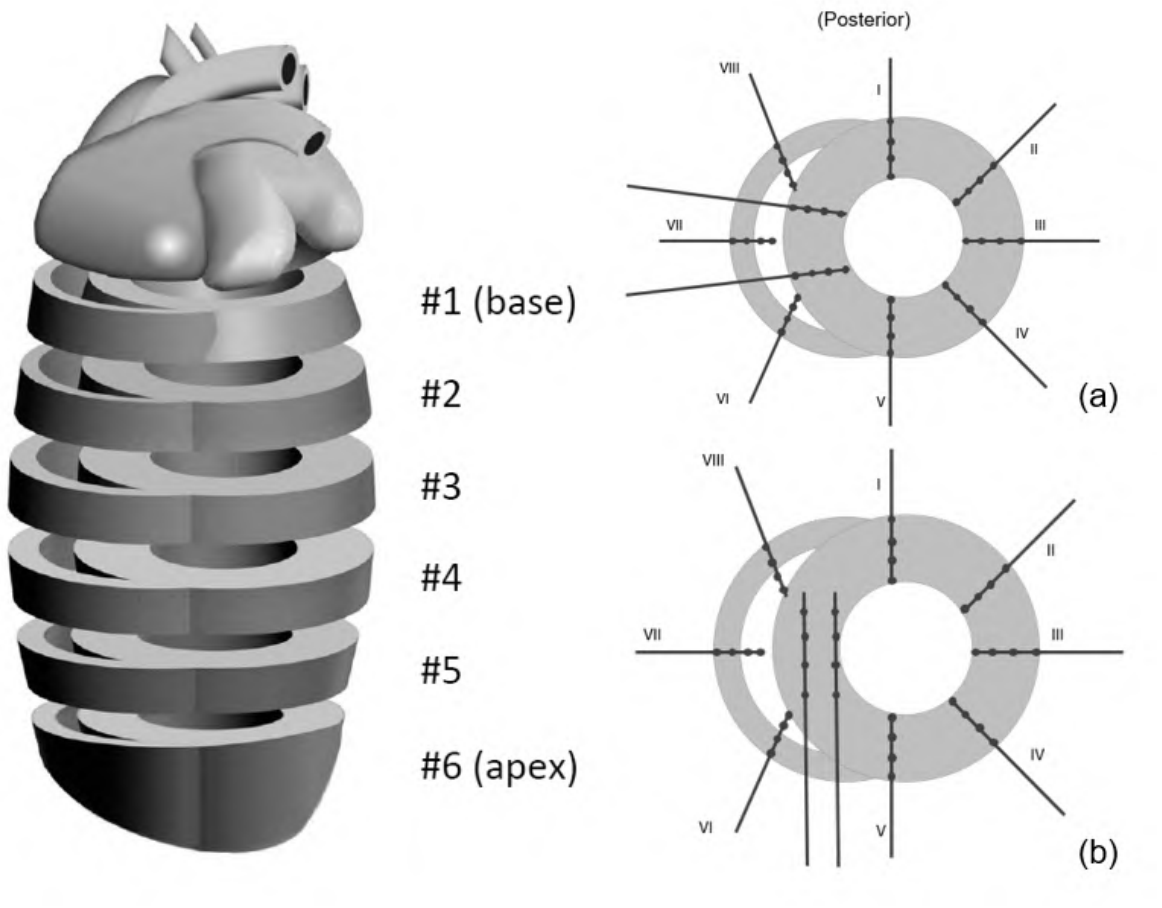

Figure 2.3: An overview of the different needle positions whereby the needles I-V (from posterior to anterior) are positioned in the left ventricle and needles VI-VII (from anterior to posterior) in the right ventricle. The different vertical slices of the heart is represented by the symbol '#' followed by the slice number. Figure adapted from Dunnink et al. (2017). Subfigures (a) and (b) denote the difference in orientation of the septal needles.

The dogs were paced at 1000 to 1500ms depending on the intrinsic activity of the ventricles. During the experiment, 2 different situations were recorded namely at baseline and during administration of dofetilide. Both situations were measured over a time period of around 10 minutes. The dosage of dofetilide depending on the weight of the dog, namely 0.025mg/kg/5min, was used to induce TdP. The administration of dofetilide was stopped after the occurrence of TdP or after 5 minutes when no had occurred. In case of a non-terminating episode of TdP, the canine heart was defibrillated. Also an electrocardiogram (ECG) was recorded during the experiment along with the signals of the needle electrodes (Dunnink et al., 2017).

In this experiment the data of 5 dogs were gathered, represented in table 2.1. All these dogs were defined as 'inducible' dogs which implies that at least 3 episodes of TdP occurred and/or one or more non-terminating episodes of TdP were observed after administration of dofetilide (Wijers et al., 2017).

Table 2.1: Overview of the different dogs

Dog number	Characteristic
901016	paced
928607	paced
938017	paced
959367	paced
963356	paced

2.3 Ethical Approval

These experiments happened with consent of the Committee for Experiments on Animals of Utrecht University which is in agreement with the European Directive for the Protection of Vertebrate Animals used for Experimental and Other Scientific Purposes (86/609/CEE) and the Dutch Law on animal experimentation.

2.4 Characteristics of the local unipolar electrogram data

The sampling frequency of the UEG recording was 2048 Hz. This implies 2048 data points are recorded within 1 second. The unipolar electrograms were recorded via the ActiveTwo system by Biosemi (Amsterdam, Netherlands) (Dunnink et al., 2017).

A UEG signal is represented in figure 2.4. Since the unipolar electrogram measures activity of a local patch of cells, the same concepts are used as in the ECG, namely QRS-complex and T-wave. Notice that no P-wave is seen due to the AV-block. Since the dogs are paced, a pacing spike is seen to initiate the beat. All these concepts are annotated on figure 2.4.

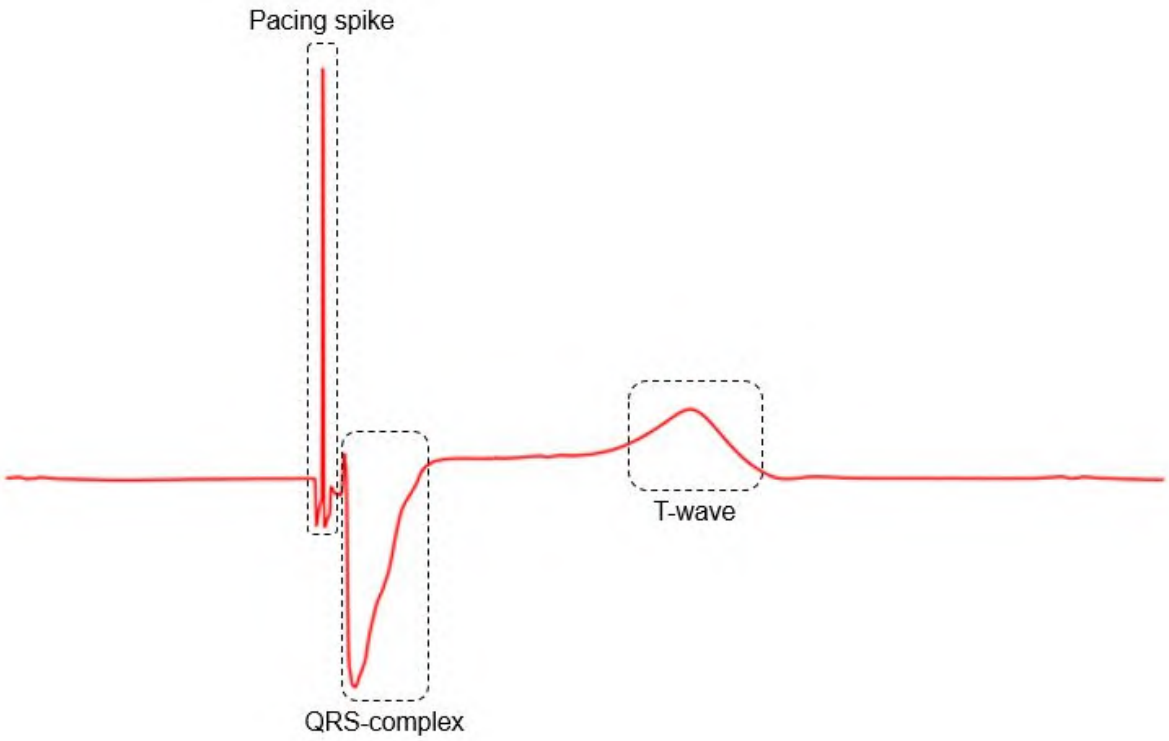

Figure 2.4: A representation of a UEG signal with annotations of the pacing spike, the QRS-complex and T-wave.

Chapter 3

Methods for quantification and representation

In this chapter, the different quantification measures and representations of an episode of Torsade de Pointes (TdP) are introduced. Also the representation of the data is explained to facilitate the interpretation of figures in the continuation of this master's dissertation.

3.1 Quantification measures

3.1.1 Definition of Torsade de Pointes

Locati, Maison-Blanche, Dejode, Cauchemez, and Coumel (1995) defined Torsade de Pointes as a ventricular arrhythmia with 5 or more consecutive beats showing a typical twisting configuration. The length of 5 consecutive beats was the minimal length in order to recognize the typical TdP-pattern (Locati et al., 1995).

This definition of TdP is now generally used in research concerning TdP. As mentioned in section 1.7.4 this definition should be used carefully since it is arbitrary.

3.1.2 Activation-recovery interval

The activation repolarization interval (ARI) is used to approach the value of the refractory period by Haws and Lux (1990). This implies that the ARI is related to the duration of the action potential duration (APD) on that specific location. The ARI is calculated based on the signal of the unipolar electrogram (UEG) as the time difference between the local time of excitation and local time of repolarization. The local time of excitation is the time of the most rapid decrease in

the QRS-complex which corresponds with the maximal negative derivative of the UEG signal (dV/dt min). In a similar way the local time of repolarization is calculated, namely the maximal positive derivative near the peak of the T-wave (dV/dt max). This method is called the 'Wyatt method' for ARI determination (Haws & Lux, 1990).

The Wyatt method for ARI determination evokes controversy when a positive T-wave morphology is considered. Chen et al. (1991) introduced an 'alternative method' for the ARI determination. In this method the maximal negative derivative of the positive T-wave was considered to obtain a more accurate value of the ARI. In the case of a negative or biphasic T-wave morphology, the maximal positive derivative of the T-wave remained a marker for the end of the ARI (Chen et al., 1991). It is believed that the ARI calculated with the Wyatt method and the alternative method have a subtle difference in its APD correlation. Approximately the ARI determined via the Wyatt method corresponds with APD_{50}, which is the time from the beginning of the action potential to the time 50% repolarization is reached, while the ARI calculated via the alternative method corresponds with APD_{90}. Since the Wyatt method is defined upon a stronger scientific reasoning, the Wyatt method is the most common preferred method for ARI determination (Western et al., 2014). An overview of these concepts are given in figure 3.1.

In 2006 a study written by Coronel et al. (2006) tried to verify the Wyatt method. It was stated that in both, negative as positive T-wave morphologies, the maximal positive derivative is the best marker for local repolarization (Coronel et al., 2006).

The ARI is an important parameter for the occurrence of TdP. As mentioned in section 1.7, an episode of TdP is often preceded by a prolongation of the QT-interval. This would imply that the ARI increases as well.

The T-wave has different morphologies, namely a positive, negative or a biphasic morphology. In the figures 3.2, 3.3 & 3.4 the different T-wave morphologies in a UEG signal are represented over the duration of 1 ventricular contraction over the same time period of the same dog.

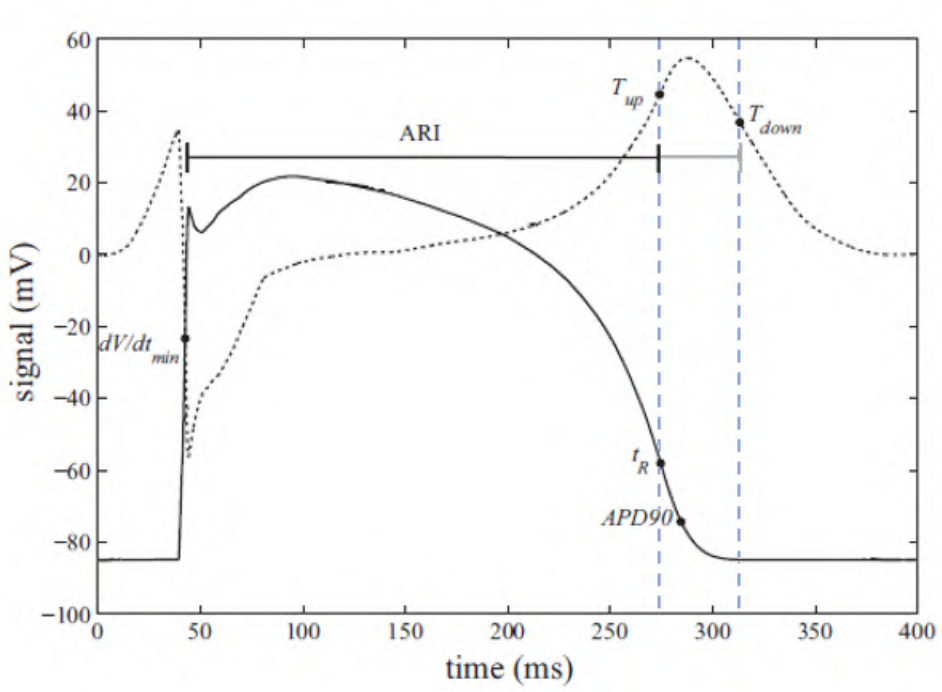

Figure 3.1: A signal of a UEG with a positive T-wave morphology and a ventricular action potential respectively represented in a dotted and solid line over time. Different points are represented with a black dot, namely dV/dt max, T_{up} and T_{down} which represent respectively the maximal positive and negative derivative of the T-wave, t_r which corresponds to the local time of excitation, the repolarization time (calculated as the maximal negative derivation of the action potential during the repolarization) and the point APD_{90}. Figure adapted from Western et al. (2014).

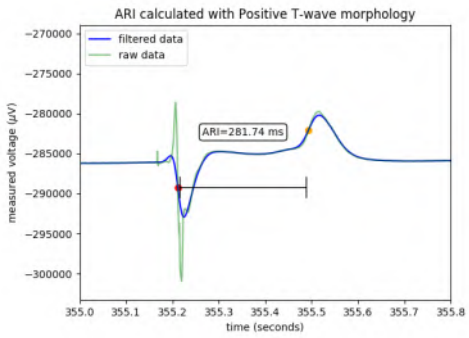

Figure 3.2: Electrode signal of 1 ventricular contraction with a positive T-wave morphology of channel 219 of dog 959367 during time 355-355.8 s. The duration of the ARI is annotated by the horizontal line. The ARI-value is shown in the box.

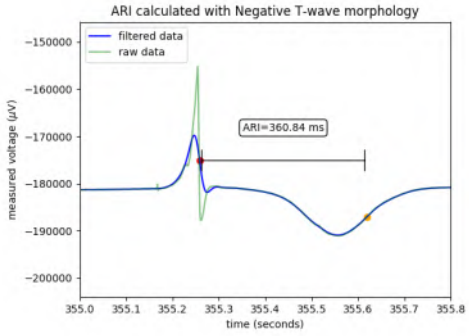

Figure 3.3: Electrode signal of 1 ventricular contraction with a negative T-wave morphology of channel 34 of dog 959367 during time 355-355.8 s. The duration of the ARI is annotated by the horizontal line. The ARI-value is shown in the box.

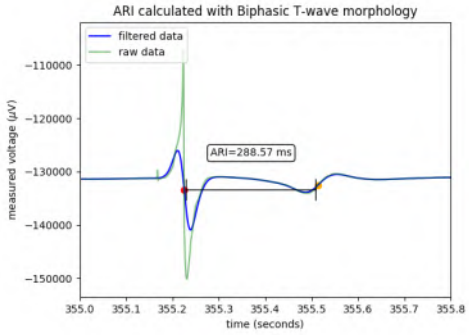

Figure 3.4: Electrode signal of 1 ventricular contraction with a biphasic T-wave morphology of channel 247 of dog 959367 during time 355-355.8 s. The duration of the ARI is annotated by the horizontal line. The ARI-value is shown in the box.

3.1.3 Short-term variability

In order to quantify the beat-to-beat variation of intervals between heartbeat, Brennan, Palaniswami, and Kamen (2001) introduced a quantification for the heart rate variability. This concept of variability, called short-term variability (STV), was then generalised to different intervals such as APD, ARI and QT-interval by Thomsen et al. (2004). The STV represents the mean orthogonal distance from the diagonal to the points of the poincaré plot. The value of the STV is thus a measure for the variability of the ARI.

$$STV = \frac{\sum_1^N |D_{n+1} - D_n|}{(N-1) \times \sqrt{2}},$$

where $N =$ number of beats taken into account,

$D =$ duration of the considered interval

The time period to calculate the STV in must contain minimal 31 consecutive beats (N $\leq$ 31) before the first offset of an ectopic beat (Wijers, Ritsema van Eck, Doevendans, Meine, & Vos, n.d.).

From intracardiac electrogram (EGM) data, it was derived that the STV of the ARI increases before the offset of TdP in either awake or anaesthetized conditions. A similar conclusion was drawn for monophasic action potential (MAP) data, namely the STV of mean action potential duration increased before the occurence of TdP concluded by Wijers et al. (2017). This increase of STV in right and left ventricle is similar unlike other parameters as the APD (Wijers et al., 2017).

3.2 Methods of representation

3.2.1 Electrode map

In this master's dissertation, the representation of the different needles is not represented as in figure 2.3 of chapter 2. An overview of the different needles and its electrodes are depicted in an electrode map. In order to facilitate the interpretation of the electrode map, shown on figure 3.5, the same description of the slice number, needle number and needle orientation are used as in figure 2.3. Electrode maps are used to present the results in a quick and easy way.

Each used electrode terminal, also called channel, is labelled by number. The electrode location varies from dog to dog. This is also seen in the figures A.1, A.2, A.3, A.4 & A.5, added in appendix A. The amount of channels per needle in the right ventricle is smaller compared to the amount of channels in the left ventricle. This is due to the difference in wall thickness,

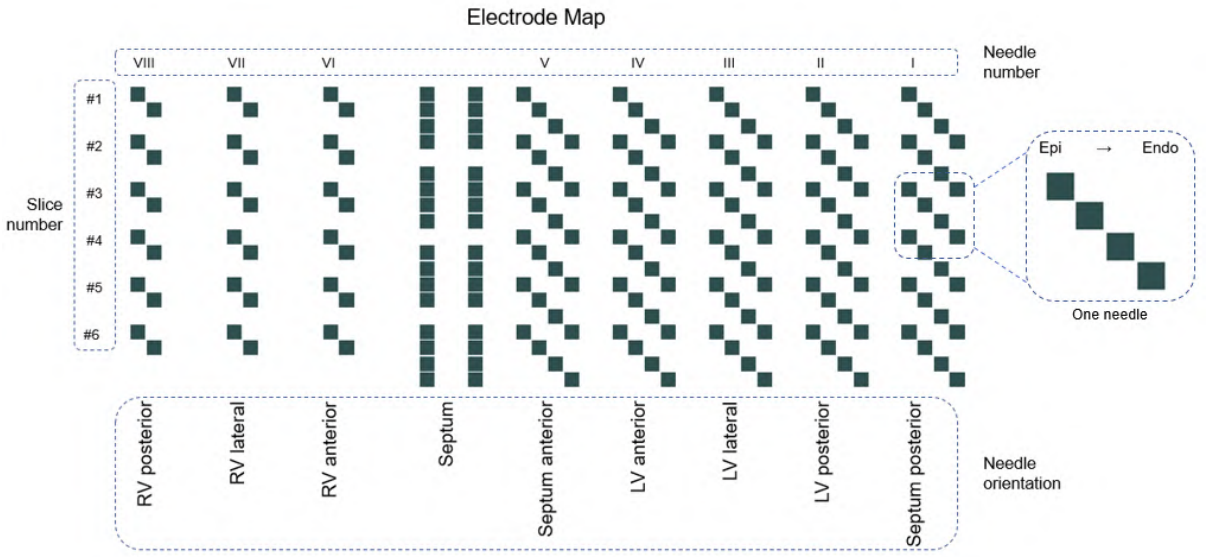

Figure 3.5: An electrode map with description of the slice number, needle number and needle orientation.

as mentioned in section 1.1.2. The thicker the wall, the more channels register a good signal. The amount of channels also varies over the different dogs. The smallest amount of channels is seen in dog 938017 (figure A.3) while in dog 928607 a larger amount of channels is seen (figure A.2). In dog 901016, the different orientation of the needles in the septum is seen in the electrode map (figure A.1) which is explained in section 2.2.

3.2.2 Poincaré plots

According to Brennan et al. (2001), poincaré plots are a valuable tool to display the non-linear characteristic of interval sequences. In this plot each duration of an interval, such as ARI, is plotted against the following interval. This way the correlation between sequential intervals and thus the beat-to-beat behaviour is easily derived from the plot.

It is stated in the study of Brennan et al. (2001) that the poincaré plots are useful for the heart-rate variability. This variability typically appears as an elongated cloud of points along the line-of-identity. In these plots the interval between 2 R-waves, called the RR interval, was used. The short-term variability is derived from the dispersion of points perpendicular to the line-of-identity (Brennan et al., 2001). The same is expected when the ARI is considered in stead of the RR interval. This method to visualize the STV was applied in the study of Thomsen et al. (2004). A graphical representation is shown in figure 3.6.

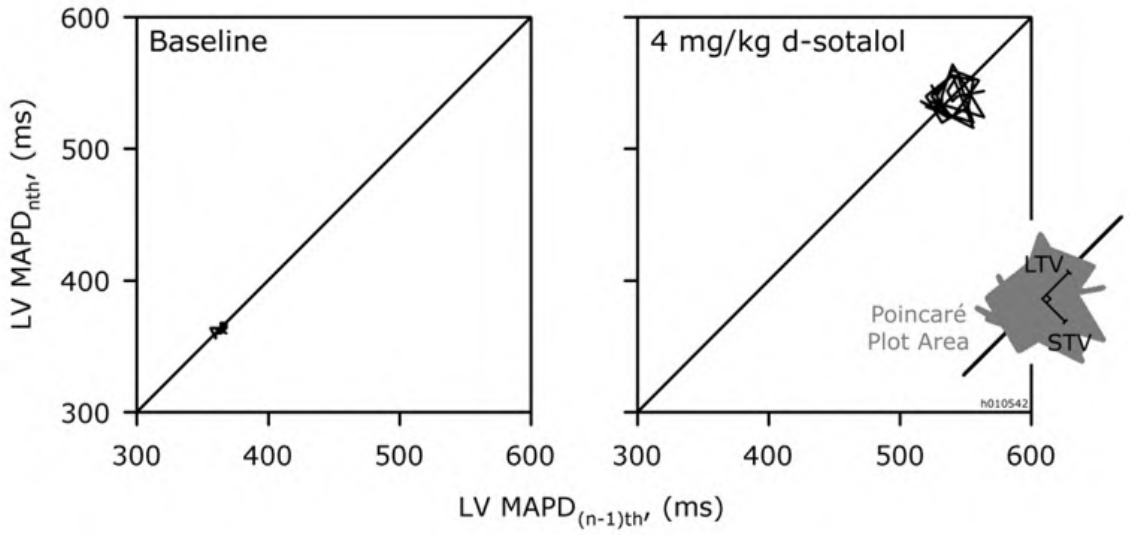

Figure 3.6: Different poincaré plots showing the plot at respectively baseline and administration of a drug, d-sotadol which induces the occurence of TdP. Notice that not the STV of the ARI is calculated but the STV of the mean APD (MAPD). Figure adapted from Thomsen et al. (2004).

Chapter 4

Clinical purpose

This research focusses on 2 parts, namely (1) whether short-term variability (STV) of the activation repolarization interval (ARI) is a good biomarker in unipolar electrogram (UEG) for the prediction of Torsade de Pointes (TdP) and (2) whether the origins of the focal beats in an episode of TdP are homogeneously or heterogeneously distributed over the heart.

From previous articles a trend is seen in intracardiac electrogram (EGM) and monophasic action potential (MAP) data: the STV increases just before the offset of the ectopic beat. A first question is whether the same trend is visible in the UEG data obtained via needles. If this trend would be visible, it would be interesting to see whether this STV increase is locally dependent or not. This outcome would be of clinical importance since it determines the optimal placement of the implantable cardiac defibrillator (ICD) electrode. In case of a homogeneous increase in STV, the location of the ICD electrode is not of importance. While when this STV increase is heterogeneous, the optimal location of the ICD electrode is of course the location where the increase is more prominent. The optimal position of the electrode would allow a faster detection of a coming episode of Torsade de Pointes and thus a faster application of the shock which might even increase the survival rate.

The theories of TdP perpetuation by focal activity have never been experimentally verified, the obtained UEG data allows to give more insight in the focal mechanism of TdP. The second part of the research focussed on which theory is more likely via determining the origin of every ectopic beat. If there are preferable locations for the focal activity, it might be of clinical relevance. It could give medical staff more insight in the arrhythmia and whether ablation of these preferable origins would be useful or not. Notice that this would only be applicable if a patient would be having only episodes of Torsade de Pointes perpetuated by focal activity.

In case there are preferable locations to start the episode of TdP and the STV increase is heterogeneously distributed over the heart, it would be interesting to investigate the correlation between both. Are the preferable origins characterised by an elevated STV increase or not?

Chapter 5

STV as Biomarker

This chapter focuses on the first research question, namely is the short-term variability (STV) of the activation repolarization interval (ARI) a useful biomarker for Torsade de Pointes (TdP) in unipolar electrogram (UEG) data? As mentioned in section 3.1.3, the STV of the ARI increases right before the offset of TdP measured via intracardiac electrogram (EGM) and monophasic action potential (MAP) data (Wijers et al., 2017). In this research the question is whether the same trend occurs in the data of the UEG and whether this increase occurs heterogeneously or homogeneously over the heart. In the continuation of this master's dissertation, the notation of STV of the ARI is shortened to just STV.

5.1 Hypothesis

The STV is a good biomarker for the prediction of TdP in UEG data. This implies that the STV increases just before the offset of the first ectopic beat. This increase is heterogeneously distributed in the heart with an elevated STV increase near the origin of the ectopic beat.

5.2 Method

Figure 5.1: Work flow of the project 'STV as Biomarker'.

5.2.1 Determination of time period for the STV calculation

In order to calculate the STV, different time periods of 31 consecutive beats were selected. It was important to select a timespan with no ectopic or escape beats. The determined time periods for every dog are depicted in table 5.1.

Table 5.1: Overview of the selected time periods to determine the STV in

Dog Number	Times [baseline] (s)	Times [dofetilide administration] (s)}
901016	578.25-620	17.5-59.6
928607	699-731.6	123.2-154.65
959367	163-40-194.90	69.74-101.5
963356	635-666.1	38.39-70.39
938017	249.341-297.7	288.6-335

Notice that the time period for the baseline recording was taken at the end of the recording to avoid influence of abnormal activity due to the insertion of the needles. For the recording during dofetilide administration, this time period was taken in the beginning of the recording just before the first ectopic beat.

Remark that it was not always possible to find a time period of 31 beats without ectopic activity at the end of the baseline recording or before the first beat. In those cases an earlier or later time period was selected.

5.2.2 Determination of local time of excitation and local time of repolarization

In order to calculate the ARI for every beat, the local time of excitation and local time of repolarization must be determined as described in section 3.1.2.

The local time of excitation was determined via deriving of the filtered signal. Filtering smooths the signal and removes noise. Often this filtering step removes the pacing spike as well, shown in figure 5.2. All the relative negative maxima of this derivative were identified. These maxima, shown on figure 5.3, had to fulfil 2 criteria to be considered as the derivative of such a 'local time of excitation': (1) the derivative had to be smaller than a certain threshold. This step ensured that no noise was selected as local time of excitation. The value of the threshold was determined via visual inspection of the data aiming towards a value which discriminates noise from subtle peaks. (2) The second criteria stated that the interval between 2 following local times of excitation had to be at least 1 second. Via the index of such a relative negative maximum of the derivative, the local time of excitation was determined on the filtered signal.

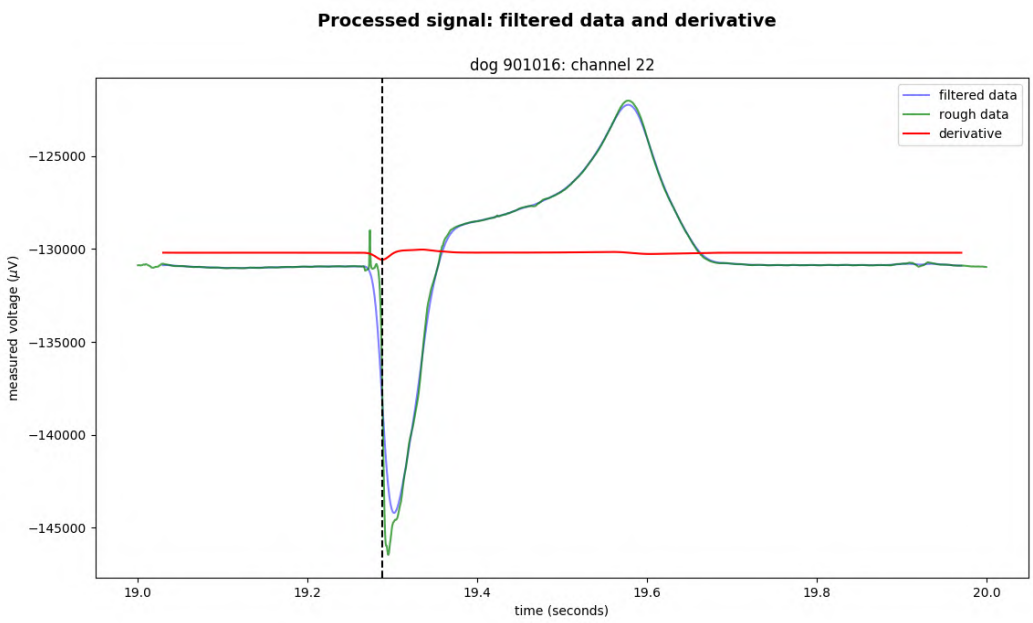

Figure 5.2: The first processing step of the signal, namely filtering and taking the derivative of this filtered signal. In this figure the rough data, filtered data and the derivative are shown respectively by the green, blue and red line. The vertical dashed line represents the time when the derivative is minimal. Notice that the filtering step removes noise as the pacing spike and this way the spike has no impact on the derivative.

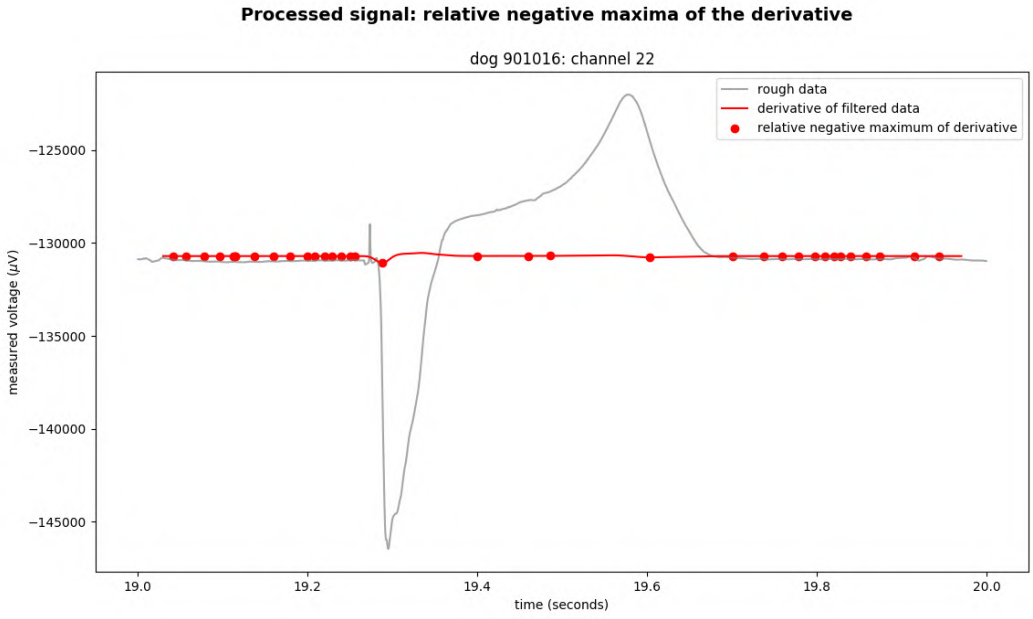

Figure 5.3: A visualisation of all the relative negative maxima on the derivative of the filtered data. The rough data is represented by the grey line. The derivative of the filtered signal and the relative negative maxima of the derivative are shown respectively by the red line and red dots.

The next step was to translate the found local time of excitation on the filtered data towards the rough data. This was done in a limited window around each previously determined local time of excitation. An important step, since the local time of excitation on the rough data slightly differs from the local time of excitation on the filtered data. This small difference is represented in figure 5.4.

Notice that the translation from the derivative towards the filtered data and the filtered data towards the rough data was based onto the index and did not make use of interpolation between 2 data points. This could result in an error of maximal $0.5/2048$ second determined by the sampling speed of the recording. This is represented in figure 5.5.

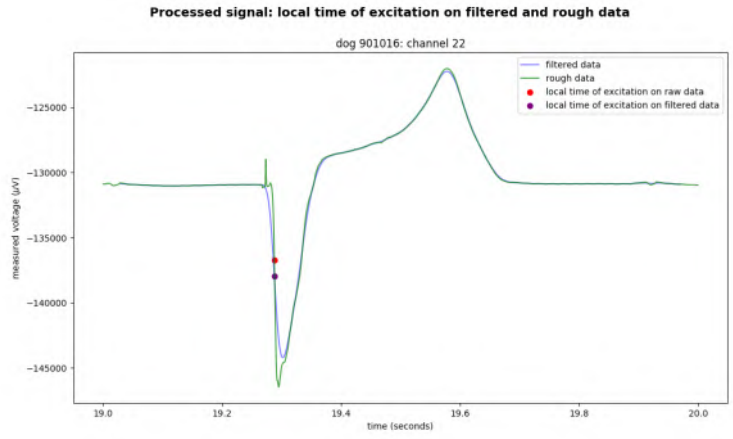

(a) General view of the local time of excitation

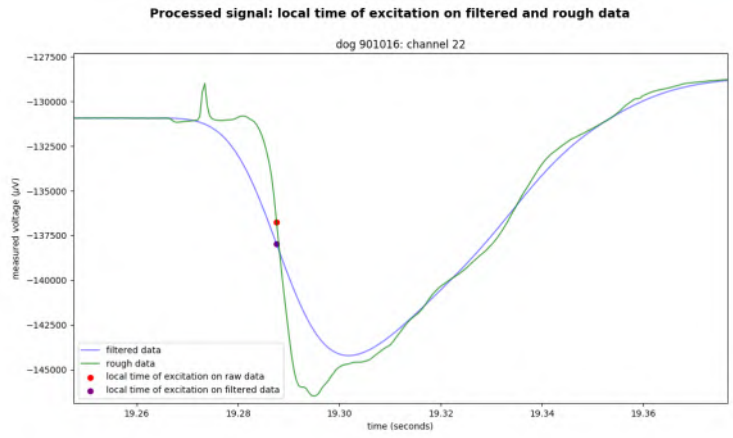

(b) Detailed view of the local time of excitation

Figure 5.4: Determination of the local time of excitation on the rough data as well as on the filtered data. Notice that the location is slightly different. The filtered data and the rough data are shown by the blue and green line. The local time of excitation on the filtered data is shown by the purple dot while the local time of excitation on the rough data is represented by a red dot.

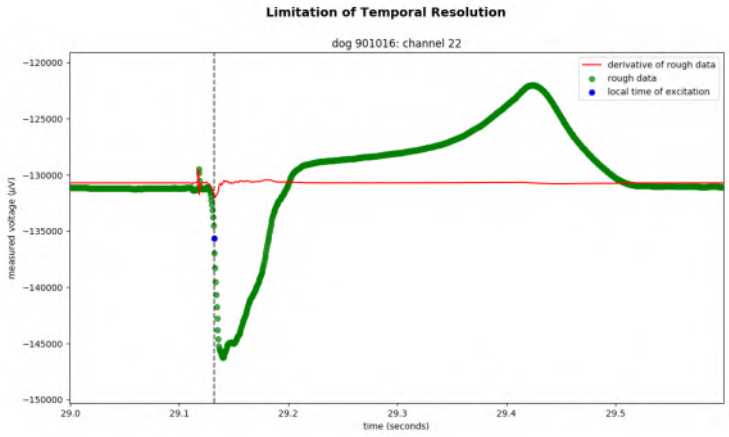

(a) General view of the local time of excitation

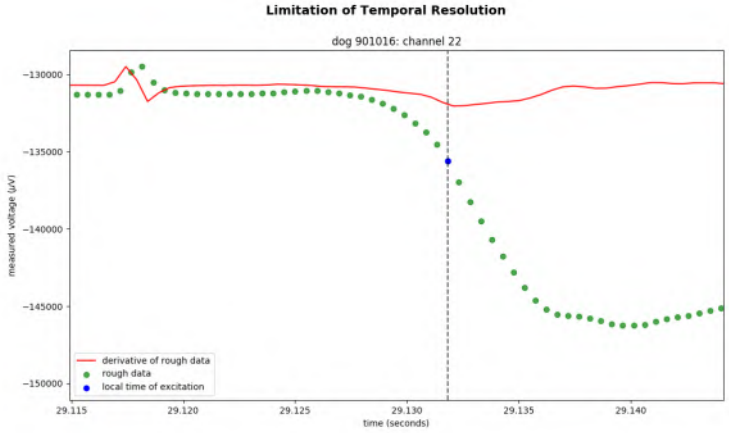

(b) Detailed view of the local time of excitation

Figure 5.5: The derivative of the rough data is shown by the red line. The green dots represent the outcome of the recording. Notice the time between 2 points is constant, namely $1/2048$ second. Due to this limitation in sampling speed, the determination of the local time of excitation could be influenced.

The local time of repolarization was determined based on the findings for the local time of excitation. For every local time of excitation, the maximal positive derivative was determined in a window after the considered local time of excitation. This was done on the filtered data thus the findings had to be translated to the rough data. In figure 5.6 the local time of excitation as well as the local time of repolarization are indicated.

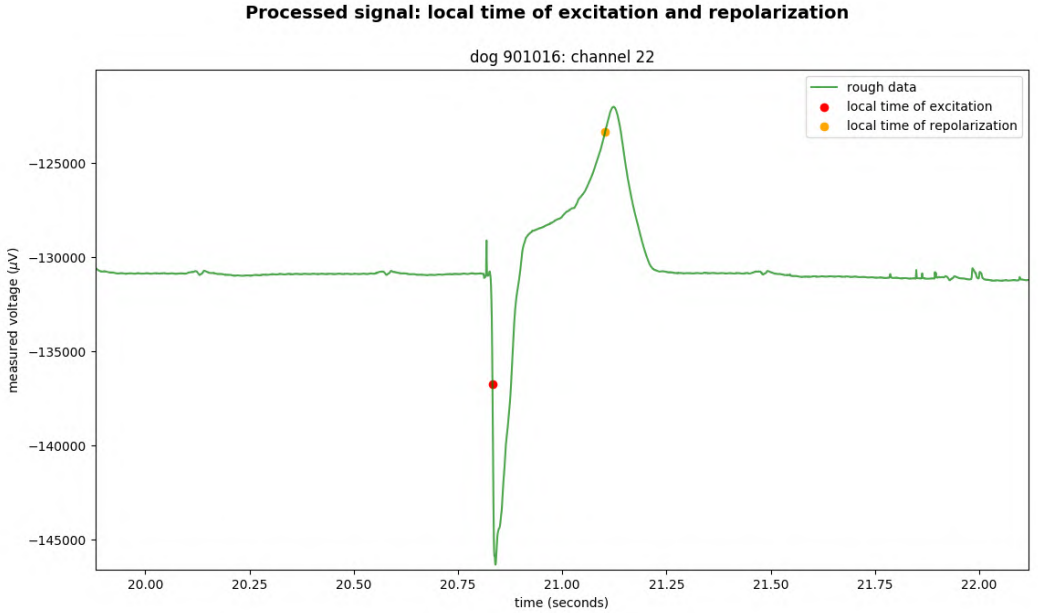

Figure 5.6: A visualisation of the local time of excitation and local time of repolarization determined on the rough data. The rough data is represented by the green line. The local time of excitation and local time of repolarization are represented by respectively the red and yellow dot.

When this algorithm was applied to all different channels of all the different dogs it was seen that in case of a distinct pacing spike, the local time of excitation was determined incorrectly. This is as expected since in those cases the pacing spike was not filtered away and had thus a significant impact on the derivative. This situation is represented in figure 5.7.

In case of distinct pacing, the algorithm for the determination of the local time of excitation was adapted. This was done via identifying the spike based on 2 criteria. (1) A first criteria was again based on a threshold for the maximal negative derivative. The threshold had a larger value since the distinct pacing spike is characterized by a very steep signal. (2) The second criteria verified whether in a window after this spike another steep slope was seen which corresponded to the QRS-complex. When a spike was identified, the local time of excitation was determined on the second steep slope. The result of this algorithm is represented in figure 5.8.

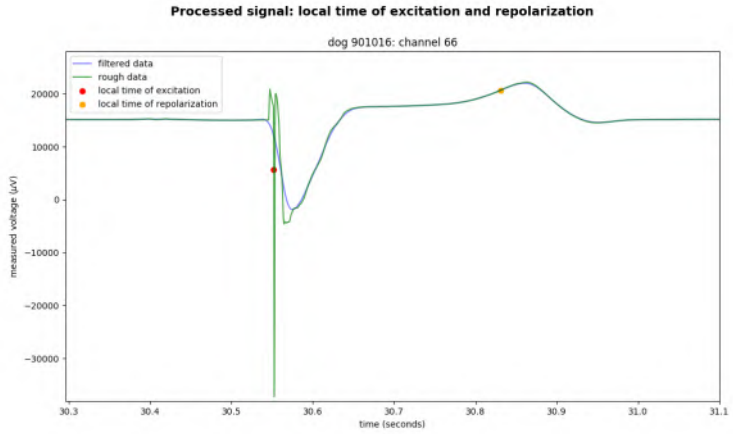

(a) General view of the local time of excitation

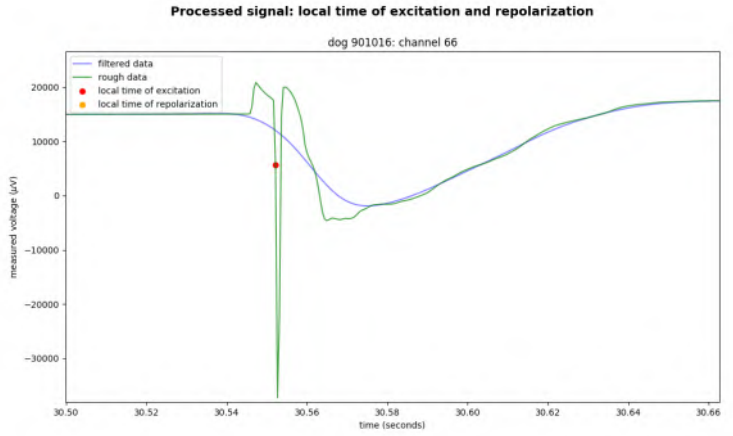

(b) Detailed view of the local time of excitation

Figure 5.7: Determination of the local time of excitation in case of a distinct pacing spike. Notice that the determination of this local time of excitation is incorrect since it is positioned onto the pacing spike.The filtered data and the rough data are represented by respectively the blue and green line. The local time of excitation and local time of repolarization are represented by respectively the red and yellow dot.

Unfortunately due to a large variability of signals, this method was not able to be generalized over all the channels of all the different dogs. The main problem was seen with signals containing a large, steep negative peak which was not the pacing spike. In these cases the algorithm misidentified a pacing spike causing a misplacement of the local time of excitation. An example of such an incorrect determination of the local time of excitation is represented in figure 5.9. Notice that this is due to a change in steepness of the QRS-complex.

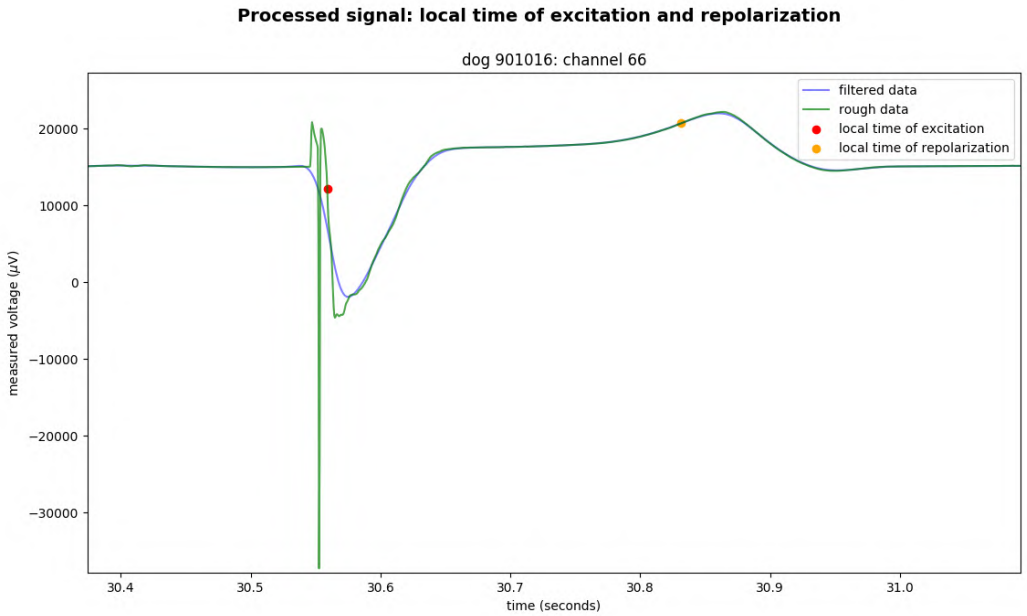

Figure 5.8: The determination of the local time of excitation in case of a distinct pacing spike using the extended algorithms. The filtered data and the rough data are represented by respectively the blue and green line. The local time of excitation and local time of repolarization are represented by respectively the red and yellow dot.

In order to avoid a parameter overload in the input of the different functions, standard parameters which remained constant over the whole analysis were introduced at the beginning of each function. The functions 'find_ max_ neg_ derivative' and 'find_ max_ pos_ derivative' determine respectively the local time of excitation and local time of repolarization. The algorithms are attached in appendix B.

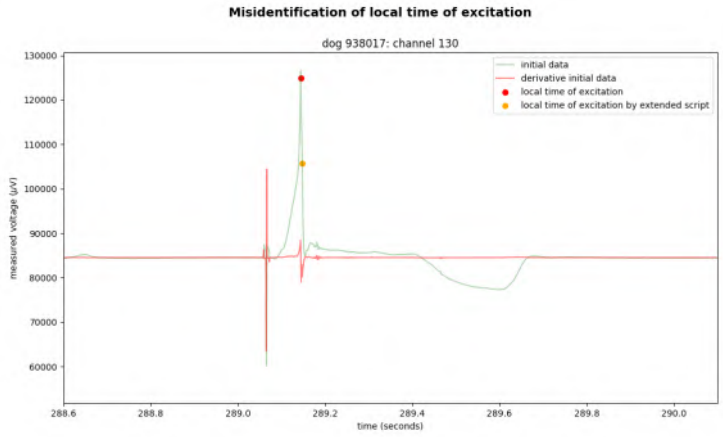

(a) General view of the local time of excitation

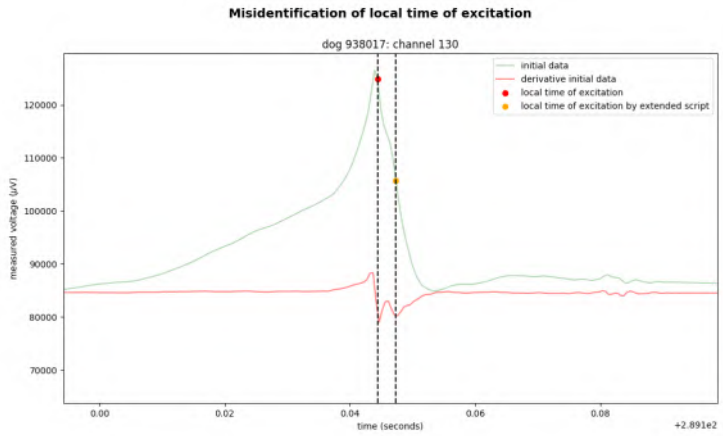

(b) Detailed view of the local time of excitation

Figure 5.9: Determination of the local time of excitation in case of a large peak causing a misplacement. The rough data is represented by respectively the green line. The local time of excitation determined by the initial algorithm is shown with the red dot. The yellow dot represents the local time of excitation found by the extended algorithm.

5.2.3 Semi-automated inspection

Since biological data is used, a high variability between the UEG signals is seen. This variability is made clear in figure 5.10 where different UEG signals are depicted over the same time period of one dog. Due to this high variability in the signals, writing an algorithm which works for all the signals is challenging. The written algorithms for this research purpose perform well however not perfect. Therefore all the determined local times of excitation and local times of repolarization had to be visually inspected and corrected if necessary. To ease this process, a graphical user interface (GUI) was written.

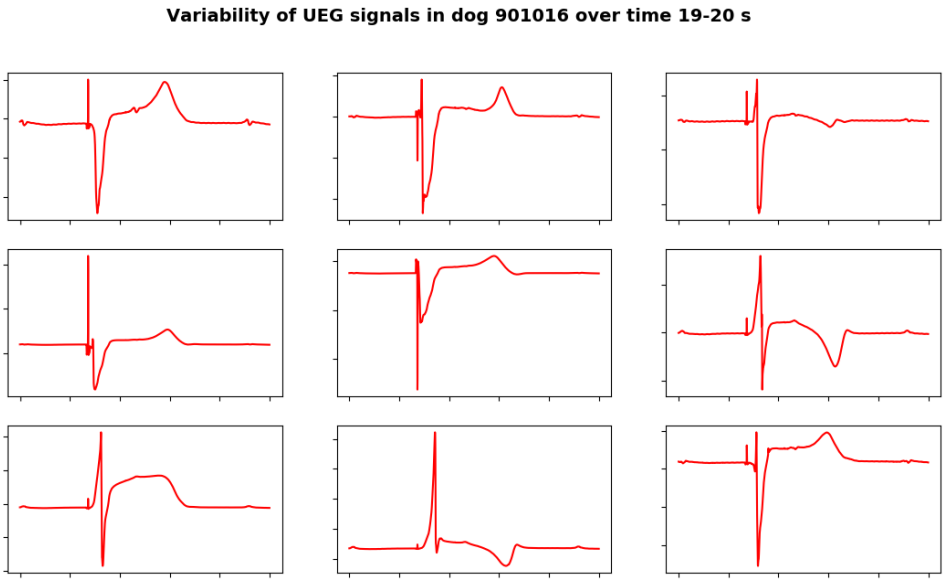

Figure 5.10: Some different types of UEG signals from the same dog during the same timespan.

The aim of the GUI was to be as user-friendly as possible since the visual inspection was done by medical researches with a limited programming background. The interface shows 2 plots of the same UEG signal: an overview plot and a more detailed view. Via dragging the window towards left or right, the shown data was moved in time. Different buttons were implemented with varying functions. The most important ones are the buttons for changing the local time of excitation and local time of repolarization. After pressing a button and clicking on a location on the plot a local time of excitation or repolarization could easily be deleted or added. Notice that a new local time of excitation or repolarization was searched within a window around the coordinates of the clicking. An option to adjust this window size was also implemented to ease the determination of the local time of excitation and repolarization. This was important to neglect the effect of noise near the important time points. However this also

has a clear disadvantage: the smaller the window size, the smaller the range to determine the maximal negative or positive derivative and thus the more subjective the determined time point becomes. Another button is the 'Spike Seen'-button which recalculated the local times of excitation in case a spike was seen, as explained in the previous section.

Every channel should be evaluated via the buttons: 'Good' and 'Bad' depending on the quality and morphology of the UEG data. When a channel was evaluated as bad, it was discarded in the further analysis. Only when the channel was evaluated, the user was able to go the evaluation of the next channel. However in case the channel was evaluated as 'Good', the time period of the channel had to contain 31 local times of excitation and 31 local times of repolarization as well in order to go to the next channel. Checking the amount of dots is important to make sure that no beat has been forgotten in the evaluation. The user was guided through the visual inspection via statements as 'Please evaluate and check the position of dots', 'Verify the amount of red dots', 'This channel is evaluated as good'. The next and previous button enabled reviewing the inspection. Another feature of the GUI was to retake the inspection after closing the window. An important characteristic since 31 beats of 185 different channels needed to be visually inspected. The design of the GUI is shown in figure 5.11. The code for this GUI is not incorporated in the appendix since it is out of the scope of the research topic.

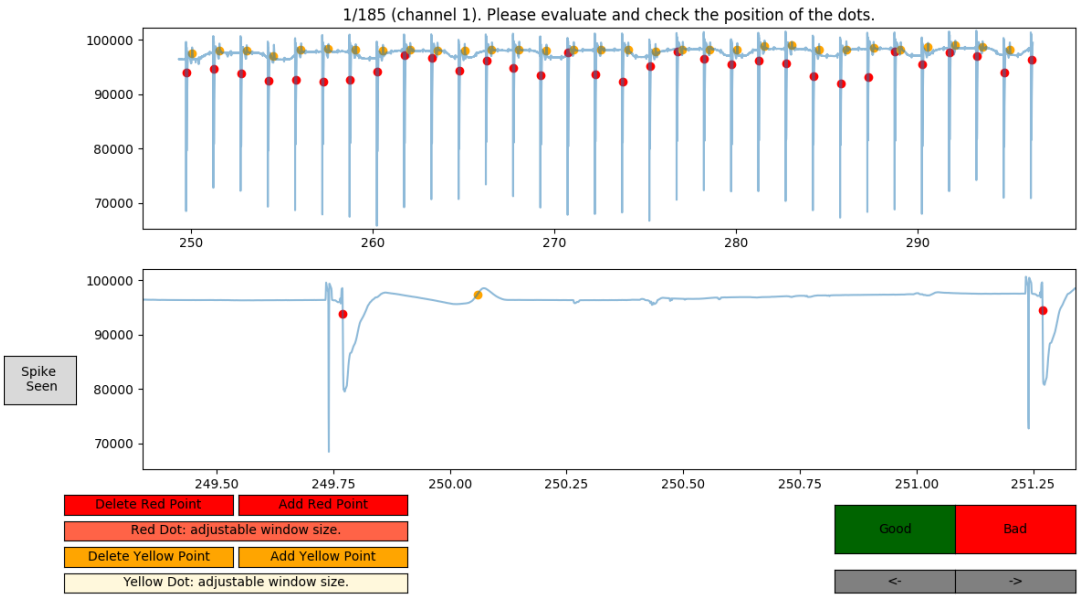

Figure 5.11: The design of the GUI to visually inspect the UEG data.

5.2.4 Calculation and representation of the STV

The first step after the visual inspection was evaluating the outcome of the inspection by determining the amount of good and bad channels. The amount of good channels must be high enough to ensure a good quality of the analysis. For every good-considered channel the STV was calculated via a dedicated for loop over the whole timespan. For every good-evaluated, the Pointcaré plot was created and its corresponding STV value was calculated and shown in an overview represented on an electrode map. Notice that in an electrode map only the good channels were depicted and bad channels were discarded in the analysis.

The most important functions for this analysis are attached in appendix B.

5.3 Results

The results of the analysis of dog 901016 are shown in this section. Unfortunately only 1 dog was analysed due to the time consuming visual inspection of all the different channels.

The selected time period for dog 901016 is represented in figures 5.12 & 5.13. Notice that even the baseline recording contains abnormal activity before and after this selected period.

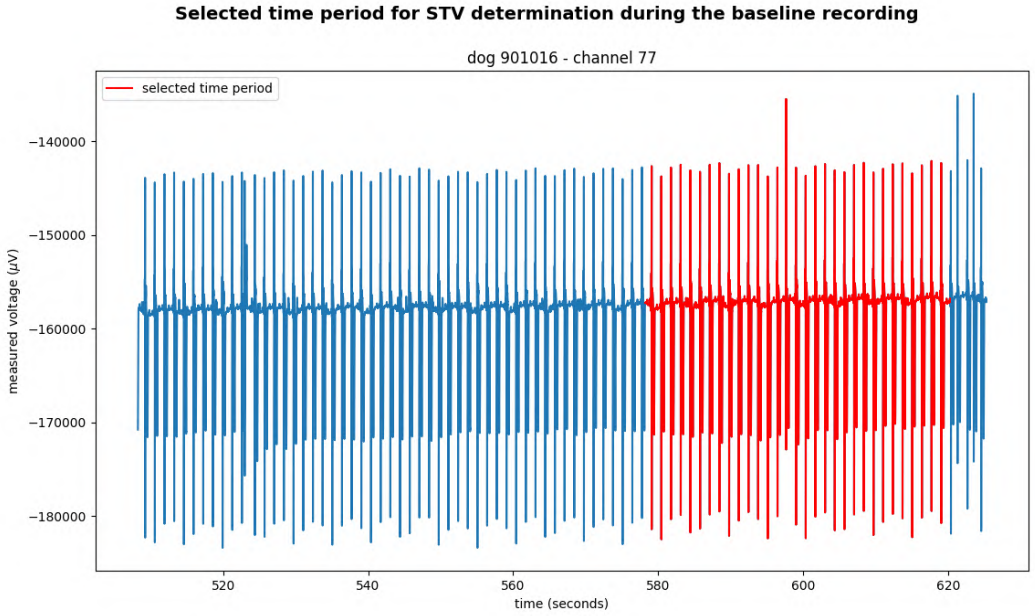

Figure 5.12: The selected time period for dog 901016 during the baseline recording is represented in red.

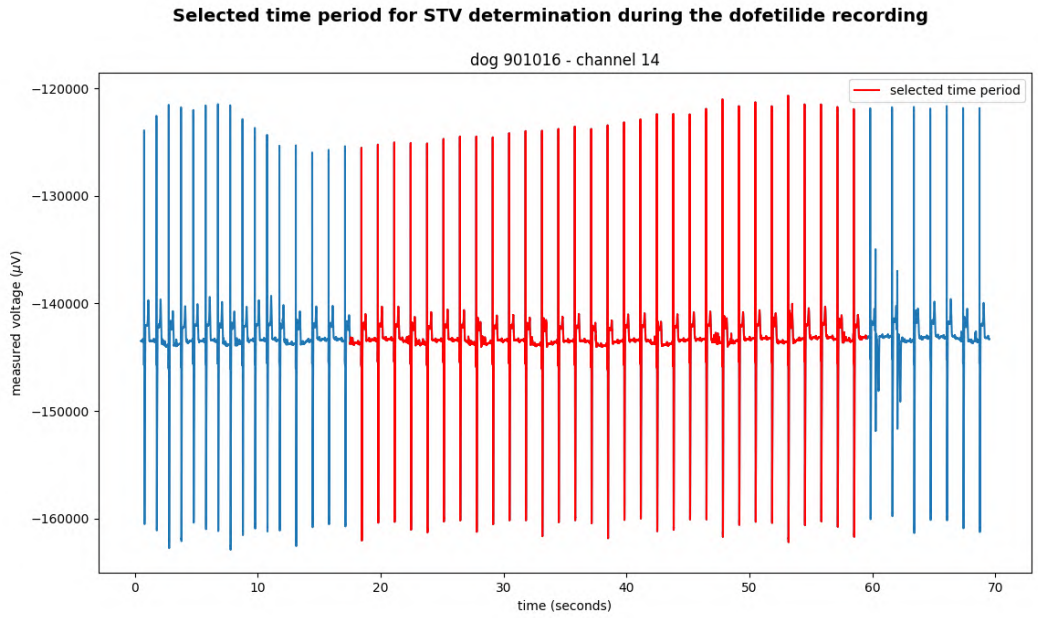

Figure 5.13: The selected time period for dog 901016 during the dofetilide recording is represented in red.

Different heat maps were made representing the STV values for each channel. This was done for the STV values during the baseline recording and during the dofetilide recording. These heat maps are represented respectively in the figures 5.14 & 5.15. The differences between the STV values of the baseline recording and dofetilide recording were calculated for every channel and represented in figure 5.16. Remark that the difference was only calculated of channels which were evaluated as good in the baseline recording as well as in the dofetilide recording. Additionally the Pointcaré plots were made of the channels with the highest and lowest STV value. The figures containing the STV heat map as well as the Pointcaré plots are shown in figures 5.17 & 5.18.

On the figures 5.14 & 5.15 is seen that the STV values are heterogeneously distributed over the heart. The STV values during the baseline recording varied between 1.2 and 10.2. For the dofetilide recording, these STV values varied between 1.0 and 9.4. When looking at figure 5.16, no clear increase or decrease in STV is seen.

The first activated channel after the time period of 31 beats during the dofetilide recording is channel 141 for dog 901016. This channel is situated endocardial, anterior of the LV ventricle. The location of the origin is shown in figure 5.19. How the origin of the ectopic beat is determined is explained in the next chapter.

The figures 5.14, 5.15 & 5.16 with annotation of the STV value are attached in the appendix F. A list with the exact value of the calculated STV of the baseline recording and the dofetilide recording for every channel is added in appendix D. This list also contains the exact difference between the STV of the baseline recording and the dofetilide recording. If this increase is positive, a 1 was added in the column 'Positive?' in order to quickly calculate the amount of increased channel. From this file is seen that only $43/139$ channels have an increased STV during the dofetilide recording. The average difference between the STV equals $-0.446ms$.

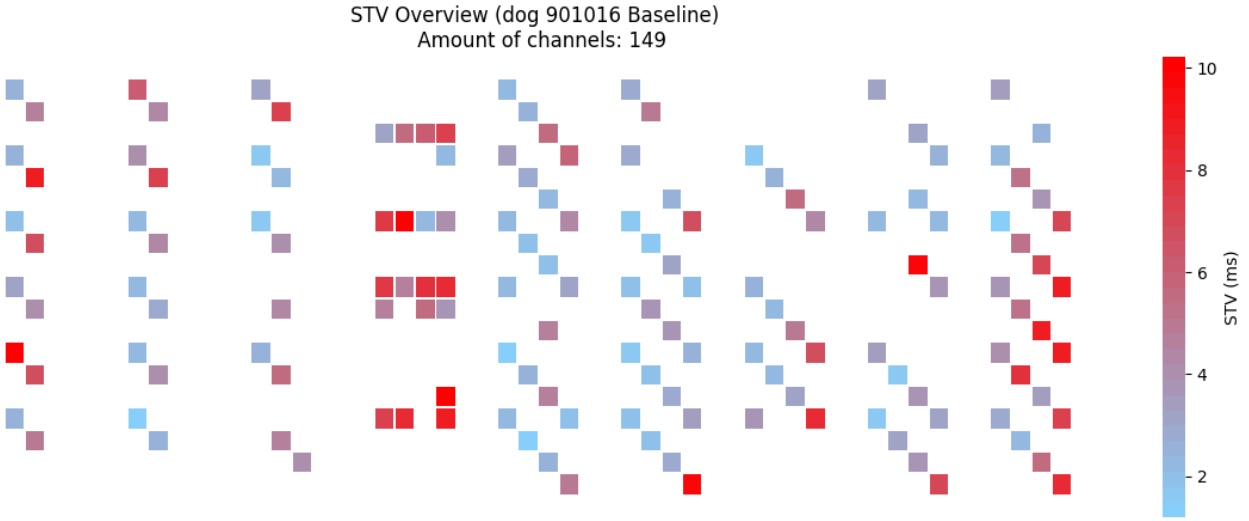

Figure 5.14: An overview of the calculated STV values for each channel during the baseline recording presented on an electrode map for dog 901016.

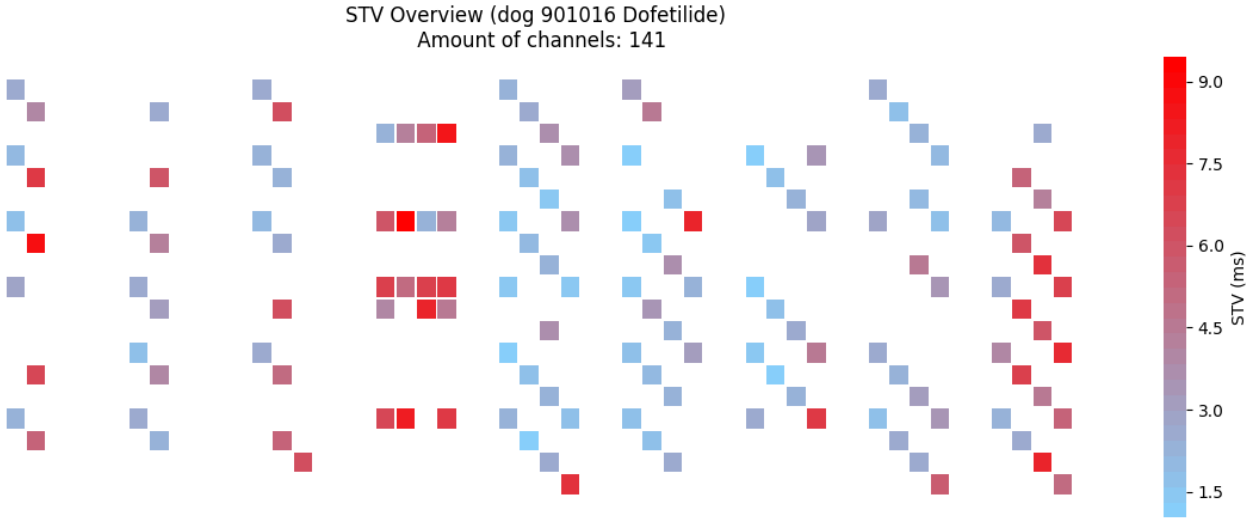

Figure 5.15: An overview of the calculated STV values for each channel during the dofetilide recording presented on an electrode map for dog 901016.

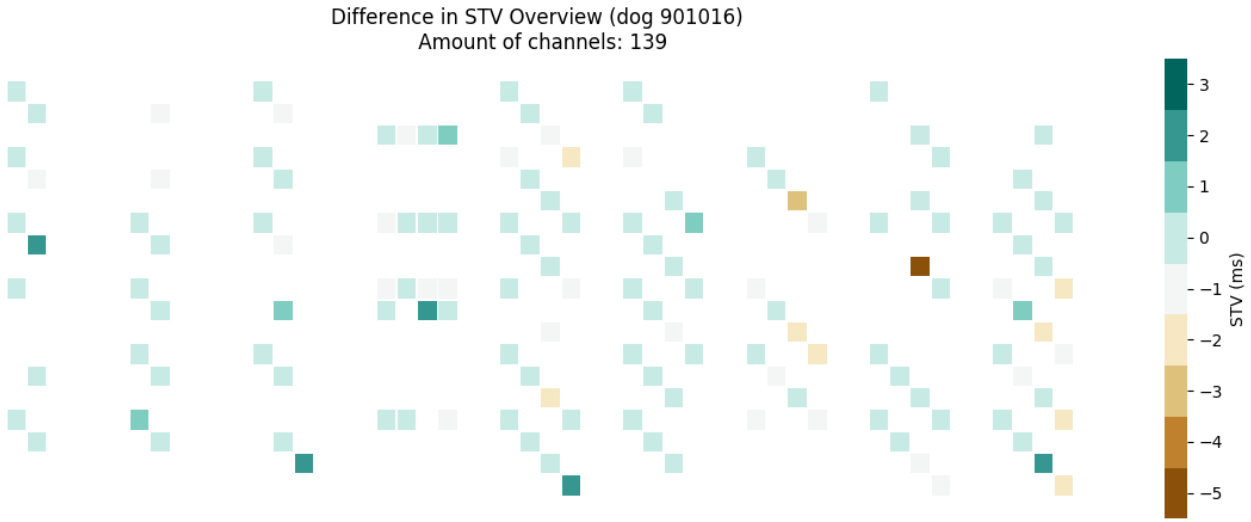

Figure 5.16: An overview of the difference in STV values for each channel presented on an electrode map for dog 901016.

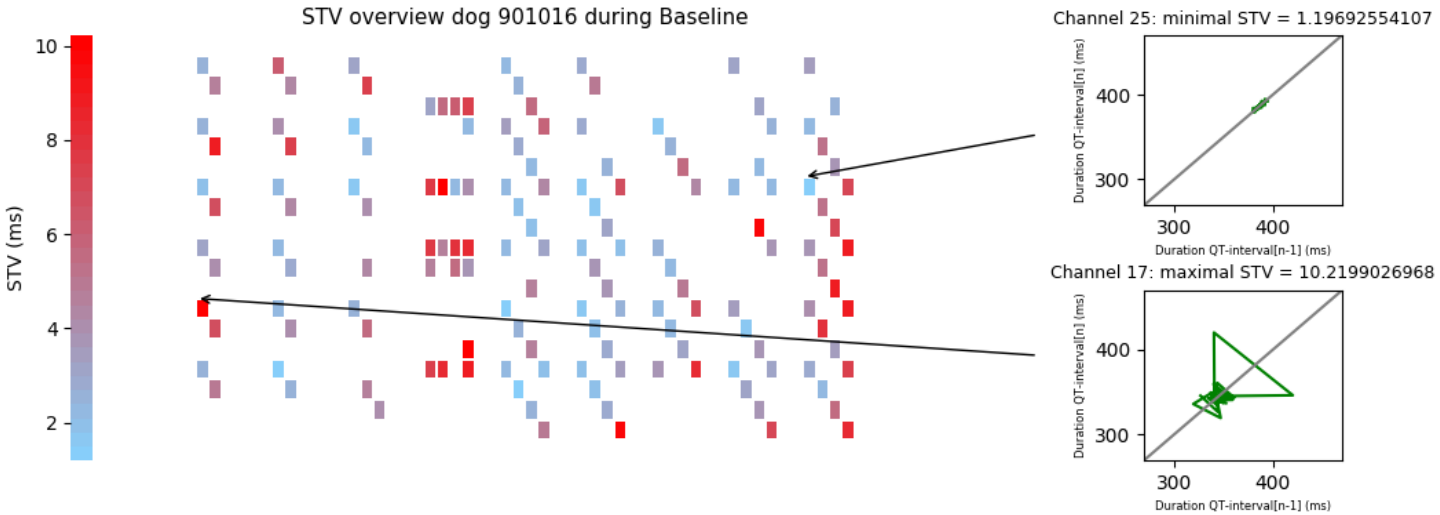

Figure 5.17: An overview of the calculated STV values for each channel during the baseline recording presented on an electrode map for dog 901016 as well as Pointcaré plots of the channels with the highest and lowest STV value.

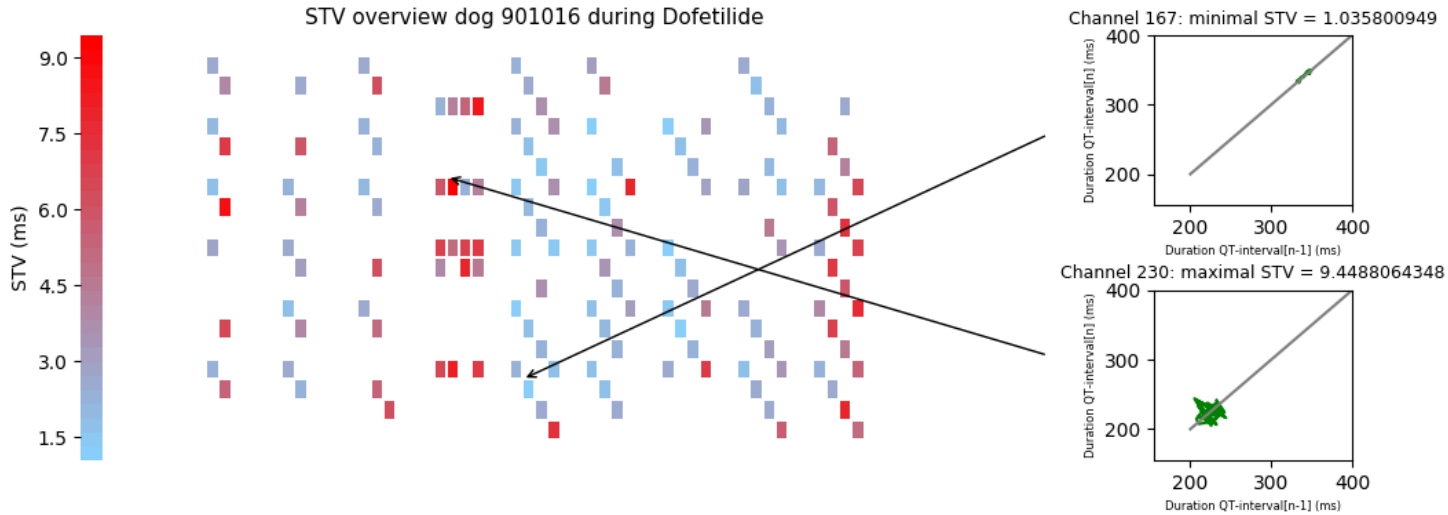

Figure 5.18: An overview of the calculated STV values for each channel during the dofetilide recording presented on an electrode map for dog 901016 as well as Pointcaré plots of the channels with the highest and lowest STV value.

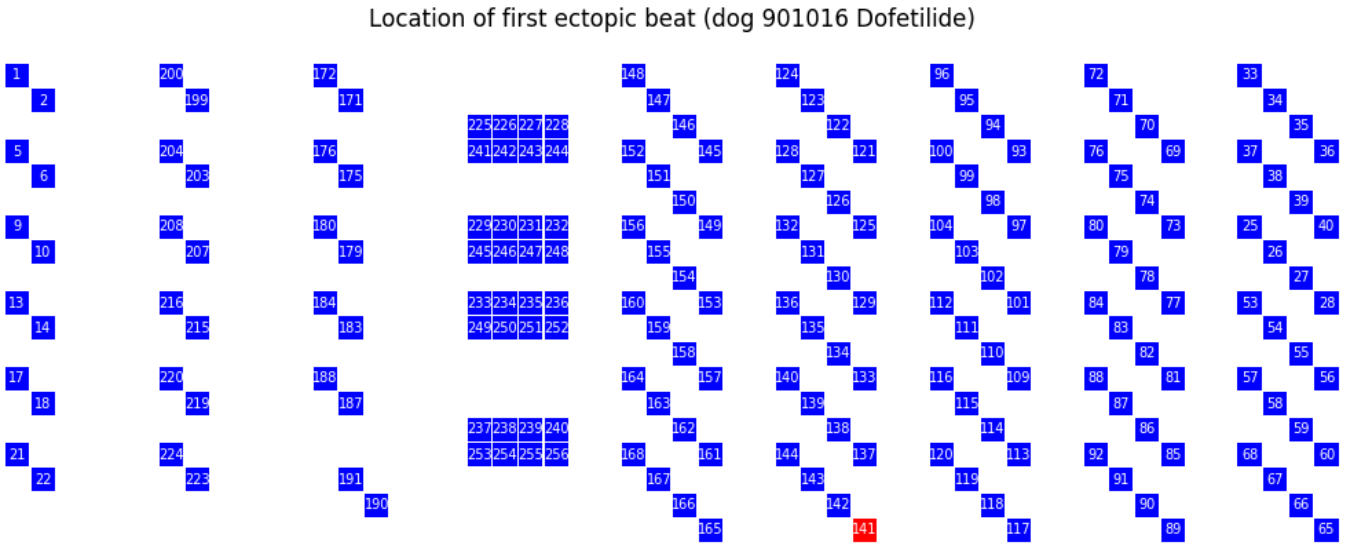

Figure 5.19: The origin of the ectopic beat after the time period of 31 beats for dog 901016.

5.4 Discussion

The STV values varied over different regions in the heart, shown in figures 5.14 & 5.15. When these figures are compared, it is seen that the STV values behave similarly. The region of the septum as the region posterior to the septum in the left ventricle showed elevated values of STV in both the baseline and the dofetilide recording.

In figure 5.16 no distinct increase in STV value is seen. This implies that this trend of an STV increase just before the offset of an ectopic beat was not seen in the UEG data of dog 901016. This could be due to different possible explanations. (1) Destructive interference between the different cells influenced the morphology of the T-wave which caused the T-wave to smooth. This would increase the uncertainty on the determination of the local time of repolarization and would thus directly affect the value of the STV. (2) The insertion of the needles damage a significant amount of cells causing a variable behaviour of repolarization. This has an impact on the distribution of the STV values. (3) The repolarization is too sensitive to noise to determine the local time of repolarization. (4) The GUI makes the determination of the local time of repolarization too subjective via adjusting the window size. (5) It might be that in dog 901016 the dominant effect of the STV increase is the remodelling of the heart. This is derived from the baseline recording which contained a significant amount of ectopic activity. The administration of dofetilide causes a minor effect which is not detectable in the analysis. However this hypothesis contradicts previous findings in literature (Wijers et al., 2017).

Since the slope of the QRS-complex is very steep, the determination of the local time of excitation is rather certain. Therefore it was presumed that the most uncertainty is introduced due to the determination of the local time of repolarization. A gradual increase of the T-wave over a broader time span as well as a smaller increase in magnitude introduces more uncertainty on the local time of repolarization. A wrong placement of a few milliseconds influences the STV of the channel directly. In figures 5.20 & 5.21 it is seen that the time interval of the ARI is highly variable.

Unfortunately channel 141, shown on figure 5.19, the channel where the ectopic beat arises was not evaluated as a a channel of good quality during the dofetilide recording. Therefore it was not depicted on figure 5.15. A beat of channel 141 during the dofetilide recording is shown in figure 5.22. Remark that due to the STV elevation and the noise, no clear T-wave is visible. However the origin of the ectopic beat could still be determined since the determination of the origin of the ectopic beat only depends on the local time of excitation. How the origin of the ectopic beat is determined is explained in the next chapter. Notice that the STV value in the region of the origin is not significantly increased.

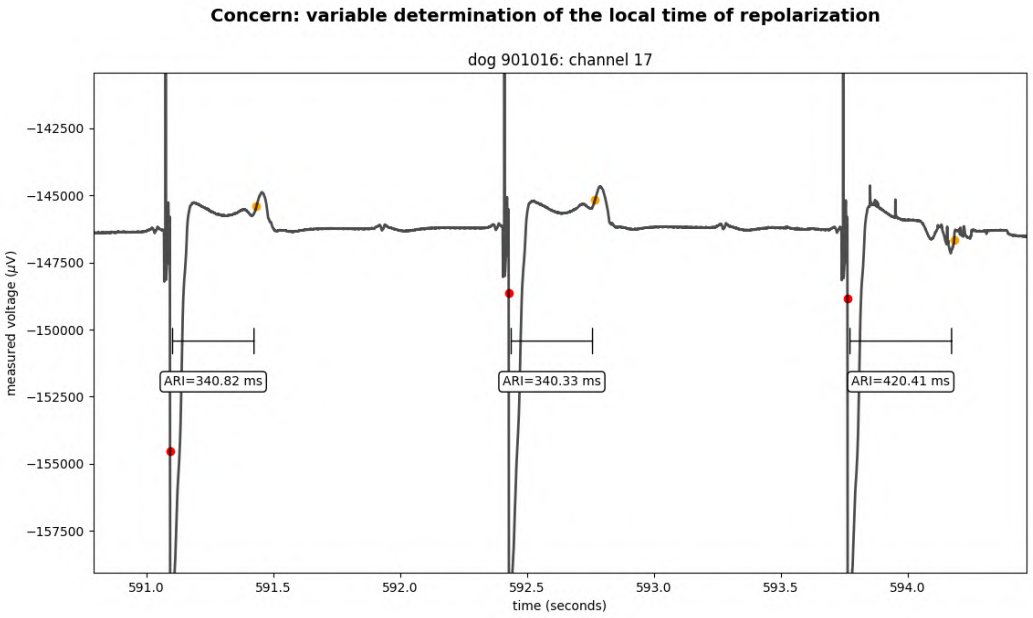

Figure 5.20: A detailed view of channel 17 during the baseline recording of dog 901016 where it is seen that the determination of the local time of repolarization is highly variable. Notice that this channel was evaluated as good and the local times of excitation and repolarization were corrected.

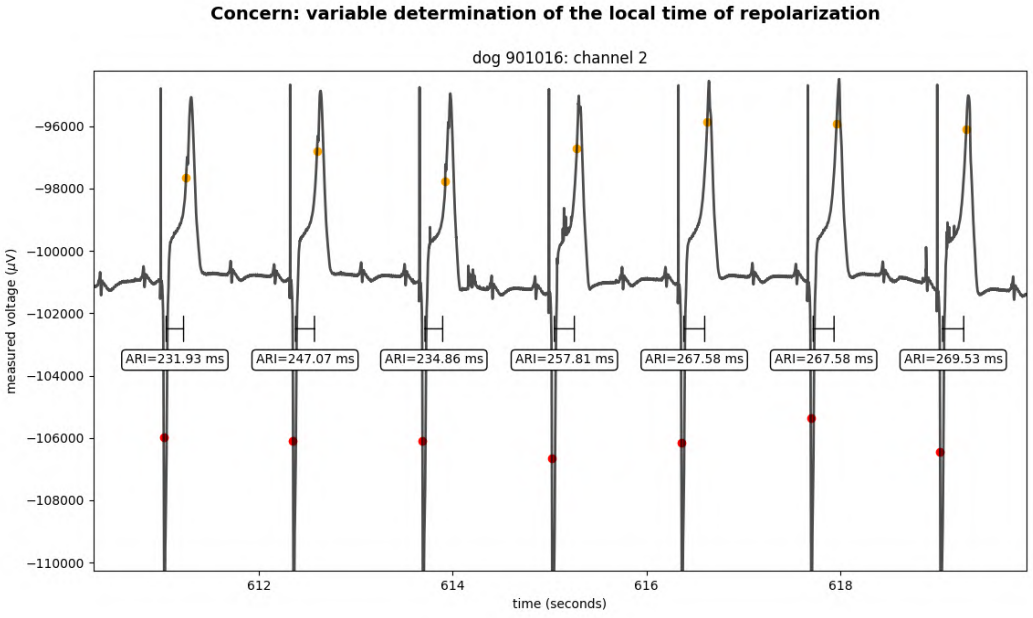

Figure 5.21: A detailed view of channel 2 during the baseline recording of dog 901016 where it is seen that the determination of the local time of repolarization is highly variable. Notice that this channel was evaluated as good and the local times of excitation and repolarization were corrected.

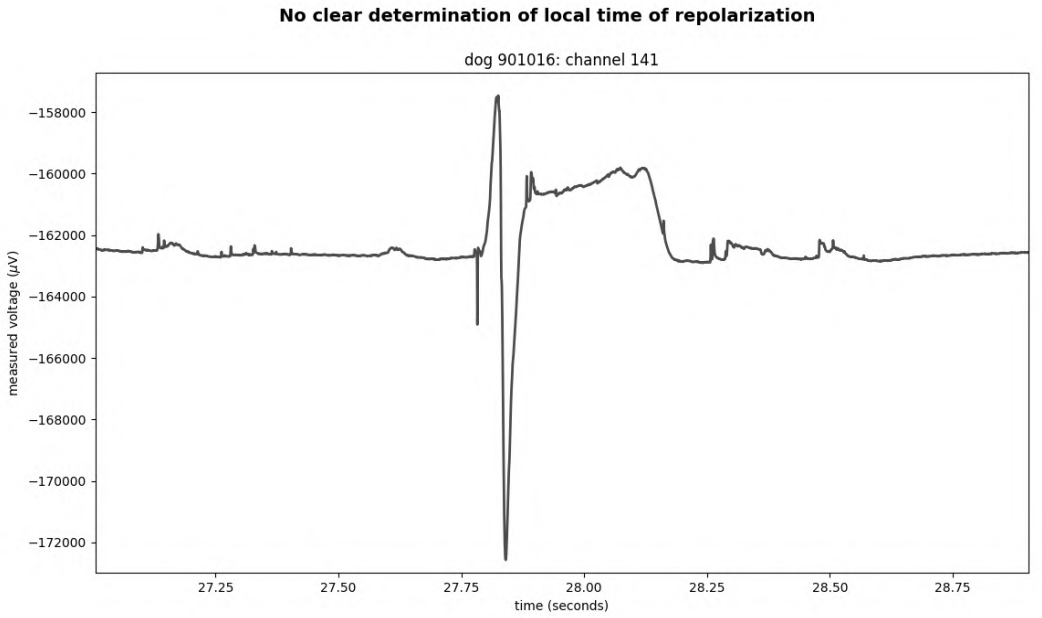

Figure 5.22: A detailed view of channel 141 during the dofetilide recording of dog 901016.

The limitation based on the sampling speed to determine the local time of excitation or repolarization was assumed to have a minor impact on the STV determination. The determination of the local time of excitation or repolarization respectively to the maximal positive or negative derivative remains the same over the whole analysis. Therefore the same error was made on the determination of local time of excitation and local time of repolarization. This was assumed to have almost no impact on the determined ARI and thus no impact on the calculated STV.

These results were not expected since the trend of an increased STV before the offset of TdP was seen in EGM data received from the inner surface of the heart. Underlying reasons why this trend was not seen in UEG data via needles could be (1) the damaging of the cardiac cells due to the needle insertion or (2) significant additional effects which were not taken into account in this analysis.

Figure 5.23 depicts different traces of EGM data. From this figure is seen that the signals are rather similar to the UEG signals. It would be interesting to compare these different types of signals in order to explain why the trend is seen in EGM data and not in UEG data.

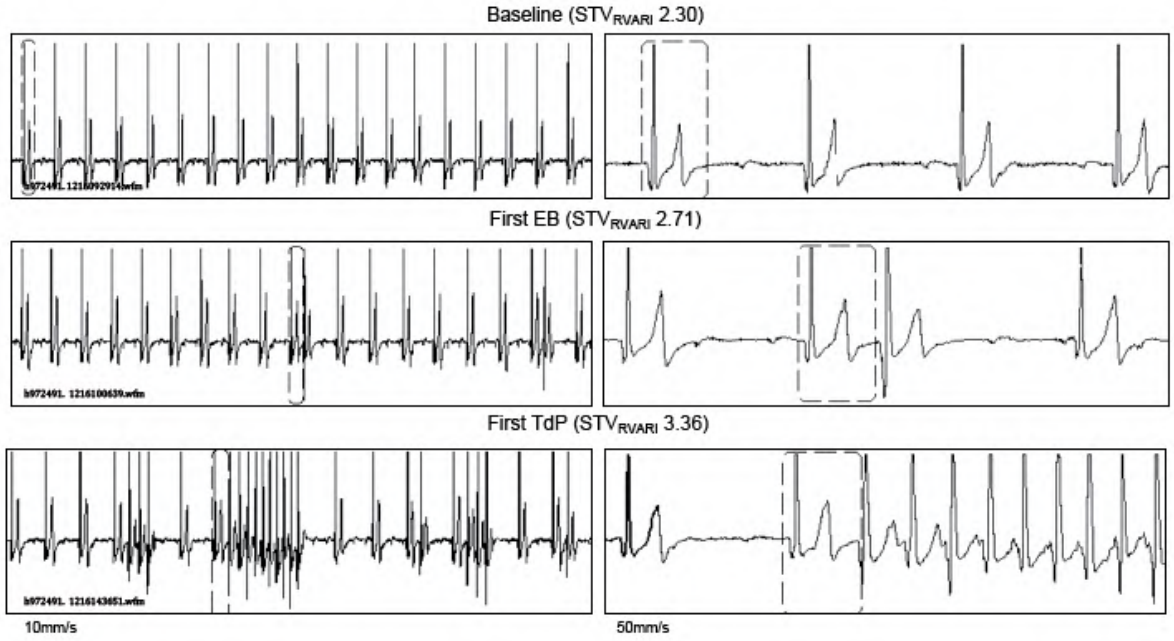

Figure 5.23: Traces of intracardiac electrogram (EGM). Figure from Wijers et al. (2017).

5.5 Conclusion

This conclusion is only applicable for the results of dog 901016. The UEG data obtained via needles did not show the trend of a STV increase just before the offset of the first ectopic beat. Therefore it was presumed that STV could not be used as biomarker for the prediction of Torsade de Pointes. The STV was highly heterogeneously distributed over the heart. Presumably the determination of STV was highly dependent on the morphology of the T-wave.

5.6 Limitations

Only one dog, namely dog 901016, was analysed which does not allow to draw a general conclusion for Torsade de Pointes. No statistical analysis has been done therefore the statement that there is no increase in STV should be carefully interpret.

5.7 Future work

The analysis must be done for all the different dogs in order to see whether there is or is not a trend visible. A statistical analysis should be preformed whether the STV increase is significant or not.

The EGM data gathered via the inner surface of the heart should be compared with the EGM data gathered via the needles. From this comparison might result why the trend is visible in the EGM on the surface of the heart and not in the EGM via needles, the UEG data. Furthermore the written algorithm should be validated with the currently used software written by Potse, Linnenbank, and Grimbergen (2002).

To determine a biomarker for the prediction of Torsade de Pointes in UEG data more research is needed. From previous studies, it was expected to see an increase in STV. It might be that additional parameters are needed to predict the offset of Torsade de Pointes. It would be interesting to know why the STV in UEG data does not show the trend of increasing before the offset of an ectopic beat.

Chapter 6

Origins of Ectopic Beats

This chapters focuses on the second research question, namely are the origins of ectopic beats homogeneously or heterogeneously distributed over the heart? As mentioned in section 1.7.1, the perpetuation of Torsade de Pointes (TdP) in the case of focal activity is still unclear. Different theories were suggested. Depending on whether the origins of ectopic beats are homogeneously or heterogeneously distributed, more insight can be given in the mechanism of the perpetuation by focal activity.

According to the theory of Vandersickel et al. (2016) the ectopic beats emerge from different heterogeneities. In that case the origins of the ectopic beats are heterogeneously distributed over the heart. The theory of de Lange et al. (2012) assumes a regionally synchronized early afterdepolarization (EAD) which propagates through the tissue. In that case the origins of the ectopic beats would be more homogenously distributed over the heart.

6.1 Hypothesis

The origins of ectopic beats are heterogeneously distributed over the heart. This statement is based on the theory of Vandersickel et al. (2016). The origins of ectopic beats are similarly distributed in episodes with only one ectopic beat compared to episodes with multiple ectopic beats.

6.2 Method

Figure 6.1: Work flow of the project 'Origins of Ectopic Beats'.

6.2.1 Determination of the ectopic beats and corresponding paced beat

In this research every ectopic beat during the dofetilide recording was analysed. A typical unipolar electrogram (UEG) signal is shown in figure 6.2. As seen in this figure, a lot of ectopic activity occurs before and after the episode of Torsade de Pointes.

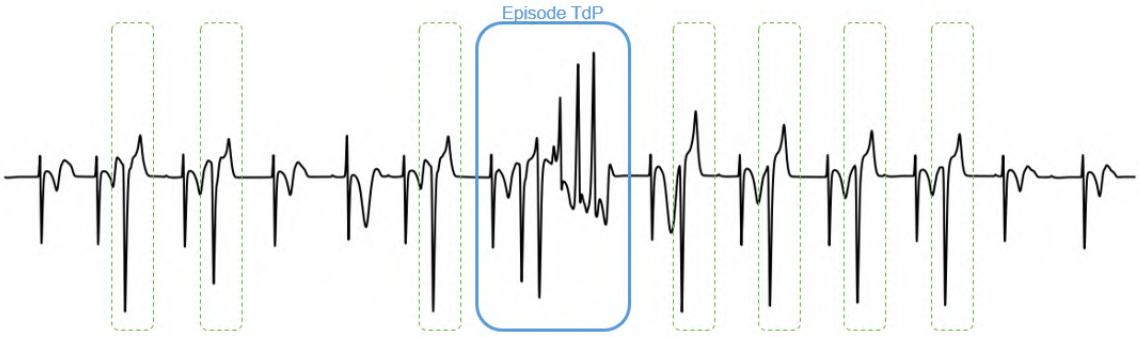

Figure 6.2: A UEG signal of channel 78 of dog 928607 during a the time period 994 - 1014 s. The blue box denotes an episode of TdP while the dashed green boxes focus on individual ectopic beats.

The local time of excitation of the ectopic beat and its previous paced beat were used to determine the origin of the ectopic beat. Analogous as in the previous chapter, first all the relative negative maxima of the derivative were calculated. These relative minima were evaluated to identify the paced beats and the ectopic beats. However compared to the algorithm in the previous project, different criteria were used. (1) A first criteria was a threshold criteria which excluded noise. This threshold for the derivative was higher compared to the algorithm to determine the local time of excitation of the paced beat in the short-term variability (STV) project. This was needed since otherwise the negative slope of some T-waves would fulfil this criteria. (2) All the relative minima of the derivative which fulfilled the first criteria, were then evaluated by the criteria based on window size. When the relative minima occurred at least 1 second after the previous beat, the beat was seen as a paced beat. In case of an ectopic beat, the local time of excitation had to lie within a time frame of $2/3$ second. In literature 500 ms is

often used as window to register an ectopic beat Wijers et al. (2017). In this research the time frame was slightly prolonged in order to generalize the algorithm. Due to the variability of the signals, a slightly bigger window allowed to incorporate less distinct ectopic beats as well. The calculation of the local time of excitation of the ectopic beats and its corresponding previous beat is shown in figure 6.3. Remark that the algorithm did not work perfectly. As mentioned earlier, it is a true challenge to find the most general algorithm which allows the best determination across all the different UEG signals. However in the next section, an extension of this algorithm is discussed to increase the performance of the algorithm.

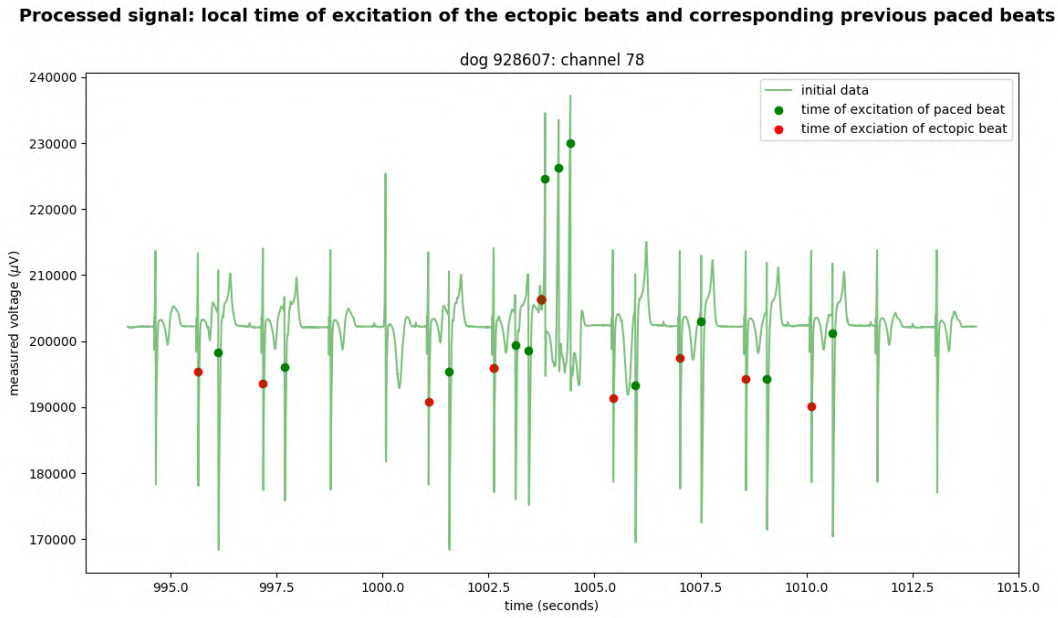

Figure 6.3: A UEG signal of channel 78 of dog 928607 during a the time period 994 -1014 s. The local times of excitation of the ectopic beats and their corresponding previous paced beats determined by the algorithm are represented by respectively the green and red dots.

The used algorithms to determine the local times of excitation of local beats and their corresponding paced beats are attached in appendix E.

6.2.2 Semi-automated inspection

The graphical user interface (GUI) written for the semi-automated inspection for the STV was adapted to be functional for this project. Notice that the local time of repolarization was not incorporated in this GUI since the local time of repolarization was not used in the analysis. The red dots were replaced by bigger stars in order to quickly see overlap between the determination of local time of excitation of ectopic and paced beats. The evaluation of the channel as a good or bad channel depending on the quality of the signal, was also required in this GUI to go to the visualization of the next channel. Figure 6.4 shows the design of the interface.

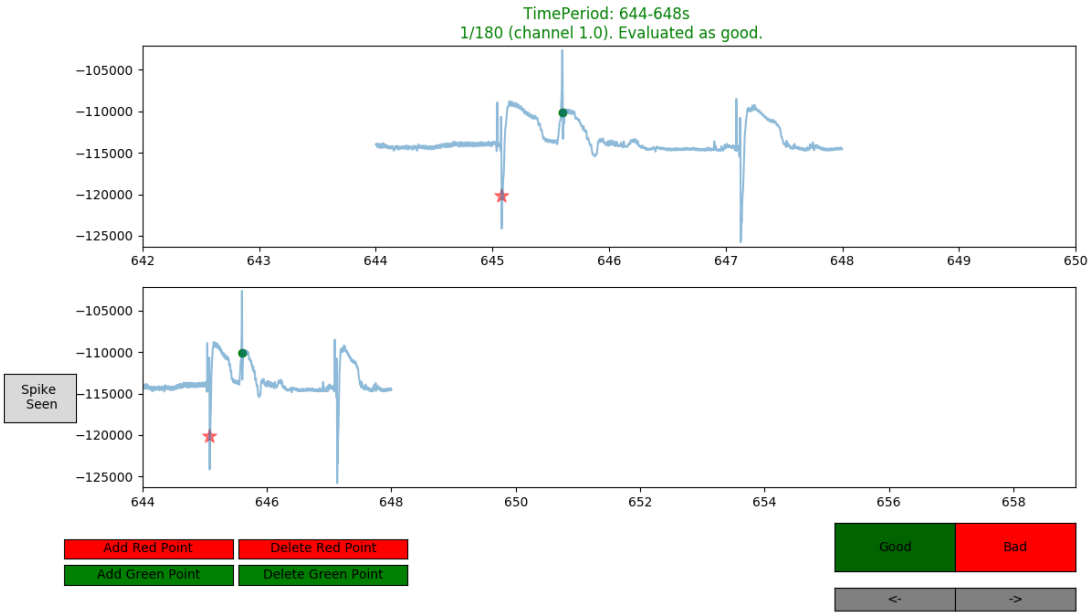

Figure 6.4: The design of the GUI to visually inspect the UEG data.

Since it was challenging to find the proper criteria which determined the local time of excitation of the ectopic beats and their corresponding previous paced beats, an extension of the algorithm was made to increase the performance of the script. When a channel was evaluated as good, it was assumed that all the local times of excitation of the ectopic beats as well as their corresponding paced beats were correctly determined. The extension of the algorithm searched a maximal negative derivative in the neighbourhood of the previously determined local times of excitation. The algorithm of the extension is also attached in appendix E.

The determination of an ectopic beat is not always straightforward. Sometimes the ectopic beat had a very mild slope or even no slope was seen. In order to make the visual inspection as objective as possible some guidelines were used:

- An ectopic beat was considered as a beat without a pacing spike.
- The ectopic beat or the series of multiple following ectopic beats had to be preceded by a paced beat.
- In case of an unclear ectopic beat due to very mild or no seen slope: the local time of excitation was removed from the analysis. When only one ectopic beat occurred which was unclear, the local times of excitation of the ectopic beat as well as the paced beat were removed.

Remark that neglecting a local time of excitation for a signal with a very mild slope does not influence the analysis to determine the first activation. The origin of the ectopic activity is often characterized by a very steep slope. Notice that the guidelines also integrate escape beats in the analysis. However since these are more likely to occur after a change in pacing rate

which did not often occur during the recording, it was seen a minor influence on the analysis. Furthermore, the visual inspection was only needed for time periods which contained ectopic activity and which were not evaluated previously for the study by Vandersickel et al. (2017). The local time of excitation is referred to as time of activation or activation time in the continuation of this thesis.

6.2.3 Determination and representation of the origins of the ectopic beats

To determine the origin of each ectopic beat, the recording was separated into different episodes. A timespan of a paced beat followed by one ectopic beat or multiple ectopic beats was denoted as 'episode'. For each episode a dictionary was made containing for all the channels evaluated as good, all activation times of the paced beat together with the ectopic activity.

Remark that for the previously analysed episodes for the article by Vandersickel et al. (2017) such a dictionary was already made. For previously analysed episodes which were re-entrant or non-terminating only the first 2 beats, namely the paced beat and following ectopic beat, were integrated in the episode since the first beat after the paced beat is always an ectopic beat.

The next step was to find the time span of each beat in every episode. This was done via the dispersion of activation times, namely finding the interval between 2 consecutive beats, called the interbeat interval. A sorted array containing all the activation times of all channels was made. The biggest differences between consecutive elements correspond to the interbeat interval. Logically the amount of interbeat intervals is equal to the amount of beats minus 1. In figure 6.5 the dispersion of activation times is shown.

The last step was to find the first activation time and first activated channel for every beat in every episode. For each beat, the activation time of each channel within that beat is evaluated compared to a reference value. In case the activation time of the channel is smaller compared to the reference value, the reference value was overwritten by the value of the smaller activation time. Also for the determination of the first activated channel a reference channel is used in the similar way. A loop over all the different channels resulted thus in the first activation time and its corresponding channel. When this was done for all beats, an array with all first activated channels and an array with all first activation times was given as output.

The algorithms corresponding to the important function are attached in appendix E.

The visual inspection could introduce bias when the position of local time of excitation of the ectopic beat or the paced beat is corrected. At the origin of a beat, the UEG signal is characterized by a steep downwards peak since the depolarization wave only travels away and thus away from the electrode. Therefore it is presumed that due to the steep downward peak of the initiating beat the determination of the first activated channel would be most of the cases correct. In figure 6.6 different channels are represented during episode 45. In the first plot the

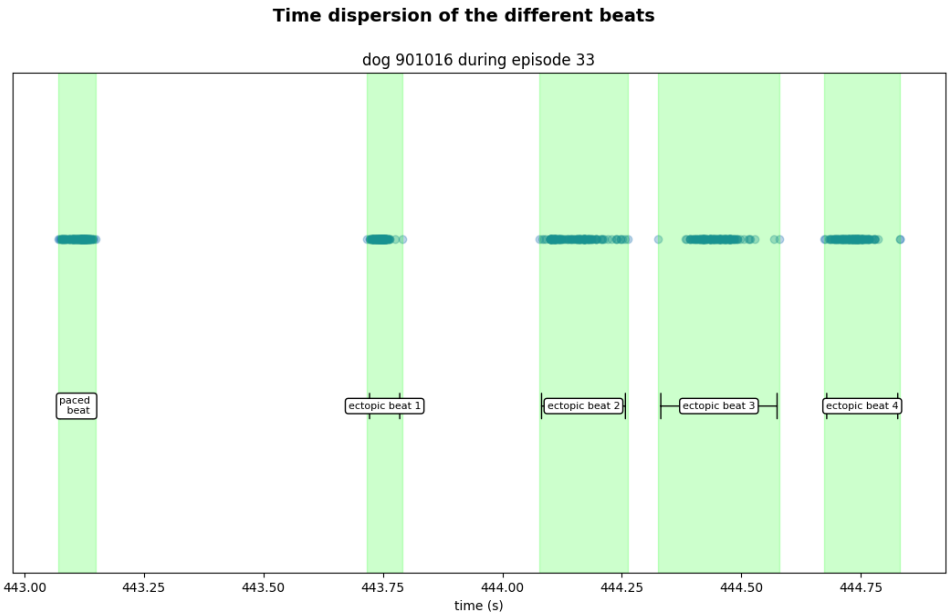

Figure 6.5: The dispersion of activation times of dog 901016 during episode 33.

data of the channel which initiates the paced beat is shown. In the second plot the data of the channel which initiates the ectopic beats is represented. Notice that these channels show a steep downward peak which is not preceded by a fast upward peak. In the third plot, a random channel is added. On this plot is seen that the depolarization wave travels towards channel 215 and goes than further which explains the upward peak followed by the downward peak in the UEG signal.

The representation of the origins was done via a heat map projected onto the electrode map of the dog. Different heat maps were created:

- Heat map containing all the origins of all ectopic activity of all the different episodes.
- Heat map containing all the origins of the first ectopic beat of every episode.
- Heat map containing all the origins of the ectopic beats in episodes which contained only 1 ectopic beat.
- Heat map containing all the origins of the ectopic beats in episodes which contained at least 2 ectopic beats.
- Heat map containing all the origins of the ectopic beats in episodes classified as re-entry or non-terminating. .
- Heat map containing all the origins of the paced beats.

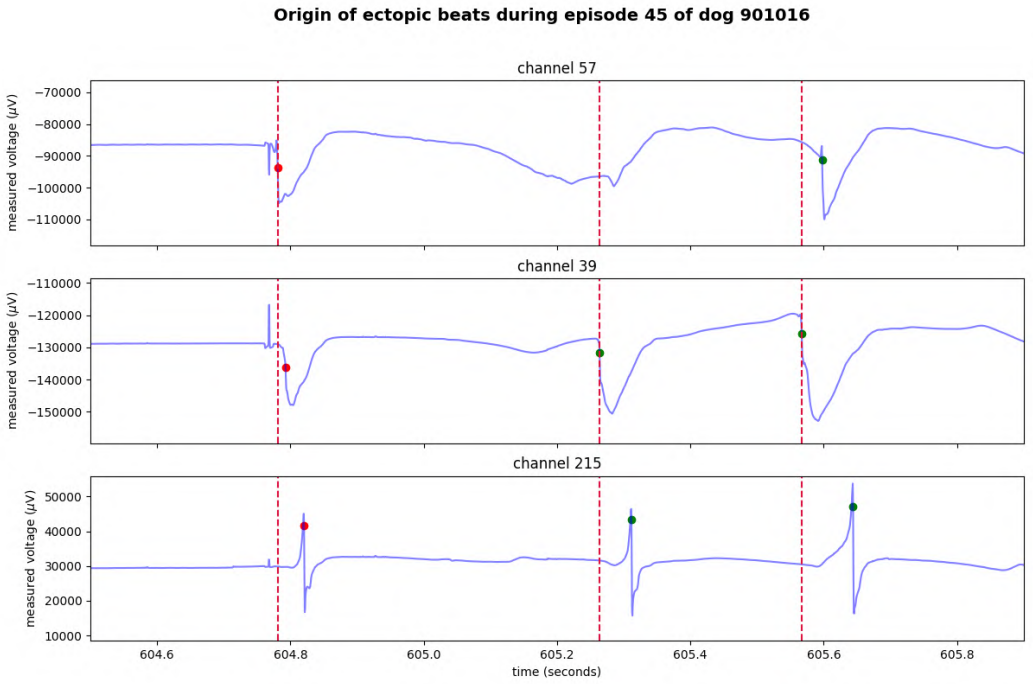

Figure 6.6: Different channels, namely channel 57, 39 & 215, for the same episode. On this figure is seen that channel 57 initiates the paced beat while channel 39 initiates the ectopic beats. The initial data is represented in blue, the red and green dot represent respectively the local time of excitation of the paced and ectopic beat. The dashed vertical lines represent the local time of excitation of the initiating beat.

The overview of all the ectopic beats would answer the question whether the origins are homogeneously or heterogeneously distributed across the heart. The other heat maps could give insight in whether the ectopic focus changes depending on episodes with one or multiple ectopic beats are considered. The heat map containing the first activity of the paced beats could give insight in how reliable the visual inspection and algorithm were. Since the pacing electrode did not change in location, it was expected that the paced beat comes consistently from the same location.

6.3 Results

Unfortunately the visual inspection was time consuming. The recording lasted 10 minutes with on average 1 beat per second, which implies on average 600 beats per channel. Since at least 180 working channels are present in the dog, around 108 000 beats had to be inspected for only one dog. Due to limited time only one dog, namely dog 901016, could be evaluated.

The heat map containing all the origins of all ectopic activity of all the different episodes is represented in figure 6.7. In figure 6.8 an overview is given of the origins of the first ectopic beats in all the different episodes during the dofetilide recording. To gain more insight in the mechanism of TdP, figures 6.9, 6.10 & 6.11 were made. The overview of the origins of the paced beats in all the episodes is given in figure 6.12. These heat maps with annotations are added in the appendix F.

On figure 6.7 which represents the origins of all the ectopic activity, it is seen that there are 3 preferable origins for the ectopic activity. These locations are (1) epicardial on needle I in slice number 4 located between the base and apex posterior to the septum in the left ventricle (2) endocardial on needle IV in slice number 6 located near the apex anterior to the left ventricle and (3) endocardial on needle I in slice number 6 located near the apex posterior to the septum in the left ventricle. A total amount of 229 ectopic beats is evaluated in this heat map. Notice that the same trend is visible in figure 6.8. The same locations initiate the first ectopic beat in re-entrant and non-terminating episodes as seen in figure 6.11. Remark that this result is based on only 6 ectopic beats.

In figure 6.9 is seen that the dominant location to initiate individual ectopic beats is situated endocardial near the apex anterior to the left ventricle. Notice that the other locations as seen in figure 6.7 are minor preferable locations. Figure 6.10 shows that for episodes with multiple ectopic beats, the dominant location shifts towards the epicardial location in the middle between the base and apex posterior to the septum in the left ventricle. The location endocardial near the apex anterior to the left ventricle initiate only 1 ectopic beat.

In figure 6.12 a heat map is represented with the origin of the paced beat of each episode. On this figure is seen that more than 80% of the paced beats start in the endocardium near the apex posterior from the septum.

All these figures with annotation are attached in the appendix F. A list with more details of every ectopic episode is attached in appendix G. For the analysis a distinction was made between time spans which were analysed previously and were not previously analysed. This list contains in the columns 't1' & 't2', the times of the previously analysed episode or the time in between those analysed episodes. In the column '# beats' the length of the episode was indicated. The '$1+$' denotes the paced beat followed by the amount of ectopic beats in the episodes. In the next column a '1' was placed in case a paced beat was considered while '0' when an ectopic beat was considered. Followed by the columns with the first local time of excitation and the first activated electrode. The next column contained the interbeat interval. This interbeat interval equals the time in between the first local times of excitation of the considered beat and the next beat. In case the last ectopic beat was considered, the interbeat interval was equal to '0'. The number of ectopic episode was shown in the next column whereby the episodes are ordered chronologically. Then the total amount of episodes was represented. Logically this number remains constant within one dog. The next column indicates whether the episode was classified as re-entrant or an ectopic episode respectively

denoted by 'R' or 'E'. In the column 'not registered?' a '1' was placed when the episode was not registered previously and a '0' when the episode was analysed for a previous study. In case of very unclear downward peaks, no local time of excitation of the beat was determined. Therefore the last column shows the amount of channels with a local time of excitation determined for that beat. Notice that this number must be high enough to ensure a correct determination of the first activation.

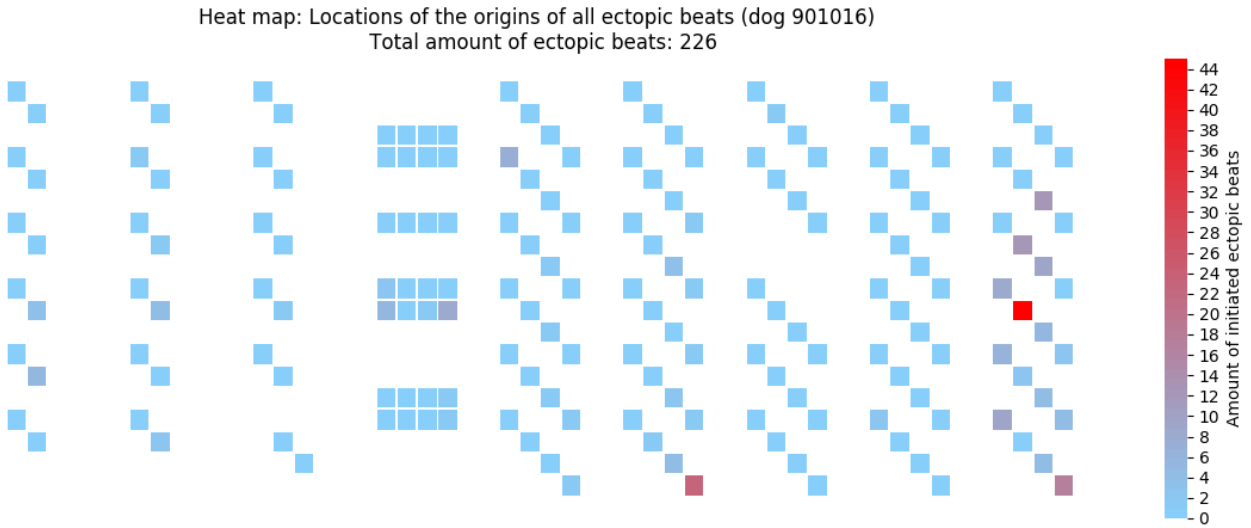

Figure 6.7: An overview of the origins of all the ectopic activity during the dofetilide recording presented on an electrode map for dog 901016.

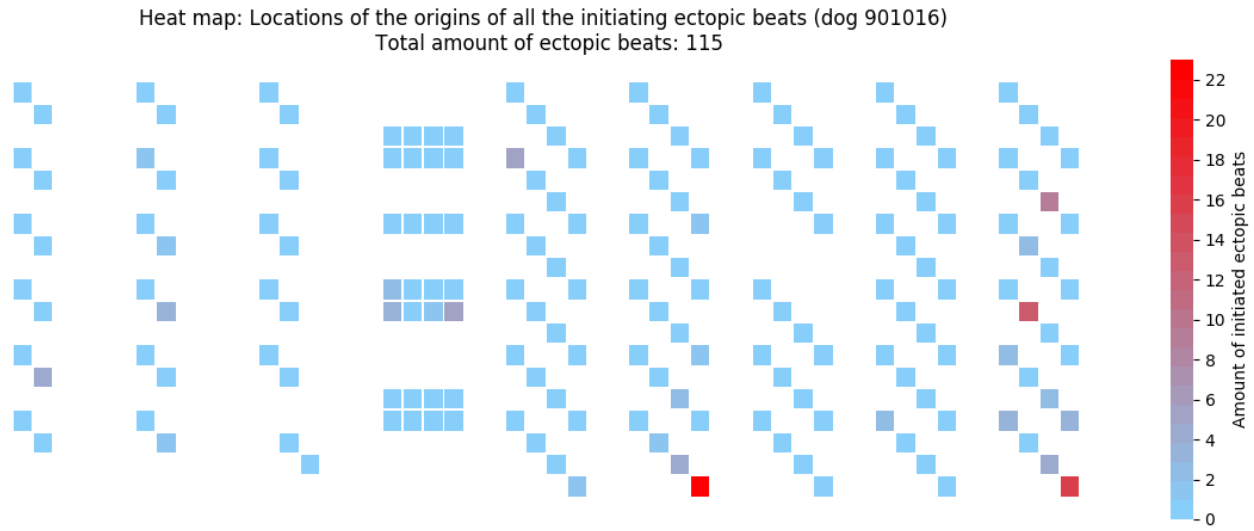

Figure 6.8: An overview of the origins of the first ectopic beat in all episodes presented on an electrode map for dog 901016.

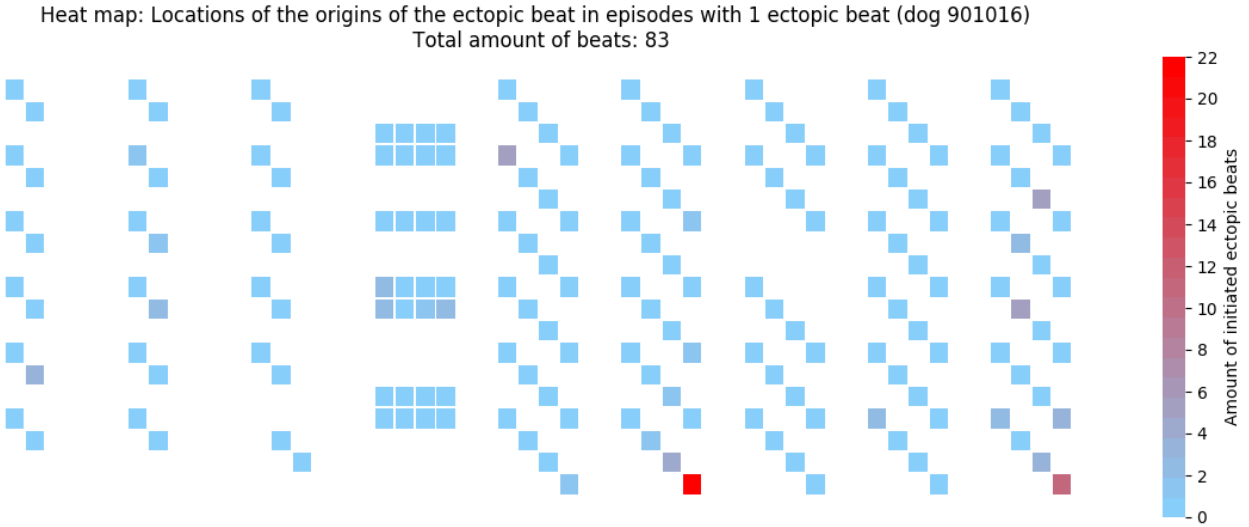

Figure 6.9: An overview of the origins of the ectopic beats in episodes with only 1 ectopic beat presented on an electrode map for dog 901016.

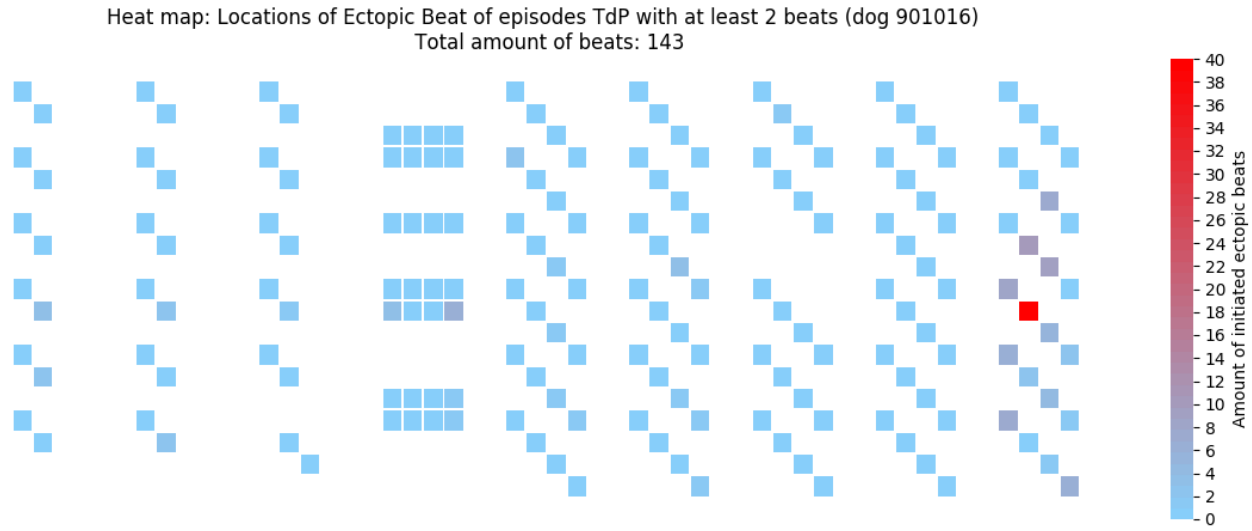

Figure 6.10: An overview of the origins of the ectopic beats in episodes with at least 2 ectopic beats presented on an electrode map for dog 901016.

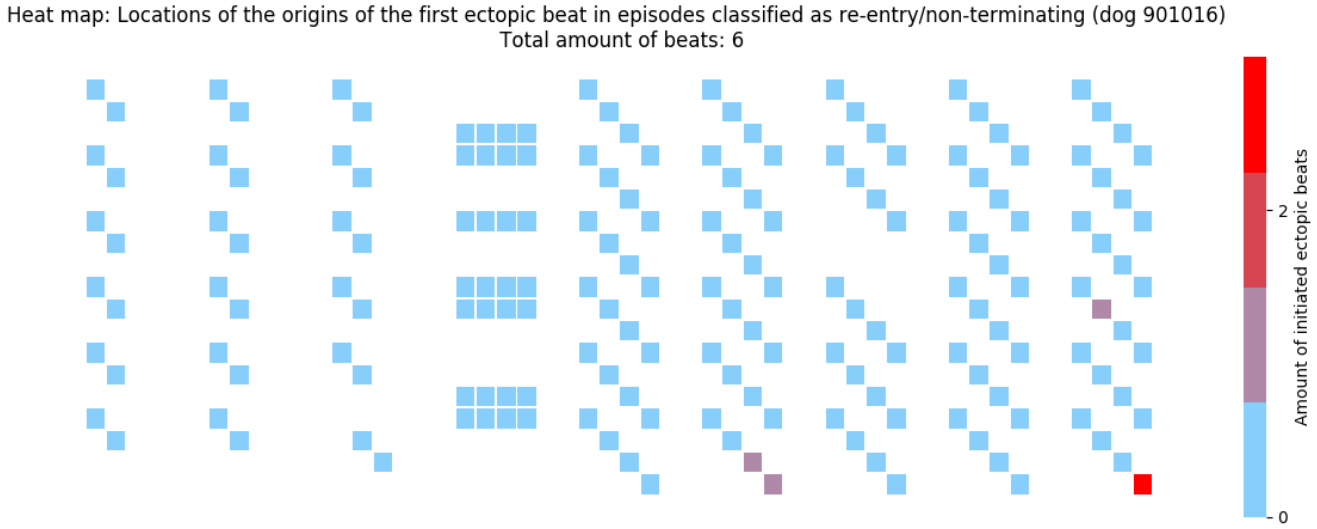

Figure 6.11: An overview of the origins of the ectopic beats in episodes classified as re-entry or non-terminating presented on an electrode map for dog 901016.

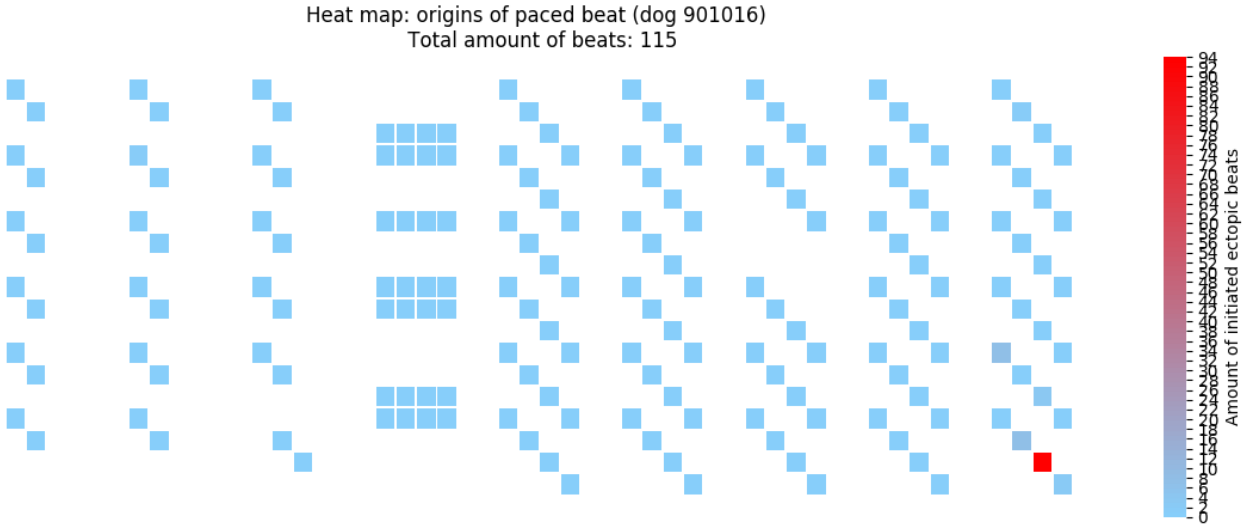

Figure 6.12: An overview of the origins of the paced beats in all episodes during the dofetilide recording presented on an electrode map for dog 901016.

6.4 Discussion

The following discussion is only applicable on the analysis of dog 901016.

From figure 6.7 it is seen that the origins of ectopic beats are heterogeneously distributed over the heart. Thereby it is presumed that the theory of Vandersickel et al. (2016) is more likely than the theory of de Lange et al. (2012). The same trend is visible in the origins of ectopic beats which initiate the episode, shown in figures 6.8 & 6.11.

Comparing the figures 6.9 & 6.10, it is observed that depending on the amount of ectopic beats in the episode, the preferable location to initiate the ectopic beat changes. This shift might be due to a difference in local characteristics of the tissue. To gain more insight in these local characteristics, the activation repolarization interval (ARI) distribution was analysed. In the study by Dunnink et al. (2017), it was concluded that regions with a high heterogeneity in repolarization time are more prone to develop TdP. A high variability in the repolarization time implies a high variability in ARI. The distribution of the ARI is shown in figure 6.13. On this figure is seen that the region posterior to the septum in the middle between the base in the left ventricle shows a high heterogeneity of repolarization. There is a clear difference when this region is compared to the region endocardial near the apex anterior to the left ventricle. This anterior region shows less heterogeneity which presumes that there is a difference in local characteristics. Figure 6.13 with annotation is added in attachment F.

On figure 6.12 is seen that almost all paced beats have an origin endocardial posterior to the septum near the apex. As expected since the pacing electrode did not change place during the recording. The location of the origin of a paced beat would be situated endocardial since the pacing electrode was placed in contact with the endocardium of the ventricular wall via the jugular vein Dunnink et al. (2017). However as written in section 2.2, this pacing electrode was placed in the right ventricular apex while on the figure is seen that the paced beat came consistently from the left ventricular apex. This can be explained by the fact that there are no needles recording the activity in the tip of the apex. Presumably, the depolarization wave moves faster towards the left ventricle than upwards in the right ventricle.

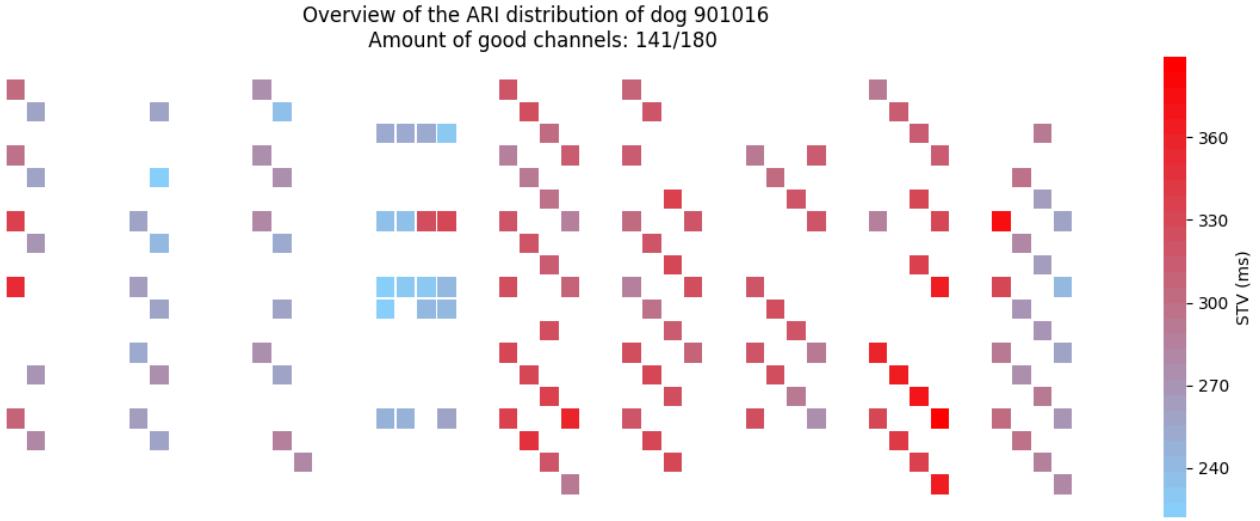

Figure 6.13: An overview of the ARI distribution presented on an electrode map for dog 901016. The ARI was determined in the last analysed beat in the time period 17.5-59.6 s during the dofetilide recording, which was analysed for the STV project.

Notice that in some cases a significant amount of channels were not of good quality. This might lead to a wrong determination of the origin of the paced beat and/or ectopic beat. An example of such an episode is episode 38. The paced beat is initiated near the base, shown in figure 6.14, in stead of near the apex. To understand this phenomenon all the UEG signals of the 5 needles posterior to the septum in the left ventricle were analysed. These UEG signals are depicted per needle in figures 6.15, 6.16, 6.17, 6.18 & 6.19. On these figures is seen that the paced beat is initiated by channel 34 since the smallest upward peak is seen at the paced beat. A possible explanation is the initiation of an ectopic beat just before the offset of the paced beat. Another possible explanation is the occurrence of human error. Since the needles are plugged into a console, these needles might be switched. This would imply the the signal comes form a different location than depicted on the electrode map.

Figure 6.14: The origin of the paced beat during episode 38 in dog 901016.

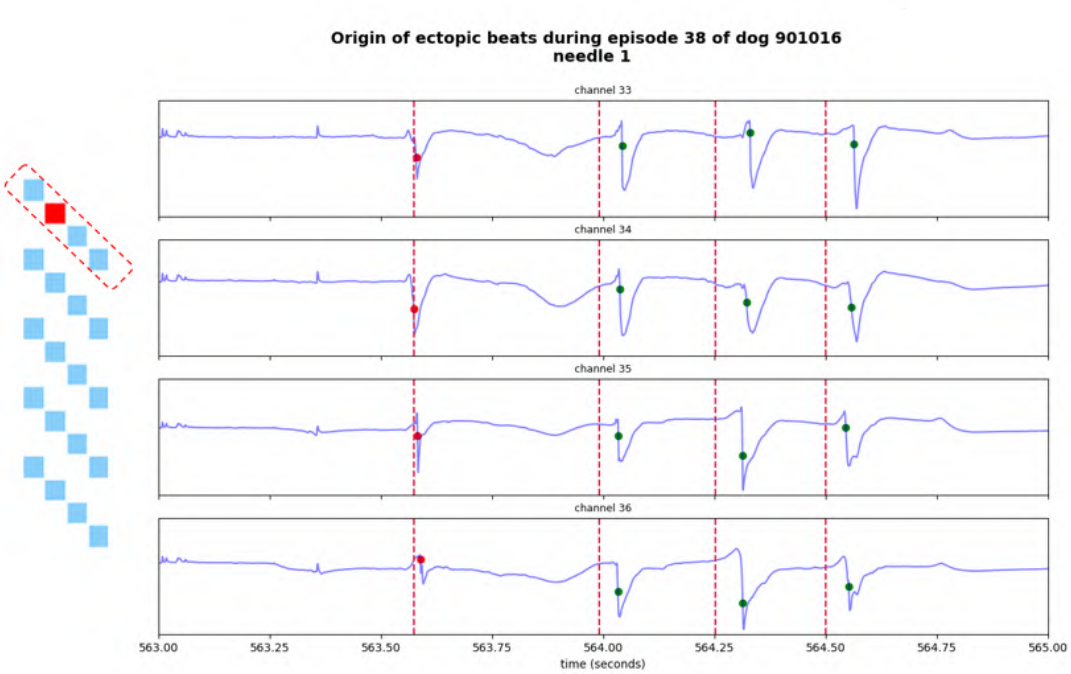

Figure 6.15: The UEG signals of channels 33 (epicardial), 34, 35 & 36 (endocardial) on the first needle during episode 38 are shown. The initial data is represented in blue, the red and green dot represent respectively the local time of excitation of the paced and ectopic beat. The dashed vertical lines represent the first local time of excitation of the beat. On the left sub-plot the considered needle is depicted in the red dashed box.

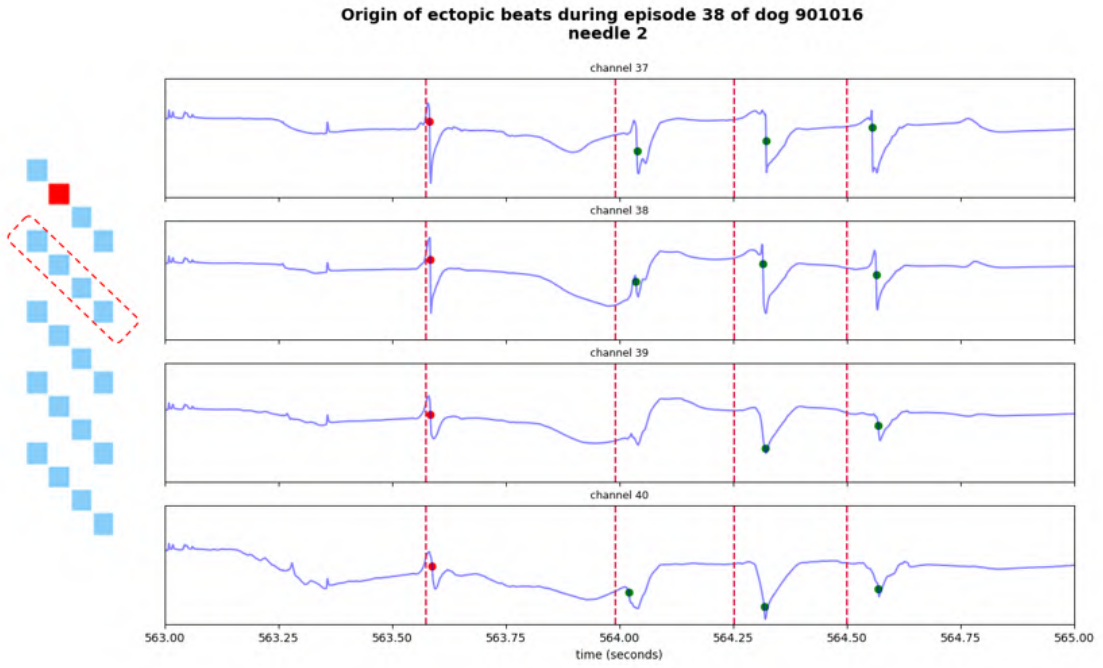

Figure 6.16: The UEG signals of channels 37 (epicardial), 38, 39 & 40 (endocardial) on the second needle during episode 38 are shown. The initial data is represented in blue, the red and green dot represent respectively the local time of excitation of the paced and ectopic beat. The dashed vertical lines represent the first local time of excitation of the beat. On the left sub-plot the considered needle is depicted in the red dashed box

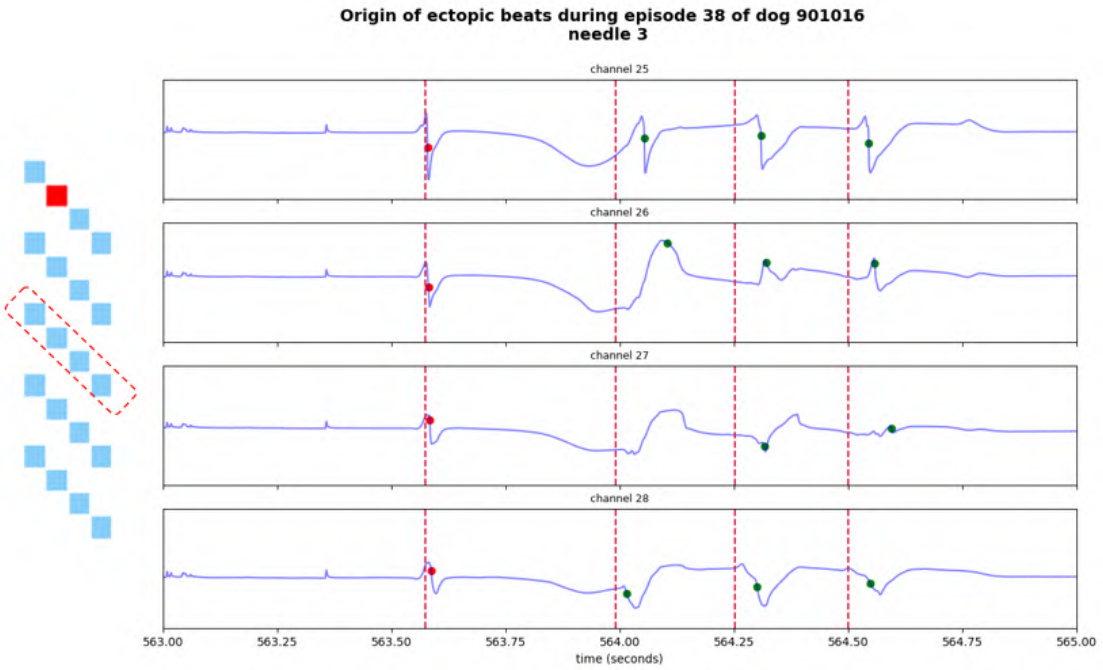

Figure 6.17: The UEG signals of channels 25 (epicardial), 26, 27 & 28 (endocardial) on the third needle during episode 38 are shown. The initial data is represented in blue, the red and green dot represent respectively the local time of excitation of the paced and ectopic beat. The dashed vertical lines represent the first local time of excitation of the beat. On the left sub-plot the considered needle is depicted in the red dashed box

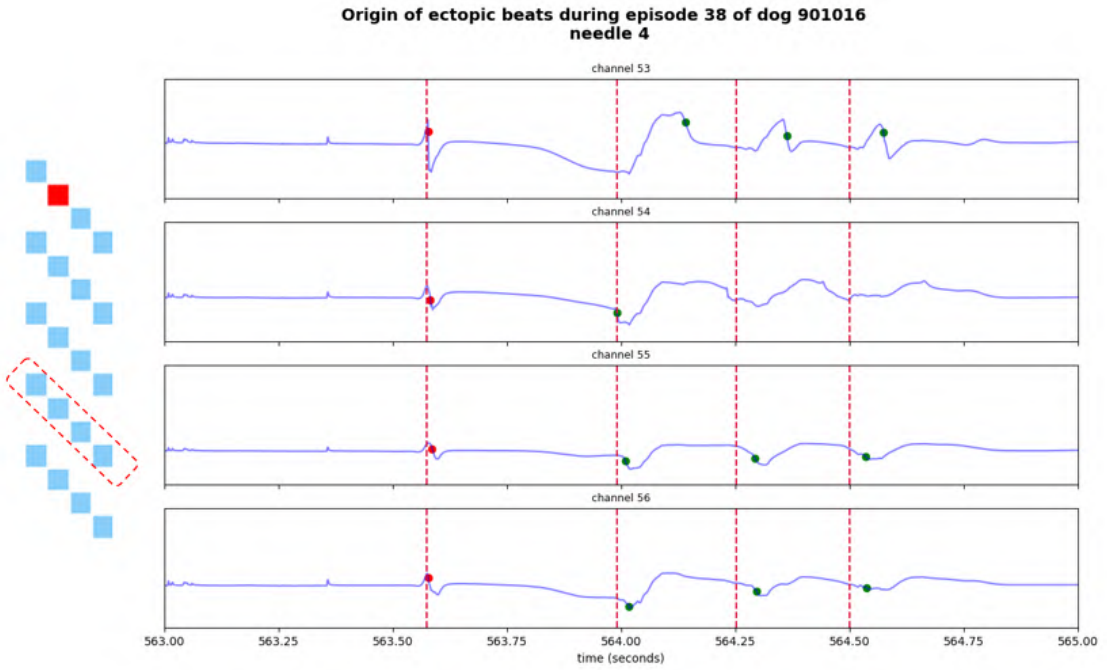

Figure 6.18: The UEG signals of channels 53 (epicardial), 54, 55 & 56 (endocardial) on the fourth needle during episode 38 are shown. The initial data is represented in blue, the red and green dot represent respectively the local time of excitation of the paced and ectopic beat. The dashed vertical lines represent the first local time of excitation of the beat. On the left sub-plot the considered needle is depicted in the red dashed box

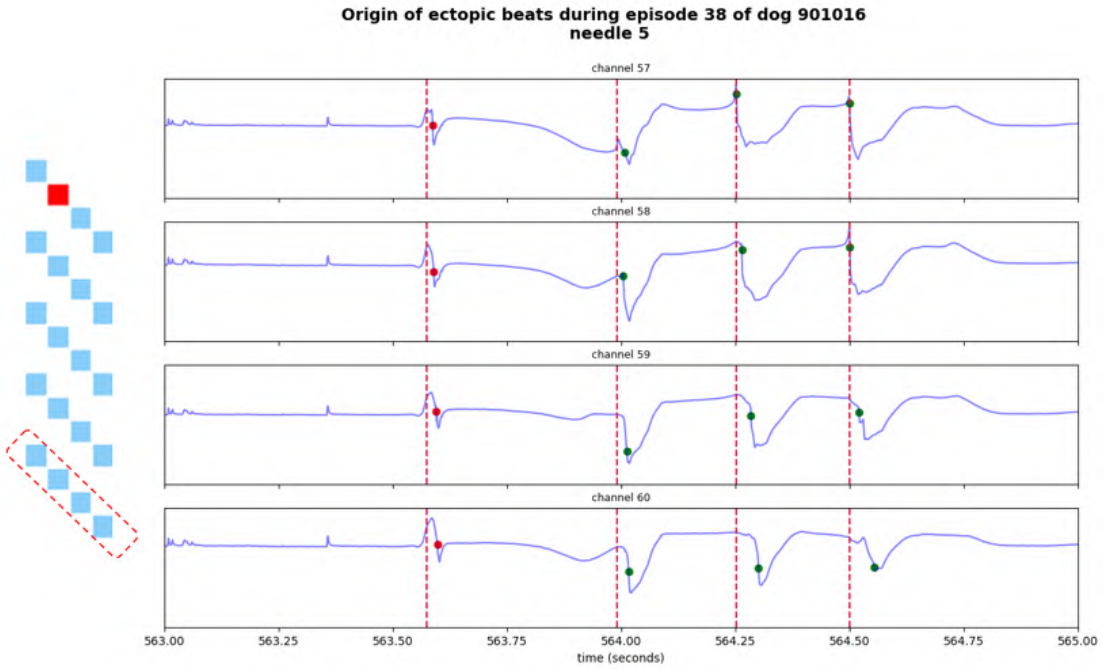

Figure 6.19: The UEG signals of channels 57 (epicardial), 58, 59 & 60 (endocardial) on the fifth needle during episode 38 are shown. The initial data is represented in blue, the red and green dot represent respectively the local time of excitation of the paced and ectopic beat. The dashed vertical lines represent the first local time of excitation of the beat. On the left sub-plot the considered needle is depicted in the red dashed box

6.5 Conclusion

For dog 901016, the distribution of origins of the ectopic beats is heterogeneous. Therefore it was concluded that the ectopic beat origins in preferable locations. It is presumed that the theory of Vandersickel et al. (2016) is more likely. Depending on the amount of beats in the episode, the preferable location to initiate the ectopic beats changes. This shift might be due to a difference in local characteristics of the tissue.

6.6 Limitations

Only one dog is analysed which does not allow to draw a general conclusion for Torsade de Pointes. Since a limited amount of episodes ($32/115$ episodes) contained more than 1 ectopic beat, questions should be posed as whether this is enough to determine a trend. The distance between the different electrodes is around 1.2 cm which does not allow to determine the exact position of the origin of the beat (Vandersickel et al., 2017).

Another limitation of this project is that it is done by myself who has a limited insight in the different UEG signals. No statistical analysis has been done therefore the statementthat distribution of origins of the ectopic beats is heterogeneous should be carefully interpret.

6.7 Future work

The analysis must be done for all the different dogs in order to see whether the trend is visible or not. A statistical analysis should be preformed to analyse whether the distribution of the ectopic beats is heterogeneous. Also a comparison between the different dogs should be made: is the left ventricle more prone for initiation ectopic beats?

Chapter 7

Conclusion

Currently no general conclusion for Torsade de Pointes (TdP) can be drawn since only 1 dog was analysed.

From the results of the analysed dog was derived that the short-term variability (STV) of the activation repolarization interval (ARI) did not show an increase in the unipolar electrogram (UEG) data just before the offset of the first ectopic beat. Presumably the determination of STV was highly dependent on the morphology of the T-wave.

Since the trend on a STV increase was not seen, no further conclusion could be drawn concerning the distribution of the STV and its correlation with the preferable locations of the origins of ectopic beats.

Further research might gain more insight in why the STV was not increased in UEG while this trend is seen in similar data as intracardiac electrogram (EGM) data and monophasic action potential (MAP) data.

For the analysed dog, the distribution of origins of the ectopic beats was heterogeneous. Therefore it is presumed that the ectopic beat are initiated in preferable locations, which implies that the theory of Vandersickel et al. (2016) is more likely. Depending on the amount of beats in the episode, the preferable location to initiate the ectopic beats changes. This shift might be due to a difference in local characteristics of the tissue.

References

Black, J. M., & Hawks, J. H. (2009). *Medical-surgical nursing*. Saunders/Elsevier,.

Boulaksil, M., Jungschleger, J. G., Antoons, G., Houtman, M. J., de Boer, T. P., Wilders, R., ... others (2011). Drug-induced torsade de pointes arrhythmias in the chronic av-block dog are perpetuated by focal activity. *Circulation: Arrhythmia and Electrophysiology*, CIRCEP–110.

Brennan, M., Palaniswami, M., & Kamen, P. (2001). Do existing measures of poincare plot geometry reflect nonlinear features of heart rate variability? *IEEE transactions on biomedical engineering*, *48*(11), 1342–1347.

Burns, Edward. (2017a). *Polymorphic vt & torsade de pointes (tdp).* Retrieved from `https://lifeinthefastlane.com/ecg-library/tdp/` ([Online; accessed November 26th, 2017])

Burns, Edward. (2017b). *Ventricular tachycardia – monomorphic.* Retrieved from `https://lifeinthefastlane.com/ecg-library/ventricular-tachycardia/` ([Online; accessed November 26th, 2017])

Cardiac action potentials in different areas of the heart. (2009). Retrieved from `https://epfellow.wordpress.com/2009/08/27/cardiac-action-potentials-in-different-areas/` ([Online; accessed March 27th, 2018])

Chen, P.-S., Moser, K. M., Dembitsky, W. P., Auger, W. R., Daily, P. O., Calisi, C. M., ... Feld, G. K. (1991). Epicardial activation and repolarization patterns in patients with right ventricular hypertrophy. *Circulation*, *83*(1), 104–118.

Clarkson. (n.d.). *Cardiac action potentials.* Retrieved from `http://www.nataliescasebook.com/tag/cardiac-action-potentials` ([Online; accessed March 25th, 2018])

Colucci, W. (2008). Pathophysiology of heart failure: Neurohumoral adaptations. *UpToDate*, *15*, 3.

Coronel, R., de Bakker, J. M., Wilms-Schopman, F. J., Opthof, T., Linnenbank, A. C., Belterman, C. N., & Janse, M. J. (2006). Monophasic action potentials and activation recovery intervals as measures of ventricular action potential duration: experimental evidence to resolve some controversies. *Heart Rhythm*, *3*(9), 1043–1050.

de Lange, E., Xie, Y., & Qu, Z. (2012). Synchronization of early afterdepolarizations and arrhythmogenesis in heterogeneous cardiac tissue models. *Biophysical journal*, *103*(2), 365–373.

Dixon, J. A., & Spinale, F. G. (2009). Large animal models of heart failure. *Circulation: Heart Failure*, *2*(3), 262–271.

Drew, B. J., Ackerman, M. J., Funk, M., Gibler, W. B., Kligfield, P., Menon, V., ... others (2010). Prevention of torsade de pointes in hospital settings. *Circulation*, *121*(8), 1047–1060.

Dunnink, A. (2016). *The relation between bradycardic dyssynchronous ventricular activation, remodeling and arrhythmogenesis* (Unpublished doctoral dissertation). Uitgeverij BOX-Press.

Dunnink, A., Stams, T. R., Bossu, A., Meijborg, V. M., Beekman, J. D., Wijers, S. C., ... Vos, M. A. (2017). Torsade de pointes arrhythmias arise at the site of maximal heterogeneity of repolarization in the chronic complete atrioventricular block dog. *EP Europace*, *19*(5), 858–865.

El-Sherif, N., Chinushi, M., Caref, E. B., & Restivo, M. (1997). Electrophysiological mechanism of the characteristic electrocardiographic morphology of torsade de pointes tachyarrhythmias in the long-qt syndrome: detailed analysis of ventricular tridimensional activation patterns. *Circulation*, *96*(12), 4392–4399.

Ep principles: Catheter positioning. (2016). Retrieved from `https://www.springboardhealthcare.com/wp-content/uploads/2017/06/13-EP-PRINCIPLES-Catheter-Positioning.pdf` ([Online; accessed April 16th, 2018])

Goldberger, J. J., & Ng, J. (2010). *Practical signal and image processing in clinical cardiology*. Springer.

Hasenfuss, G. (1998). Animal models of human cardiovascular disease, heart failure and hypertrophy. *Cardiovascular research*, *39*(1), 60–76.

Haws, C. W., & Lux, R. L. (1990). Correlation between in vivo transmembrane action potential durations and activation-recovery intervals from electrograms. effects of interventions that alter repolarization time. *Circulation*, *81*(1), 281–288.

Hu, R., Stevenson, W. G., & Lilly, L. S. (2012). Clinical aspects of cardiac arrhythmias. In L. S. Lilly (Ed.), *Pathophysiology of heart disease: a collaborative project of medical students and faculty* (p. 279-300). Boston: Lippincott Williams & Wilkins.

Hu, R., Stevenson, W. G., Strichartz, G. R., & Lilly, L. S. (2012). Mechanisms of cardiac arrhythmias. In L. S. Lilly (Ed.), *Pathophysiology of heart disease: a collaborative project of medical students and faculty* (p. 261-278). Boston: Lippincott Williams & Wilkins.

Huikuri, H. V., Castellanos, A., & Myerburg, R. J. (2001). Sudden death due to cardiac arrhythmias. *New England Journal of Medicine*, *345*(20), 1473–1482.

Kadish, A. (2004). *What is a monophasic action potential?* Elsevier Science.

Kay, N. G., Dosdall, D. J., & Shepard, R. B. (2011). Cardiac electrical stimulation. In K. A. Ellenbogen, B. L. Wilkoff, G. N. Kay, C. P. Lau, & A. Auricchio (Eds.), *Clinical cardiac pacing, defibrillation and resynchronization therapy* (p. 1-39). Elsevier Health Sciences.

Klabunde, Richard E. (2016). *Electrocardiogram (ekg, ecg).* Retrieved from `http://www.cvphysiology.com/Arrhythmias/A009` ([Online; accessed November 24th, 2017])

Kozhevnikov, D. O., Yamamoto, K., Robotis, D., Restivo, M., & El-Sherif, N. (2002). Electrophysiological mechanism of enhanced susceptibility of hypertrophied heart to acquired torsade de pointes arrhythmias: tridimensional mapping of activation and recovery patterns. *Circulation*, *105*(9), 1128–1134.

Lin, K. Y., Edelmand, E. R., Strichartz, G., & Lilly, L. S. (2012). Basic cardiac structure and function. In L. S. Lilly (Ed.), *Pathophysiology of heart disease: a collaborative project of medical students and faculty* (p. 1-27). Boston: Lippincott Williams & Wilkins.

Locati, E. H., Maison-Blanche, P., Dejode, P., Cauchemez, B., & Coumel, P. (1995). Spontaneous sequences of onset of torsade de pointes in patients with acquired prolonged repolarization: quantitative analysis of holter recordings. *Journal of the American College of Cardiology*, *25*(7), 1564–1575.

Marieb, E. N., & Hoehn, K. (2016). *Human anatomy & physiology* (10th ed.). Pearson Education.

Potse, M., Linnenbank, A. C., & Grimbergen, C. A. (2002). Software design for analysis of multichannel intracardial and body surface electrocardiograms. *Computer methods and programs in biomedicine*, *69*(3), 225–236.

Roden, D. M. (1998). Taking the "idio" out of "idiosyncratic": predicting torsades de pointes. *Pacing and Clinical Electrophysiology*, *21*(5), 1029–1034.

Romedli, S. R., & Lilly, L. S. (2012). The electrocardiogram. In L. S. Lilly (Ed.), *Pathophysiology of heart disease: a collaborative project of medical students and faculty* (p. 75-112). Boston: Lippincott Williams & Wilkins.

Schmitt, H., Cabo, C., Costeas, C., Coromilas, J., & Wit, A. L. (2001). Mechanisms for spontaneous changes in qrs morphology sometimes resembling torsades de pointes during reentrant ventricular tachycardia in a canine infarct model. *Journal of cardiovascular electrophysiology*, *12*(6), 686–694.

Schreiner, K. D., Voss, F., Senges, J. C., Becker, R., Kraft, P., Bauer, A., ... Schoels, W. (2004). Tridimensional activation patterns of acquired torsade-de-pointes-tachycardias in dogs with chronic av-block. *Basic research in cardiology*, *99*(4), 288–298.

Schwartz, P. J., & Woosley, R. L. (2016). Predicting the unpredictable: drug-induced qt prolongation and torsades de pointes. *Journal of the American College of Cardiology*, *67*(13), 1639–1650.

Sieroslawska, Alexandra. (2017). *Cardiac skeleton.* Retrieved from `https://www.kenhub.com/en/library/anatomy/cardiac-skeleton` ([Online; accessed December 13th, 2017])

Stevenson, W. G., & Soejima, K. (2005). Recording techniques for clinical electrophysiology. *Journal of cardiovascular electrophysiology*, *16*(9), 1017–1022.

Swerdlow, C., Chow, T., Das, M., Gillis, A. M., Zhou, X., Abeyratne, A., & Ghanem, R. N. (2011). Intracardiac electrogram t-wave alternans/variability increases before spontaneous ventricular tachyarrhythmias in implantable cardioverter-defibrillator patientsclinical perspective: A prospective, multi-center study. *Circulation*, *123*(10), 1052–1060.

Thomsen, M. B., Verduyn, S. C., Stengl, M., Beekman, J. D., de Pater, G., van Opstal, J., ... Vos, M. A. (2004). Increased short-term variability of repolarization predicts d-sotalol–induced torsades de pointes in dogs. *Circulation*, *110*(16), 2453–2459.

Tse, G. (2016). Mechanisms of cardiac arrhythmias. *Journal of arrhythmia*, *32*(2), 75–81.

Vandael, E., Vandenberk, B., Vandenberghe, J., Pincé, H., Willems, R., & Foulon, V. (2017). Incidence of torsade de pointes in a tertiary hospital population. *International Journal of Cardiology*.

Vandael, E., Vandenberk, B., Vandenberghe, J., Willems, R., & Foulon, V. (2017). Cases of drug-induced torsade de pointes: a review of belgian cases in the eudravigilance database. *Acta Clinica Belgica*, 1–6.

Vandersickel, N., Boer, T. P., Vos, M. A., & Panfilov, A. V. (2016). Perpetuation of torsade de pointes in heterogeneous hearts: competing foci or re-entry? *The Journal of physiology*, *594*(23), 6865–6878.

Vandersickel, N., Bossu, A., De Neve, J., Dunnink, A., Meijborg, V. M., van der Heyden, M. A., ... Panfilov, A. V. (2017). Short-lasting episodes of torsade de pointes in the chronic atrioventricular block dog model have a focal mechanism, while longer-lasting episodes are maintained by re-entry. *JACC: Clinical Electrophysiology*, *3*(13), 1565–1576.

Vornanen, M. (2016). *The temperature dependence of electrical excitability in fish hearts* (Vol. 219) (No. 13). The Company of Biologists Ltd.

Vos, M., De Groot, S., Verduyn, S., Van der Zande, J., Leunissen, H., Cleutjens, J., ... others (1998). Enhanced susceptibility for acquired torsade de pointes arrhythmias in the dog with chronic, complete av block is related to cardiac hypertrophy and electrical remodeling. *Circulation*, *98*(11), 1125–1135.

Walcott, G. P., Pogwizd, S. M., & Ideker, R. E. (2011). Principles of defibrillation: From cellular physiology to fields and waveforms. In K. A. Ellenbogen, B. L. Wilkoff, G. N. Kay, C. P. Lau, & A. Auricchio (Eds.), *Clinical cardiac pacing, defibrillation and resynchronization therapy* (p. 41-55). Elsevier Health Sciences.

Webdicine, Smarter Medical Care. (2011). *heartrhythm.* Retrieved from `http://www.webdicine.com/abnormal-heart-rate.html/heartrhythm` ([Online; accessed November 24th, 2017])

Western, D., Hanson, B., & Taggart, P. (2014). Measurement bias in activation-recovery intervals from unipolar electrograms. *American Journal of Physiology-Heart and Circulatory Physiology*, *308*(4), H331–H338.

Wijers, S. C., Ritsema van Eck, H., Doevendans, P. F., Meine, M., & Vos, M. A. (n.d.). Fiducial segment averaging for accurate determination of the inflection points on the 12-lead surface ecg and semi automatic measurement of qt variability.

Wijers, S. C., Sprenkeler, D. J., Bossu, A., Dunnink, A., Beekman, J. D., Varkevisser, R., ... Vos, M. A. (2017). Beat-to-beat variations in activation-recovery interval derived from the right ventricular electrogram can monitor arrhythmic risk under anesthetic and awake conditions in the canine chronic atrioventricular block model. *Heart rhythm*.

Appendix A

Electrode Maps

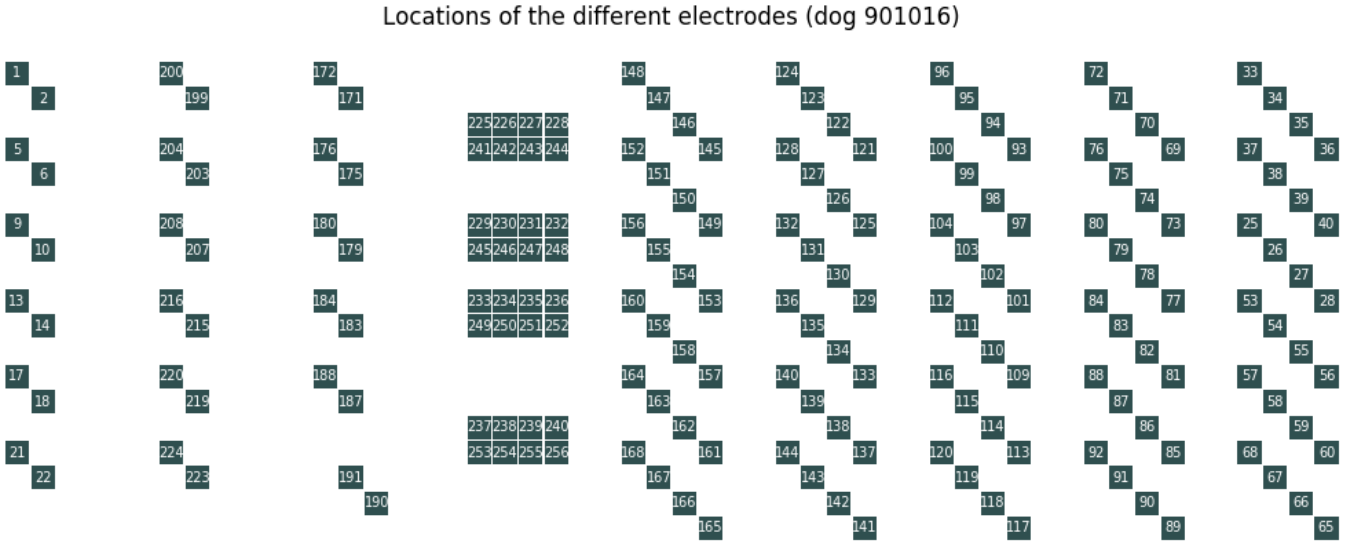

Figure A.1: An electrode map with the electrode labels for dog 901016.

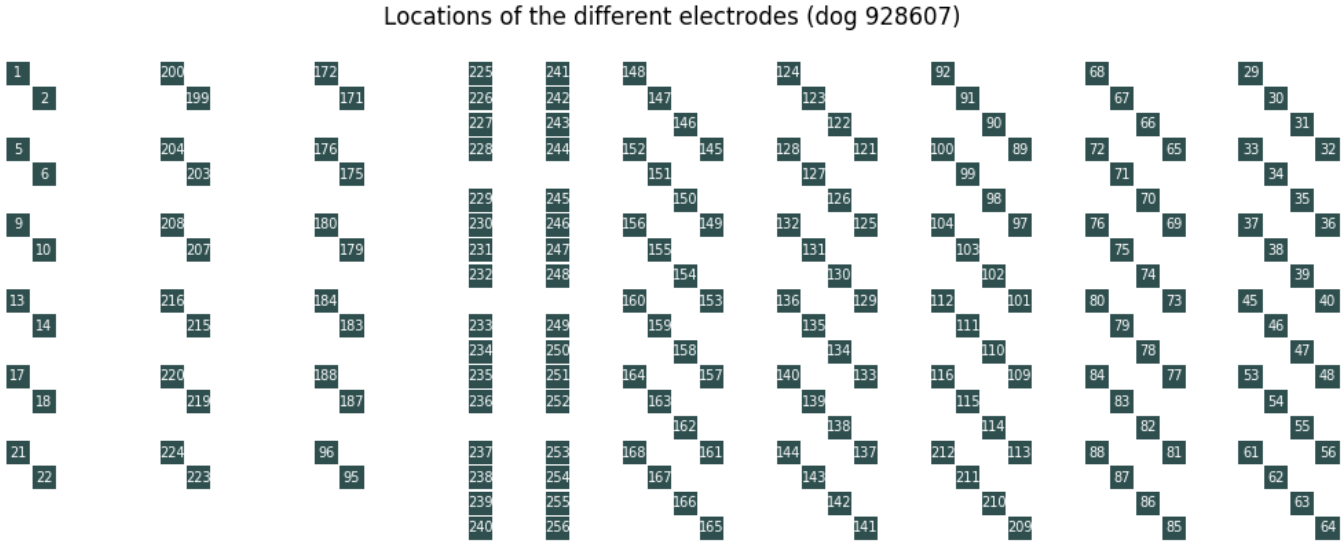

Figure A.2: An electrode map with the electrode labels for dog 928607.

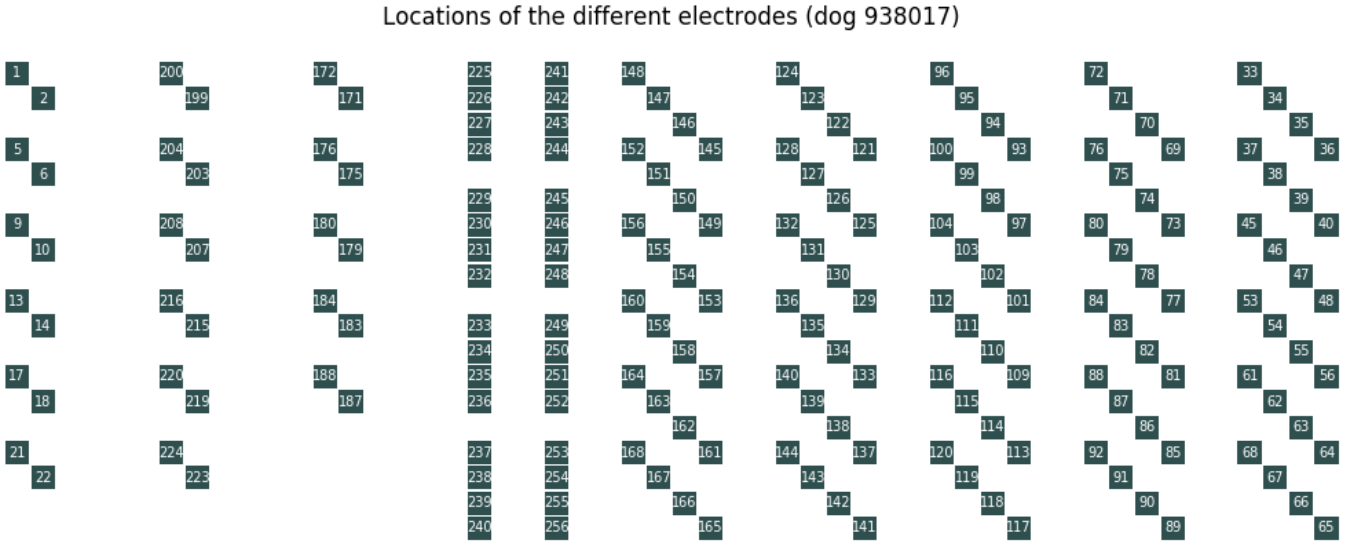

Figure A.3: An electrode map with the electrode labels for dog 938017.

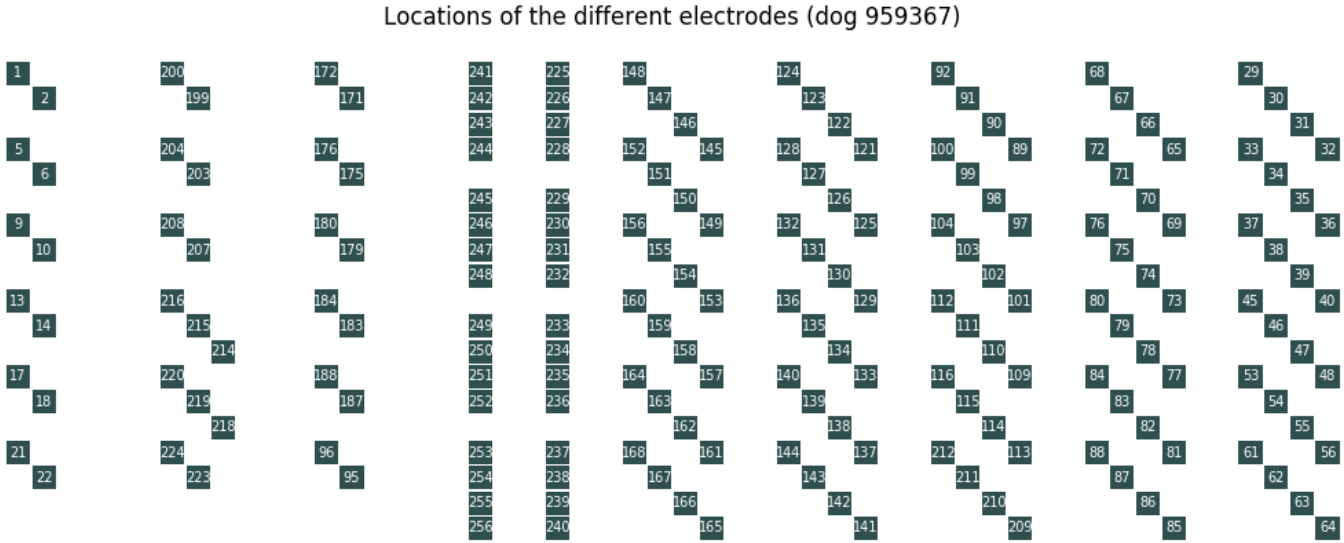

Figure A.4: An electrode map with the electrode labels for dog 959367.

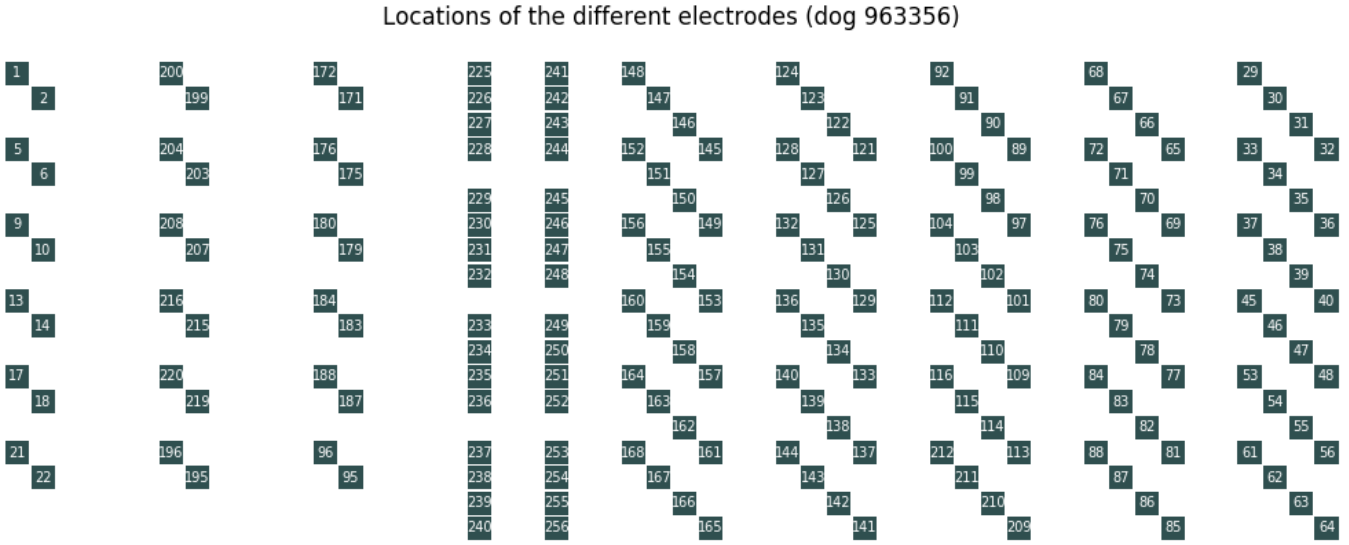

Figure A.5: An electrode map with the electrode labels for dog 963356.

Appendix B

Scripts ’STV as Biomarker’

```
import numpy as np
from scipy.signal import argrelextrema
from data_analysis import gauss_filter

def filter(initialdata, t1):
      ''' This function filters the data in order to smooth the signal and
      makes it this way less sensitive to noise.
       initial data    - initial data which needs to be filtered
       t1              - start time of the initial data
       returns the filtered signal and the corresponding time '''

    # parameters
    dt = 1.0 / 2048     # time (s) between two data points of the bdf trace
    sigma = 15          # standard deviation - characteristic needed for
                        filtering
    artefactgauss = 60  # removal of data points which are artefact of the
                        gaussian filter

    # filtering and correction for the artefact of the filter
    initialdata = gauss_filter(initialdata, sigma)
    data = initialdata[artefactgauss:len(initialdata) - artefactgauss]

    # corresponding time
    time = range(len(data))
    time = [(t + artefactgauss)*dt + t1 for t in time]
    return data, time


def find_max_neg_derivative(derivative, initial_data, t1):
      ''' This function filters finds the local time of excitation and its
      corresponding data point.
       derivative      - derivative of the filtered data
       t1              - start time of the initial data
      returns the points of excitation and the indices of these points on
      the initial data '''

    # parameters
    threshold = -35         # threshold for derivative
    window = 2048           # amount of data points within 1 second
   window_raw_data = 40    # defined window for searching the steepest
                             negative derivative
    artefactgauss = 60      # removal of data points which are artefact of
                             the gaussian filter
    dt = 1.0 / 2048         # time (s) between two data points of the bdf
                             trace

    # find the relative negative maxima of the negative derivative
    inirelmin = list(argrelextrema(derivative, np.less)[0])
```

```
# find the relative negative maxima which correspond to the local time
      of excitation
   # first criteria: the derivative must be steep enough to ensure that no
      noise is elected
   # second criteria: the derivative must at least 1 second after the
      previous beat
    relmin = []
    for index in inirelmin:
        if derivative[index] < threshold and relmin==[]:
            relmin = np.append(relmin, index)
        if derivative[index] < threshold and index > relmin[-1]+window:
            relmin = np.append(relmin, index)
    # transfer to raw data
    indices_to_rawdata = [int(index + artefactgauss) for index in relmin]

# find around these indices the steepest derivative on the raw data in the
     neighbourhood of these indices
    datapoints = []
    indices = []
    for index in indices_to_rawdata:
        data = initial_data[index-window_raw_data:index+window_raw_data]
        derivative = np.diff(data)
        minimum_index_derivative = np.argmin(derivative)
        minimum_index = index - window_raw_data + minimum_index_derivative
        minimum_data = data[minimum_index_derivative]
        datapoints = np.append(datapoints,minimum_data)
        indices = np.append(indices,minimum_index)

    # transfer indices to time points
    timepoints = [index * dt + t1 for index in indices]

    # combine time points and data points
    points = np.array(zip(timepoints, datapoints))

    return points, indices
```

```
def find_max_pos_derivative(indices_excitation, derivative, initial_data,
t1):
      ''' This function filters finds the local time of repolarization and
      its corresponding data point.
       indices_excitation  - indices of points of excitation on the initial
                             data
       derivative          - derivative of the filtered data
       t1                  - start time of the initial data
       returns the points of repolarization '''

    # parameters
    window = 2048           # amount of data points within 1 second
    removepeak = 300        # amount of data points which are part of the
                              upward slope after local time of excitation
    dt = 1.0 / 2048         # time (s) between two data points of the bdf
                              trace
    window_raw_data = 50    # defined window for searching the steepest
                              positive derivative
    artefactgauss = 60      # removal of data points which are artefact of
                              the gaussian filter


    # transfer indices of excitation to filtered data
    indices_excitation_filtered = [int(index - artefactgauss) for index in
    indices_excitation]

    # find after the local time of excitation the local time of
       repolarization on the filtered data
    relmax = []
    for index in indices_excitation_filtered:
        set = derivative[int(index) + removepeak:int(index) + window / 2]
        if set != []:
            set = derivative[int(index) + removepeak:int(index) + window / 2]
            setmax = np.argmax(set)
            setmax = index + setmax + removepeak
            relmax = np.append(relmax, setmax)

    # transfer to rough data
    indices_to_roughdata = [int(index) + 60 for index in relmax]

    # find around these indices the steepest derivative on the raw data in
       the neighbourhood of these indices
    datapoints = []
    indices = []
    for index in indices_to_roughdata:
        data = initial_data[index-window_raw_data:index+window_raw_data]
        derivative = np.diff(data)
        maximum_index_derivative = np.argmax(derivative)
        maximum_index = index - window_raw_data + maximum_index_derivative
        maximum_data = data[maximum_index_derivative]
        datapoints = np.append(datapoints,maximum_data)
        indices = np.append(indices,maximum_index)

    # transfer indices to time points
    timepoints = [index*dt + t1 for index in indices]

    # combine time points and data points
    points = np.array(zip(timepoints, datapoints))

    return points, indices
```

```
import matplotlib.pyplot as plt
import math
import numpy as np
import os
import CreateHeatmap as Heat
import pickle

def identification_channel(dict_evaluation):
    ''' This function evaluates the outcome of the visual inspection.
       dict_evaluation     - a dictionary with the channel as key and as
                             value 'good' or 'bad'
       returns the amount good and bad channels as well as an array
      containing all the good channels '''

    # initial parameters
    amount_good=0
    amount_bad=0
    good_channels=[]

    # for-loop over all channels in the dictionary
    for key in dict_evaluation.keys():
        if dict_evaluation[key]=='good':
            amount_good += 1
            good_channels=np.append(good_channels,key)
        if dict_evaluation[key]=='bad':
            amount_bad += 1

    return amount_good,amount_bad,good_channels


def STV_calculation(times_min,times_max,channel):
    ''' This function calculates the value of the STV of one channel.
       times_min   - local times of excitation
       times_max   - local times of repolarization
       channel     - channel number
       returns a value for the STV (returns a STV = 0 for bad channels) '''

    # remove duplicates
    times_min = np.unique(times_min)
    times_max = np.unique(times_max)

    # amount of local times of excitation and local times of repolarization
    amount_red=len(times_min)
    amount_yellow=len(times_max)

    # amount of times must be equal to 31 in order to calculate the STV
    if amount_red < 31:
        print('Channel {0}: Not enough beats to calculate the STV. Missing
              red dot?'.format(int(channel)))
    if amount_yellow < 31:
        print('Channel {0}: Not enough beats to calculate the STV. Missing
              yellow dot?'.format(int(channel)))
```

```
# for every channels containing 31 beats the STV is calculated
if amount_red == 31 and amount_yellow == 31:
    # initial parameters
    sum_D=0
    duration_ARIs = []
    # loop over all the beats during the time period to calculate the
   STV
    for index in range(0,amount_red):
        duration_ARI=abs(times_max[index]-times_min[index])*1000
   #calculation in ms
        if index != 0:
            D=abs(duration_ARI-duration_ARIs[-1])
            duration_ARIs = np.append(duration_ARIs, duration_ARI)
            sum_D += D
        else:
            duration_ARIs = np.append(duration_ARIs, duration_ARI)
    STV=sum_D/(30*math.sqrt(2))

else:
    print('No STV calculated from channel {0}'.format(channel))
    STV=0

return STV
```

```
def pointcare_plot(times_min,times_max,channel,STV,title,path):
    ''' This function creates a pointcare plot for the considered channel.
        times_min    - local times of excitation
        times_max    - local times of repolarization
        channel      - channel number
        STV          - value of the STV
        title        - title of the pointcare plot
        path         - path the save the figure '''

    # check whether 31 beats are present
    if len(np.unique(times_min)) != len(np.unique(times_max)):
        print('There is a different amount of Red and Yellow Points in
       channel {0}'.format(int(channel)))
    else:
        # create the data which needs to be plotted against each other
        ARI_duration=[(times_max[index]-times_min[index])*1000 for index in
       range(0,len(times_min))]

        amount=len(ARI_duration)
        ARI_duration_xvalues=ARI_duration[0:amount-1]
        ARI_duration_yvalues=ARI_duration[1:amount]

        # plot the data
        plt.plot(ARI_duration_xvalues, ARI_duration_yvalues, color='green')
        plt.title(title)
        plt.xlabel('Duration QT-interval[n-1] (ms)')
        plt.ylabel('Duration QT-interval[n] (ms)')
        plt.xlim(200, 400)
        plt.ylim(200, 400)
        # plot a straight line
        x = np.linspace(200, 600, 100)
        plt.plot(x, x, color='grey')
        plt.text(400,380,
       'STV={0}'.format(STV),horizontalalignment='right',verticalalignment=
       'top')
        plt.savefig(path,format='svg', dpi=1200)
        plt.close()
```

```
def
STV_channels(filename_evaluation,filename_min,filename_max,dog,base,PCplot)
:
    ''' This is a function combining the previous function to calculate the
       STV, make pointcare plots of all channels and makes overview plotted
       on an electrode map.
        filename_evaluation     - pickle filename with the dictionary
                                containing for each channel 'good'/'bad'
        filename_min            - pickle filename with the dictionary
                                containing for each channel all the local
                                times of excitation
        filename_max            - pickle filename with the dictionary
                                containing for each channel all the local
                                times of repolarization
        dog                     - dog number
        base                    - 1/0 depending respectively whether the
                                baseline recording is considered or not
        PCplot                  - True/False: when True all the pointcare
                                plots created and saved
        returns a dictionary with all good channels as key the corresponding
       STV as value
         '''

    # loading the pickle files
    dict_evaluation = pickle.load(open(filename_evaluation, 'rb'))
    dict_min = pickle.load(open(filename_min, "rb"))
    dict_max = pickle.load(open(filename_max, "rb"))

    # calculate the amount of good and bad channels as an array containing
       all the good channels
    (amount_good, amount_bad, good_channels) =
identification_channel(dict_evaluation)
    print('Amount of good channels:{0}'.format(amount_good))
    print('Amount of bad channels:{0}'.format(amount_bad))

    # make note in order to save the figures correctly
    if base == 1:
        note='Baseline'
    else:
        note='Dofetilide'

    # initial parameter
    channel_STV=dict()
```

```
# for-loop over all the good channels
    for key in good_channels:
        channel=int(key)
        times_min=np.array(dict_min[key])
        times_max=np.array(dict_max[key])
        STV=STV_calculation(times_min,times_max,channel)
        channel_STV[channel]=STV
        # make pointcare plot
        if PCplot == True and STV != 0:
            title_PC='Channel {2} \n Pointcare plot (dog {0}
              {1})'.format(dog,note,channel)
            directory_PC = 'ResultsUtrecht/PointcarePlots/{0}'.format(dog)
            if os.path.exists(directory_PC) == False:
                os.makedirs(directory_PC)

path_PC='ResultsUtrecht/PointcarePlots/{0}/PointcarePlot_{2}_channel{1}'.fo
rmat(dog,channel,note)
            pointcare_plot(times_min,times_max,channel,STV,title_PC,path_PC)
    # make an overview of the STV values plotted on the electrode map
    # notice: 2 times an overview is made (with and without annotations of
       the values)
    title='STV Overview (dog {0} {1})'.format(dog, note)
    directory='ResultsUtrecht/STVOverview/'
    if os.path.exists(directory) == False:
        os.makedirs(directory)
    path='ResultsUtrecht/STVOverview/STV_Map_{0}_{1}'.format(dog,note)
    for element in [True, False]:
        labels=element
        Heat.make_heatmap(dog,channel_STV,dict_evaluation,title,path,labels)
    return channel_STV
```

Appendix C

Additional figures ’STV as Biomarker’

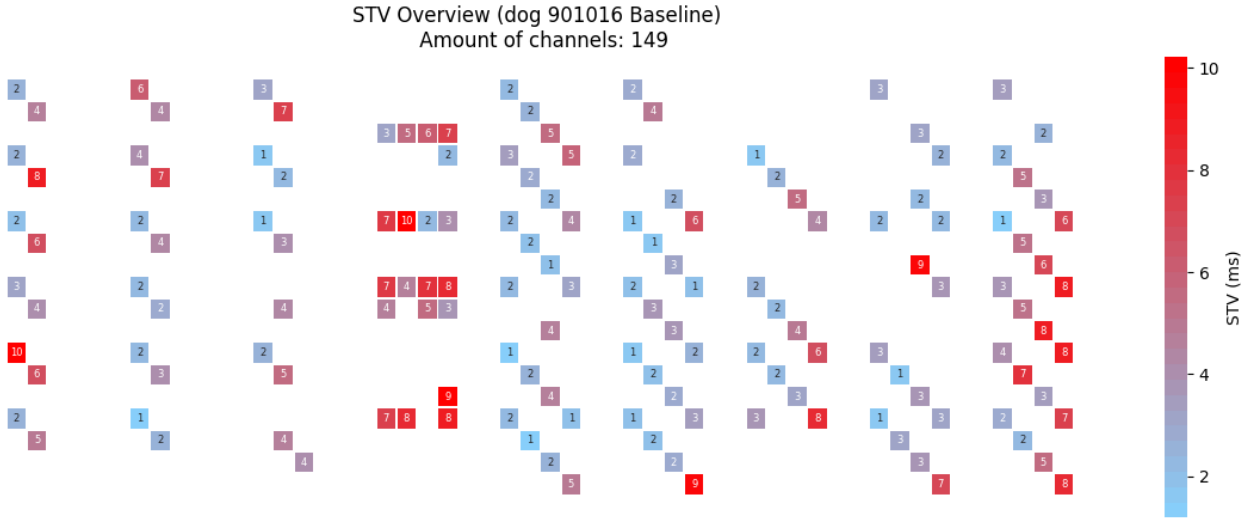

Figure C.1: An overview of the calculated STV values for each channel during the baseline recording presented on an electrode map with annotations for dog 901016.

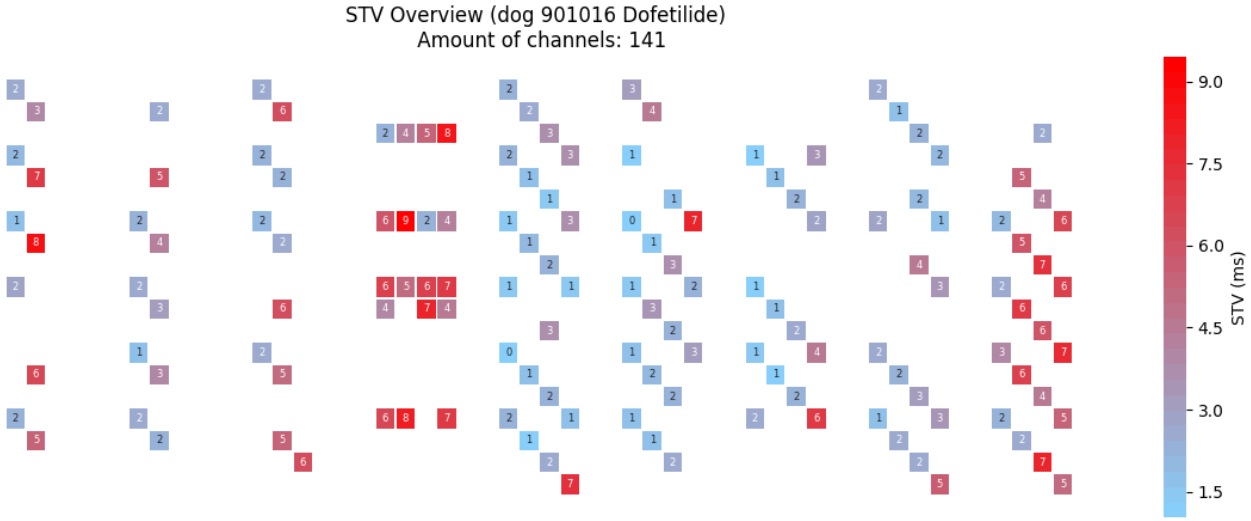

Figure C.2: An overview of the calculated STV values for each channel during the dofetilide recording presented on an electrode map with annotations for dog 901016.

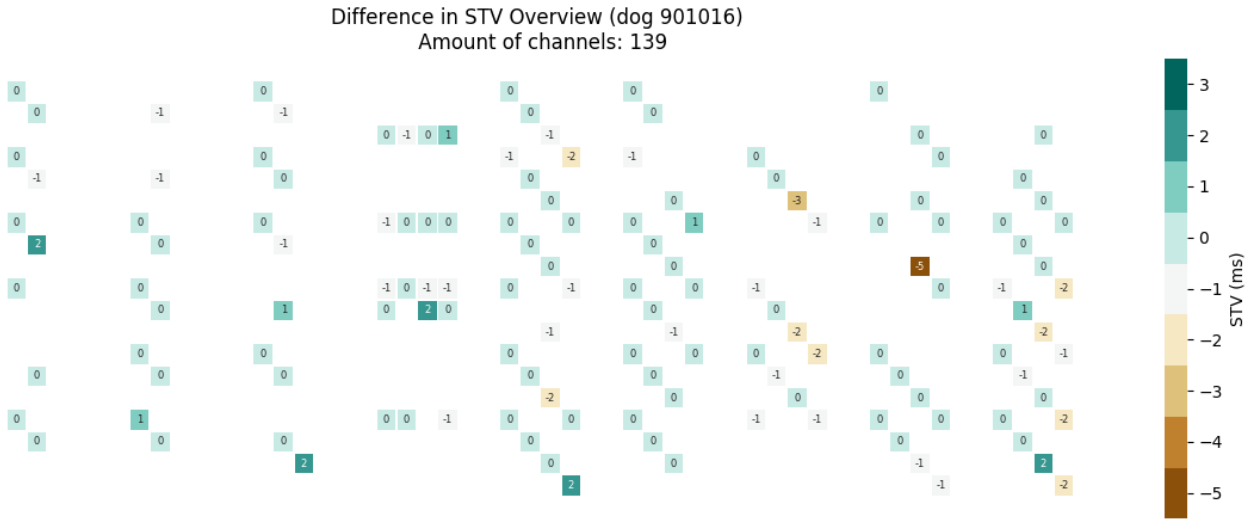

Figure C.3: An overview of the difference in STV values for each channel presented on an electrode map with annotations for dog 901016.

Appendix D

File containing the exact STV values

dog	channel	STV baseline (ms)	STV dofetilide (ms)	Difference (ms)	Positive?
901016	1	2.566484574	2.624029071	0.057544497	1
901016	2	4.776193265	3.890008008	-0.886185256	0
901016	5	2.485922278	2.117637496	-0.368284782	0
901016	6	8.804308067	7.043446453	-1.760861613	0
901016	9	2.094619697	1.806897211	-0.287722486	0
901016	10	6.617617174	8.666201273	2.048584099	1
901016	13	3.118911746	2.923260456	-0.19565129	0
901016	18	6.629126074	6.468001482	-0.161124592	0
901016	21	2.577993473	2.221217591	-0.356775882	0
901016	22	5.098442449	5.409182734	0.310740285	1
901016	25	1.196925541	2.0370752	0.840149659	1
901016	26	5.225040343	5.846520912	0.621480569	1
901016	27	6.985901956	7.331168939	0.345266983	1
901016	28	8.804308067	6.767232867	-2.0370752	0
901016	35	2.64704687	2.451395579	-0.19565129	0
901016	38	5.190513644	5.351638237	0.161124592	1
901016	39	3.728883416	4.26980169	0.540918273	1
901016	40	6.951375258	6.375930286	-0.575444972	0
901016	53	3.705865618	2.63553797	-1.070327647	0
901016	54	5.167495846	6.962884157	1.795388312	1
901016	55	8.896379262	6.019154404	-2.877224858	0
901016	56	8.919397061	7.699453721	-1.21994334	0
901016	57	4.051132601	3.85548131	-0.19565129	0
901016	58	7.998685106	6.847795163	-1.150889943	0
901016	59	3.533232126	4.419417382	0.886185256	1
901016	60	7.377204537	5.328620438	-2.048584099	0
901016	65	8.182827497	5.213531443	-2.969296054	0
901016	66	5.581816225	7.92963171	2.347815484	1
901016	67	2.359324384	2.681573568	0.322249184	1
901016	68	2.750626965	2.382342183	-0.368284782	0
901016	69	2.42837778	2.117637496	-0.310740285	0
901016	70	3.095893948	2.221217591	-0.874676357	0
901016	72	3.141929545	2.63553797	-0.506391575	0
901016	73	2.278762088	1.657281518	-0.621480569	0
901016	74	2.347815484	2.117637496	-0.230177989	0
901016	77	3.878499109	3.464178729	-0.41432038	0
901016	78	9.736528921	4.592050874	-5.144478047	0
901016	80	2.163673093	2.750626965	0.586953871	1
901016	85	3.141929545	3.326071936	0.184142391	1
901016	86	3.809445712	3.118911746	-0.690533966	0
901016	87	1.530683625	2.416868881	0.886185256	1
901016	88	3.429652031	2.497431177	-0.932220854	0
901016	89	7.204571045	5.777467516	-1.42710353	0
901016	90	3.901516908	2.497431177	-1.404085731	0
901016	91	3.03834945	2.63553797	-0.40281148	0
901016	92	1.737843814	1.680299317	-0.057544497	0
901016	97	4.315837288	2.900242657	-1.41559463	0
901016	98	5.466727231	2.198199792	-3.268527439	0
901016	99	2.658555769	1.783879412	-0.874676357	0

dog	channel	STV baseline (ms)	STV dofetilide (ms)	Difference (ms)	Positive?
901016	100	1.645772619	1.277487837	-0.368284782	0
901016	109	6.629126074	4.47696188	-2.152164194	0
901016	110	4.810719963	2.543466775	-2.267253188	0
901016	111	2.175181993	1.749352714	-0.425829279	0
901016	112	2.693082467	1.070327647	-1.62275482	0
901016	113	8.274898693	6.951375258	-1.323523435	0
901016	114	3.118911746	2.278762088	-0.840149659	0
901016	115	2.290270987	1.116363245	-1.173907742	0
901016	116	2.290270987	1.519174725	-0.771096262	0
901016	120	3.85548131	2.554975674	-1.300505636	0
901016	123	4.937317857	4.569033075	-0.368284782	0
901016	124	2.762135864	3.015331652	0.253195788	1
901016	125	6.732706169	7.814542715	1.081836547	1
901016	126	2.497431177	1.783879412	-0.713551765	0
901016	128	2.877224858	1.127872144	-1.749352714	0
901016	129	1.898968407	2.267253188	0.368284782	1
901016	130	3.210982942	3.820954612	0.60997167	1
901016	131	1.691808217	1.358050133	-0.333758084	0
901016	132	1.691808217	0.989765351	-0.702042865	0
901016	133	2.681573568	3.141929545	0.460355977	1
901016	134	3.786427914	2.23272649	-1.553701424	0
901016	135	3.613794422	3.464178729	-0.149615693	0
901016	136	2.071601898	1.484648027	-0.586953871	0
901016	138	2.785153663	2.175181993	-0.60997167	0
901016	139	2.002548501	2.106128596	0.103580095	1
901016	140	1.691808217	1.63426372	-0.057544497	0
901016	142	2.739118065	2.520448976	-0.218669089	0
901016	143	2.014057401	1.63426372	-0.379793681	0
901016	144	1.841423909	1.772370513	-0.069053397	0
901016	145	5.823503113	3.613794422	-2.209708691	0
901016	146	5.512762829	3.636812221	-1.875950608	0
901016	147	2.566484574	2.485922278	-0.080562296	0
901016	148	2.370833283	2.301779887	-0.069053397	0
901016	149	4.304328388	3.832463511	-0.471864877	0
901016	150	2.140655295	1.41559463	-0.725060664	0
901016	151	2.716100266	1.864441708	-0.851658558	0
901016	152	3.510214327	2.23272649	-1.277487837	0
901016	153	3.24550964	1.519174725	-1.726334915	0
901016	154	1.933495105	2.290270987	0.356775882	1
901016	155	2.071601898	1.979530703	-0.092071195	0
901016	156	2.370833283	1.381067932	-0.989765351	0
901016	158	4.776193265	3.636812221	-1.139381044	0
901016	160	2.24423539	1.565210323	-0.679025067	0
901016	161	1.945004004	1.703317116	-0.241686888	0
901016	162	4.546015276	2.405359982	-2.140655295	0
901016	163	2.405359982	1.852932809	-0.552427173	0
901016	164	1.484648027	0.920711955	-0.563936072	0
901016	165	5.063915751	7.469275732	2.405359982	1
901016	166	2.405359982	2.612520171	0.20716019	1

dog	channel	STV baseline (ms)	STV dofetilide (ms)	Difference (ms)	Positive?
901016	167	1.41559463	1.035800949	-0.379793681	0
901016	168	2.301779887	2.393851082	0.092071195	1
901016	171	7.480784632	6.249332392	-1.231452239	0
901016	172	3.234000741	2.554975674	-0.679025067	0
901016	175	2.359324384	2.42837778	0.069053397	1
901016	176	1.576719222	2.405359982	0.828640759	1
901016	179	3.993588103	2.681573568	-1.312014535	0
901016	180	1.737843814	2.152164194	0.41432038	1
901016	183	4.212257193	6.0997167	1.887459507	1
901016	187	5.547289527	5.225040343	-0.322249184	0
901016	188	2.508940076	2.658555769	0.149615693	1
901016	190	4.005097003	6.341403588	2.336306585	1
901016	191	4.787702164	5.443709432	0.656007268	1
901016	199	4.453944081	2.566484574	-1.887459507	0
901016	203	7.411731235	5.89255651	-1.519174725	0
901016	207	4.212257193	4.189239394	-0.023017799	0
901016	208	2.198199792	2.42837778	0.230177989	1
901016	215	2.808171462	3.095893948	0.287722486	1
901016	216	2.140655295	2.566484574	0.425829279	1
901016	219	3.970570305	3.878499109	-0.092071195	0
901016	220	2.290270987	1.668790418	-0.621480569	0
901016	223	2.601011272	2.186690892	-0.41432038	0
901016	224	1.438612429	2.63553797	1.196925541	1
901016	225	3.026840551	2.416868881	-0.60997167	0
901016	226	5.570307326	4.166221595	-1.404085731	0
901016	227	6.306876889	5.317111538	-0.989765351	0
901016	228	7.411731235	8.424514385	1.01278315	1
901016	229	7.756998218	6.007645504	-1.749352714	0
901016	230	10.2083938	9.448806435	-0.759587363	0
901016	231	2.221217591	2.301779887	0.080562296	1
901016	232	3.959061405	4.189239394	0.230177989	1
901016	233	7.803033816	6.663652772	-1.139381044	0
901016	234	4.546015276	5.132969147	0.586953871	1
901016	235	7.92963171	6.836286263	-1.093345446	0
901016	236	8.125283	7.066464252	-1.058818748	0
901016	249	4.661104271	4.085659299	-0.575444972	0
901016	251	5.501253929	7.826051615	2.324797686	1
901016	252	3.86699021	4.46545298	0.598462771	1
901016	253	7.503802431	6.537054878	-0.966747552	0
901016	254	8.136791899	8.263389793	0.126597894	1
901016	256	8.804308067	7.020428654	-1.783879412	0
			total amount of increase channels:		**43**
			average STV difference:		**-0.4462**

Appendix E

Scripts 'Origin of Ectopic Beats'

```
import ARIpoints_exp as ARI
import numpy as np
from scipy.signal import argrelextrema

def find_ectopic_beat(derivative, initial_data, t1):
      ''' This function finds the local time of excitation and its
      corresponding data point of the ectopic beat.
       derivative      - derivative of the filtered data
       initial data    - initial data
       t1              - start time of the initial data
      returns points of excitation and the indices of these points on the
      initial data of the ectopic beats'''

   # parameters
   threshold = -130        # threshold for derivative
   window = 2048           # amount of data points within 1 second
   window_raw_data = 30    # defined window for searching the steepest
                             negative derivative
   dt = 1.0 / 2048     # time (s) between two data points of the bdf trace

   # find the relative negative maxima of the negative derivative
   inirelmin = list(argrelextrema(derivative, np.less)[0])

   # find the relative negative maxima which correspond to the local time
     of excitation
   # beats-array contains all the registered 'normal' beats
   # ectopic-array contains all the registered ectopic beats
   beats = []
   ectopic = []
   for index in inirelmin:
      if derivative[index] < threshold and beats == []:
         beats = np.append(beats, index)
      else:
         if derivative[index] < threshold and index > beats[-1] + window:
            beats = np.append(beats, index)
         else:
            if derivative[index] < threshold and beats[-1] <index <
                beats[-1] + window/1.5:
               beats = np.append(beats, index)
               ectopic = np.append(ectopic, index)

   # transfer to raw data
   indices_to_rawdata = [int(index) + 60 for index in ectopic]
```

```
    # find around these indices the steepest derivative on the raw data in the
    neighbourhood of these indices
        datapoints = []
        indices = []
        for index in indices_to_rawdata:
            data = initial_data[index - window_raw_data:index + window_raw_data]
            derivative = np.diff(data)
            minimum_index_derivative = np.argmin(derivative)
            minimum_index = index - window_raw_data + minimum_index_derivative
            minimum_data = data[minimum_index_derivative]
            datapoints = np.append(datapoints, minimum_data)
            indices = np.append(indices, minimum_index)

        # transfer indices to time points
        timepoints = [index * dt + t1 for index in indices]

        # combine time points and data points
        points = np.array(zip(timepoints, datapoints))

        return points, indices
```

```
def FEB_points(initial_data,t1):
    ''' This function determines all the local times of excitation of
       ectopic beats as corresponding paced beats.
        initial data    - initial data
        t1              - start time of the initial data
        returns local times of excitation of the ectopic beats and
       corresponding paced beats'''

    # parameters
    window = 2048  # amount of data points within 1 second

    # filtering of the data and calculating the derivative
    (filtered_data,filtered_time)=ARI.filter(initial_data, t1)
    derivative = np.diff(filtered_data)

    # calculating the points of excitation for the ectopic beats
    (points,indices)=find_ectopic_beat(derivative,initial_data,t1)

    # calculating the points of excitation for all the normal beats during
       the considered period
    (points_r, indices_minder) = ARI.find_max_neg_derivative(derivative,
initial_data, t1)

    # find the corresponding/previous paced beat for every ectopic beat
    # initial parameters
    times_red=[]
    data_red=[]

    # for-loop over all the indices of local time of excitation of the
       ectopical beats as the paced beats
    for index_ect in indices:
        for index_r in indices_minder:
            if index_ect - window < index_r < index_ect + window:
                index_in_array=np.where(indices_minder==index_r)
                times_red=np.append(times_red,points_r[index_in_array][0][0])
                data_red=np.append(data_red,points_r[index_in_array][0][1])

    # combine time points and data points
    points_red=np.array(zip(times_red,data_red))

    return points,points_red
```

```
def find_important_points(initial_data, t1, times_red, times_green,
evaluation_channel):
    ''' This function determines all the local times of excitation of
       ectopic beats as corresponding paced beats based on the local times
       of a good analyzed channel of the same time period and same dog.
        initial data     - initial data
        t1               - start time of the initial data
        times_red        - dictionary with the channels as keys and as values
                           all the local times of excitation of the paced
                           beats
        times_green      - dictionary with the channels as keys and as values
                           all the local times of excitation of the ectopic
                           beats
        evaluation_channel  - a dictionary with the channel as key and as
                              value 'good' or 'bad'
        returns local times of excitation of the ectopic beats and
       corresponding paced beats'''

    # parameters
    dt = 1.0 / 2048          # time (s) between two data points of the bdf
                               trace
    window_raw_data = 150    # defined window for searching the steepest
                               positive derivative

    # filtering of the data and calculating the derivative
    (filtered_data, filtered_time) = ARI.filter(initial_data, t1)
    derivative = np.diff(filtered_data)

    # if a good channel is evaluated
    # in a good channel the position of the local time of excitation is
assumed to be correct
    if 'good' in evaluation_channel.values():
        good_key =
evaluation_channel.keys()[evaluation_channel.values().index('good')]
        timepoints_red = times_red[good_key]
        timepoints_green = times_green[good_key]
        (points_r, indices_minder) = ARI.find_max_neg_derivative(derivative,
initial_data,
       t1)
        # search the local time of excitation in a window around the local
       time of excitation of another channel of the paced beats as the
       ectopic beats
        new_timepoints_red = []
        new_datapoints_red = []
        for time in timepoints_red:
            index_nearest = find_nearest_index(points_r[:, 0], time)
            new_timepoints_red = np.append(new_timepoints_red,
points_r[index_nearest][0])
            new_datapoints_red = np.append(new_datapoints_red,
points_r[index_nearest][1])
        new_timepoints_green = []
        new_datapoints_green = []
```

```
for time in timepoints_green:
          index = (time - t1) / dt
          reduced_data = initial_data[int(index -
window_raw_data):int(index +
            window_raw_data)]
          reduced_derivative = np.diff(reduced_data)
          minimum_index_derivative = np.argmin(reduced_derivative)
          minimum_index = index - window_raw_data +
minimum_index_derivative
          minimum_time = minimum_index * dt + t1
          minimum_data = initial_data[int(minimum_index)]
          new_timepoints_green = np.append(new_timepoints_green,
minimum_time)
          new_datapoints_green = np.append(new_datapoints_green,
minimum_data)

      # combine time points and data points
      points_red = np.array(zip(new_timepoints_red, new_datapoints_red))
      points_green = np.array(zip(new_timepoints_green,
new_datapoints_green))

   else:
      # in case no channels have been evaluated as 'good'
      (points_green, points_red) = FEB.FEB_points(initial_data, t1)

   return points_red, points_green
```

```
import numpy as np

def SegregateBeats(dictionary_of_episode,length):
    ''' This function finds based on the activation times of the data the
       timeslot of the different beats in the episode.
        dictionary_of_episode    - dictionary of the episode containing the
                                   activation times of all good channels
        length          - length of the episode corresponding to the amount
                          of beats in the episode
        returns a dictionary with the time period of each beat '''

    # create an array containing all the activation times of the episode
       (over all different channels)
    all_times = []
    for key in dictionary_of_episode.keys():
        all_times = np.append(all_times, dictionary_of_episode[key])
    all_times = np.array(sorted(all_times))

    # find the biggest interbeat interval between these times
    differences = np.diff(all_times)
    maximal_differences =
np.array(sorted(differences,reverse=True))[0:int(length)-1]

    # indices of these differences
    indices_differences = []
    for element in maximal_differences:
        index = np.where(differences == element)
        indices_differences = np.append(indices_differences,index)
    indices_differences = np.array(sorted(indices_differences))

    # make a dictionary of the times aligning each beat
    timedispersion_beats = {}
    n_beat = 0
    for n_index in range(len(indices_differences)):
        #case 1: before first interbeat section
        if n_index == 0:
            t1 = all_times[0]
            t2 = all_times[int(indices_differences[n_index])]
            timedispersion_beats[n_beat] = [t1,t2]
            if n_index == len(indices_differences)-1:
                n_beat += 1
                t1=all_times[int(indices_differences[n_index])+1]
                t2=all_times[-1]
                timedispersion_beats[n_beat] = [t1, t2]
            else:
                n_beat += 1
                t1 = all_times[int(indices_differences[n_index]) + 1]
                t2 = all_times[int(indices_differences[n_index + 1])]
                timedispersion_beats[n_beat] = [t1, t2]
        else:
            n_beat += 1
            #case 2: after last interbeat section
            if n_index == len(indices_differences)-1:
                t1 = all_times[int(indices_differences[n_index]) + 1]
                t2 = all_times[-1]
                timedispersion_beats[n_beat] = [t1,t2]
```

```
#case 3: in between 2 interbeat intervals
          else:
              t1 = all_times[int(indices_differences[n_index])+1]
              t2 = all_times[int(indices_differences[n_index+1])]
              timedispersion_beats[n_beat] = [t1, t2]

    return timedispersion_beats


def FindFirstActivationPerBeat(dictionary_of_episode,length):
    ''' This function finds the first activation times and first activated
       channels of an episode.
        dictionary_of_episode - dictionary of the episode containing the
                                activation times of all good channels
        length          - length of the episode corresponding to the amount
                          of beats in the episode
        returns arrays with the first activated channels and first
       activation times of each beat '''

    # create a dictionary with the time period of each beat
    timedispersion_beats = SegregateBeats(dictionary_of_episode, length)

    # initial parameters
    FirstChannels = []
    FirstTimes = []
    # for-loop over each beat
    for n_beat in range(length):
        # take a good channel to begin with
        # the taken time is the latest activation time of the channel
        channel_first = dictionary_of_episode.keys()[0]
        time_first = dictionary_of_episode[channel_first][-1]
        # for-loop over each channel in the dictionary
        for key in dictionary_of_episode.keys():
            channel = key
            activation_times =
np.unique(np.array(dictionary_of_episode[channel]))
            if len(activation_times) == length :
                time_beat = activation_times[n_beat]
                if time_beat < time_first:
                    time_first = time_beat
                    channel_first = channel
            else:
                time_beat =
any_value_between(activation_times,timedispersion_beats[n_beat])
                if time_beat != None:
                    if time_beat < time_first:
                        time_first = time_beat
                        channel_first = channel

        # append outcome to array
        FirstChannels = np.append(FirstChannels,channel_first)
        FirstTimes = np.append(FirstTimes,time_first)

    return FirstChannels,FirstTimes
```

```
def any_value_between(array_activation,array_time_beat):
    ''' This function gives the value in the array which lies between a
      given time period.
       array_activation    - array with activation times
       array_time_beat     - time period as an array eg: [t1,t2]
       returns the activation time which lies between the time period '''
    value=None
    for element in array_activation:
       if array_time_beat[0] <= element <= array_time_beat[1]:
          value = element
    return value
```

Appendix F

Additional figures ’Origin of Ectopic Beats’

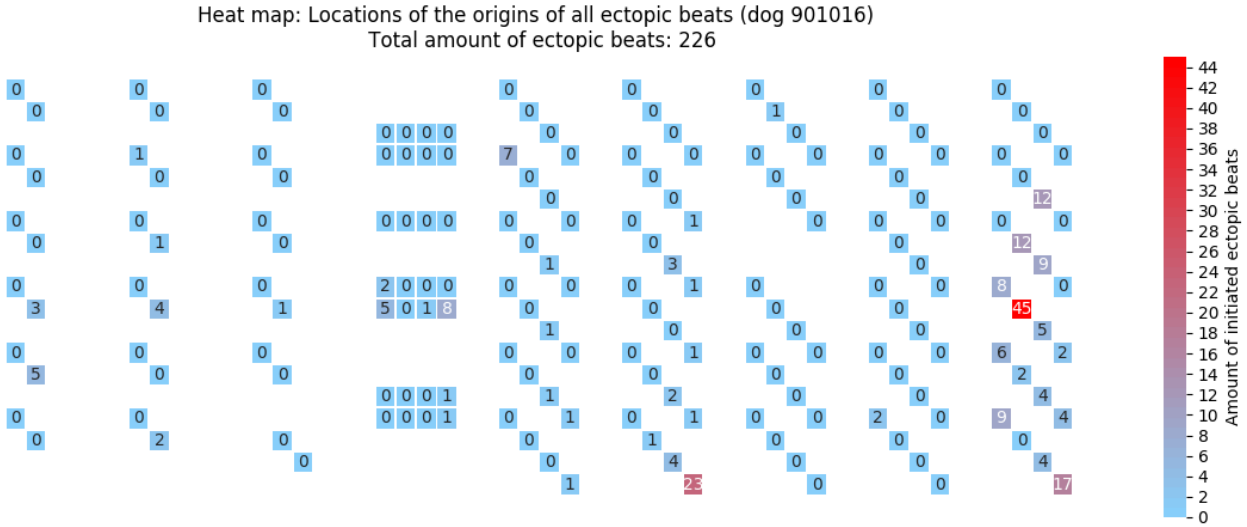

Figure F.1: An overview of the origins of all the ectopic activity during the dofetilide recording presented on an electrode map with annotation for dog 901016.

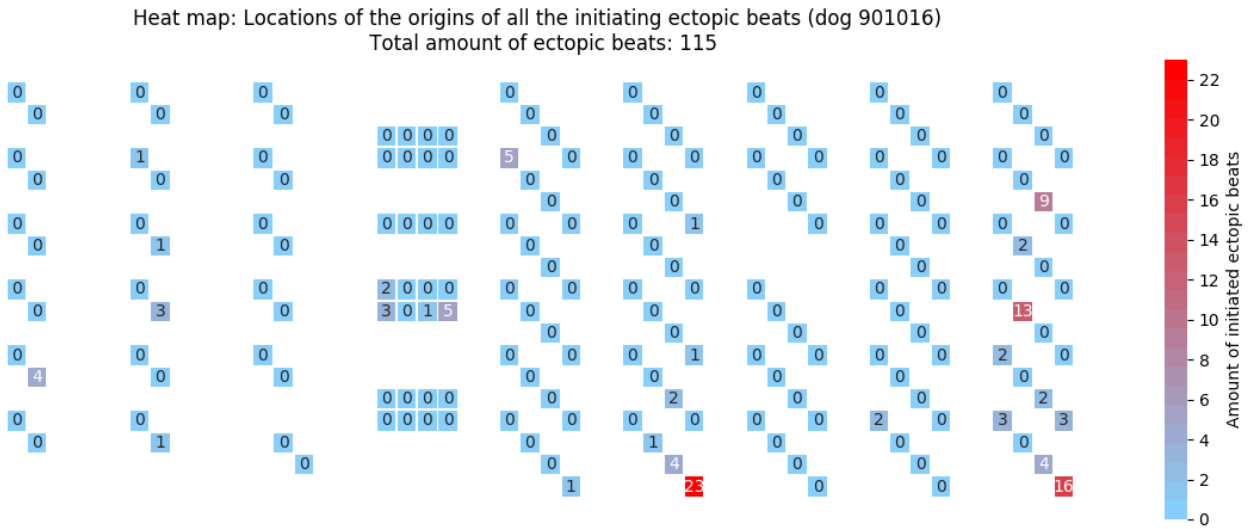

Figure F.2: An overview of the origins of the first ectopic beat in all episodes presented on an electrode map with annotation for dog 901016.

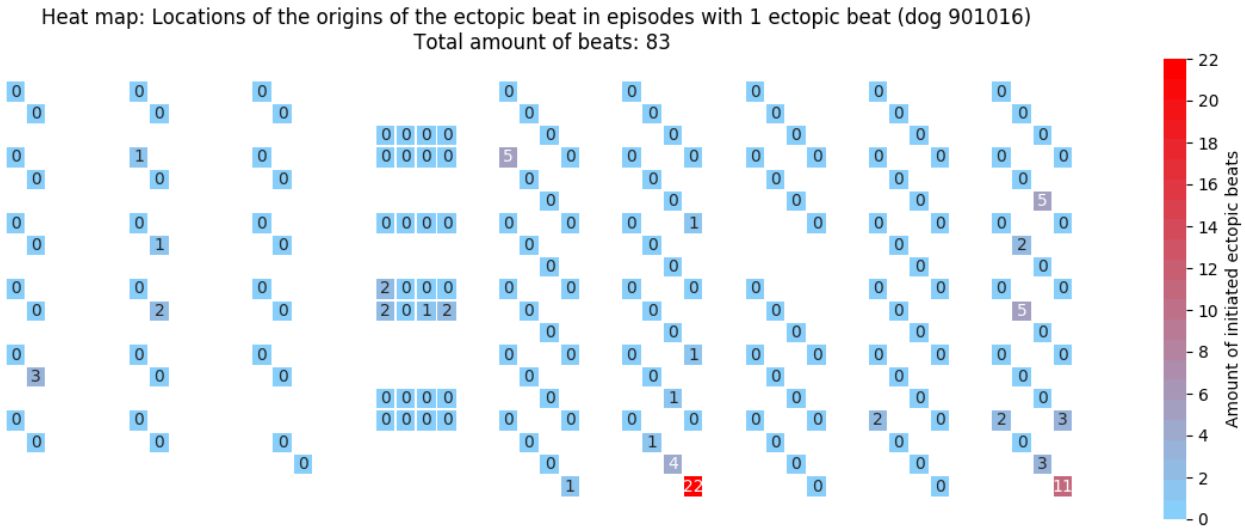

Figure F.3: An overview of the origins of the ectopic beats in episodes with only 1 ectopic beat presented on an electrode map with annotation for dog 901016.

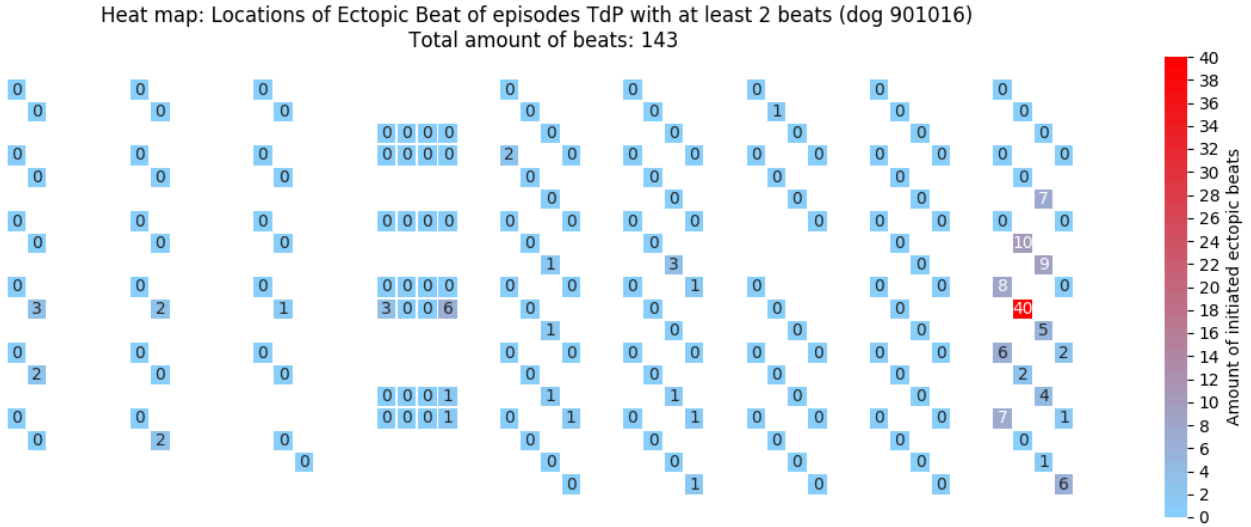

Figure F.4: An overview of the origins of the ectopic beats in episodes with at least 2 ectopic beats presented on an electrode map with annotation for dog 901016.

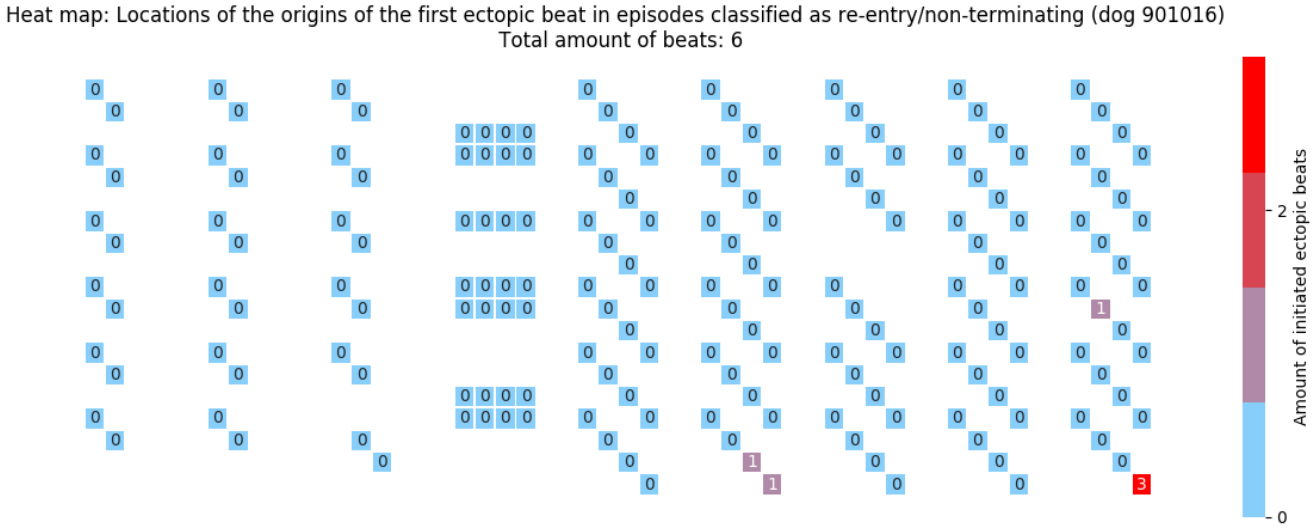

Figure F.5: An overview of the origins of the ectopic beats in episodes classified as re-entry or non-terminating presented on an electrode map with annotation for dog 901016.

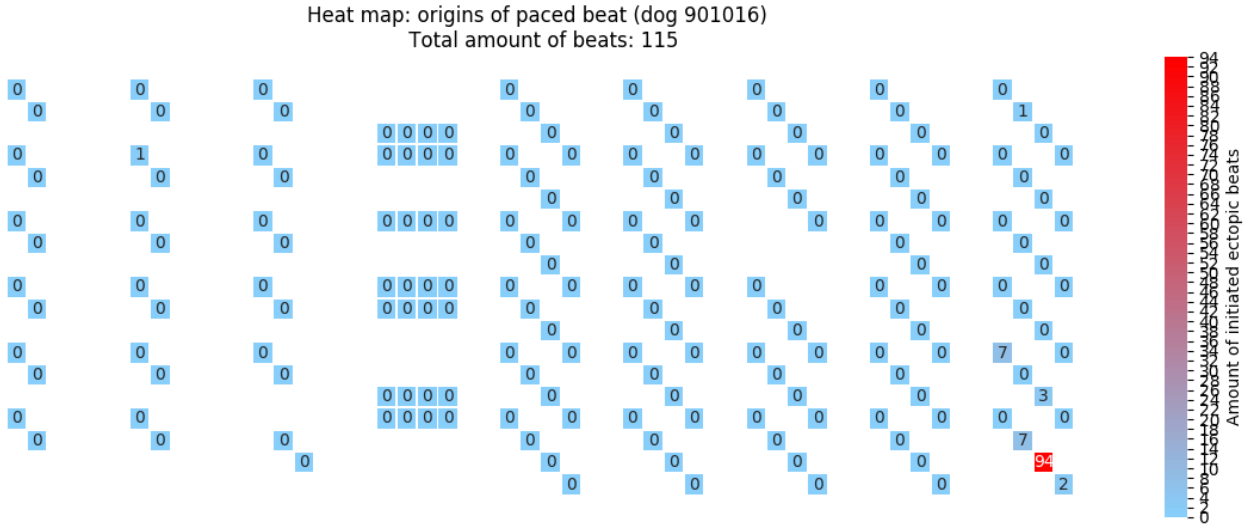

Figure F.6: An overview of the origins of the paced beats in all episodes during the dofetilide recording presented on an electrode map with annotation for dog 901016.

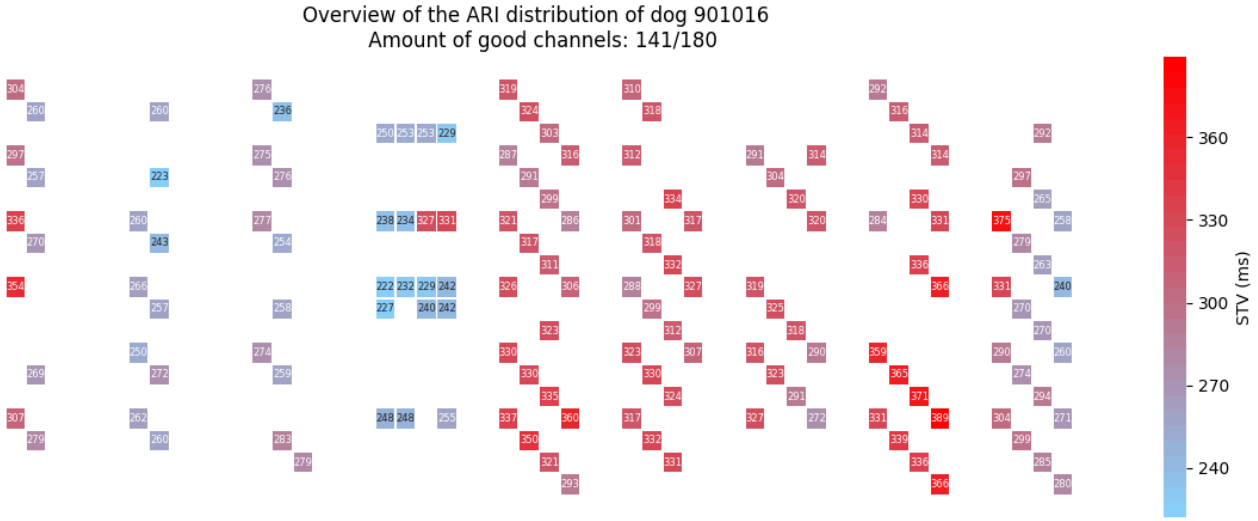

Figure F.7: An overview of the ARI distribution presented on an electrode map with annotations for dog 901016. The ARI was determined in the last analysed beat in the time period 17.5-59.6 s during the dofetilide recording, which was analysed for the STV project.

Appendix G

File containing more detailed information on ectopic beats

dog	t1	t2	# beats	paced	time (s)	electrode	interbeat (ms)	ectopic episode	total # episodes	E/R	not registered?	# analyzed beats
901016	12	482	1+1	1	59.328125	66	379.8828125	1	115	E	1	155
901016	12	482	1+1	0	59.70800781	141	0	1	115	E	1	155
901016	12	482	1+1	1	61.10302734	66	376.953125	2	115	E	1	156
901016	12	482	1+1	0	61.47998047	141	0	2	115	E	1	156
901016	12	482	1+2	1	96.25146484	66	885.2539063	3	115	E	1	156
901016	12	482	1+2	0	97.13671875	138	397.4609375	3	115	E	1	156
901016	12	482	1+2	0	97.53417969	137	0	3	115	E	1	156
901016	12	482	1+1	1	98.94628906	66	383.7890625	4	115	E	1	156
901016	12	482	1+1	0	99.33007813	141	0	4	115	E	1	155
901016	12	482	1+1	1	124.7607422	66	416.5039063	5	115	E	1	156
901016	12	482	1+1	0	125.1772461	60	0	5	115	E	1	156
901016	12	482	1+1	1	155.8994141	66	1105.957031	6	115	E	1	156
901016	12	482	1+1	0	157.0053711	133	0	6	115	E	1	156
901016	12	482	1+2	1	178.4389648	66	1104.003906	7	115	E	1	156
901016	12	482	1+2	0	179.5429688	252	1135.253906	7	115	E	1	156
901016	12	482	1+2	0	180.6782227	252	0	7	115	E	1	156
901016	12	482	1+1	1	196.7431641	66	1282.714844	8	115	E	1	156
901016	12	482	1+1	0	198.0258789	215	0	8	115	E	1	156
901016	12	482	1+1	1	199.4130859	66	1078.613281	9	115	E	1	156
901016	12	482	1+1	0	200.4916992	215	0	9	115	E	1	156
901016	12	482	1+2	1	201.8779297	66	914.0625	10	115	E	1	156
901016	12	482	1+2	0	202.7919922	215	857.421875	10	115	E	1	156
901016	12	482	1+2	0	203.6494141	215	0	10	115	E	1	156
901016	12	482	1+3	1	233.0717773	66	1039.550781	11	115	E	1	156
901016	12	482	1+3	0	234.1113281	252	561.0351563	11	115	E	1	156
901016	12	482	1+3	0	234.6723633	252	622.5585938	11	115	E	1	155
901016	12	482	1+3	0	235.2949219	252	0	11	115	E	1	156
901016	12	482	1+2	1	255.3662109	66	724.1210938	12	115	E	1	156
901016	12	482	1+2	0	256.090332	223	527.8320313	12	115	E	1	156
901016	12	482	1+2	0	256.6181641	223	0	12	115	E	1	156
901016	12	482	1+2	1	287.3500977	66	930.6640625	13	115	E	1	156

dog	t1	t2	# beats	paced	time (s)	electrode	interbeat (ms)	ectopic episode	total # episodes	E/R	not registered?	# analyzed beats
901016	12	482	1+2	0	288.2807617	252	565.4296875	13	115	E	1	156
901016	12	482	1+2	0	288.8461914	249	0	13	115	E	1	155
901016	12	482	1+1	1	291.5649414	66	549.3164063	14	115	E	1	156
901016	12	482	1+1	0	292.1142578	207	0	14	115	E	1	156
901016	12	482	1+1	1	304.1850586	204	1064.941406	15	115	E	1	156
901016	12	482	1+1	0	305.25	204	0	15	115	E	1	156
901016	12	482	1+1	1	307.9643555	66	1173.828125	16	115	E	1	156
901016	12	482	1+1	0	309.1381836	249	0	16	115	E	1	156
901016	12	482	1+1	1	321.1987305	66	877.9296875	17	115	E	1	156
901016	12	482	1+1	0	322.0766602	249	0	17	115	E	1	156
901016	12	482	1+1	1	342.9580078	66	641.6015625	18	115	E	1	156
901016	12	482	1+1	0	343.5996094	141	0	18	115	E	1	156
901016	12	482	1+1	1	346.6479492	66	679.6875	19	115	E	1	156
901016	12	482	1+1	0	347.3276367	141	0	19	115	E	1	156
901016	12	482	1+1	1	348.8779297	66	628.4179688	20	115	E	1	156
901016	12	482	1+1	0	349.5063477	141	0	20	115	E	1	156
901016	12	482	1+1	1	352.5576172	66	630.3710938	21	115	E	1	156
901016	12	482	1+1	0	353.1879883	141	0	21	115	E	1	156
901016	12	482	1+1	1	359.2373047	66	578.125	22	115	E	1	156
901016	12	482	1+1	0	359.8154297	68	0	22	115	E	1	156
901016	12	482	1+1	1	371.8720703	66	644.53125	23	115	E	1	156
901016	12	482	1+1	0	372.5166016	141	0	23	115	E	1	156
901016	12	482	1+1	1	374.0668945	66	648.4375	24	115	E	1	156
901016	12	482	1+1	0	374.715332	143	0	24	115	E	1	156
901016	12	482	1+1	1	382.2817383	66	677.2460938	25	115	E	1	156
901016	12	482	1+1	0	382.9589844	141	0	25	115	E	1	156
901016	12	482	1+1	1	387.5063477	66	655.7617188	26	115	E	1	156
901016	12	482	1+1	0	388.1621094	141	0	26	115	E	1	156
901016	12	482	1+1	1	391.2114258	66	983.3984375	27	115	E	1	156
901016	12	482	1+1	0	392.1948242	252	0	27	115	E	1	156
901016	12	482	1+1	1	393.7363281	66	598.1445313	28	115	E	1	156

dog	t1	t2	# beats	paced	time (s)	electrode	interbeat (ms)	ectopic episode	total # episodes	E/R	not registered?	# analyzed beats
901016	12	482	1+1	0	394.3344727	68	0	28	115	E	1	156
901016	12	482	1+1	1	401.8710938	66	890.625	29	115	E	1	156
901016	12	482	1+1	0	402.7617188	138	0	29	115	E	1	156
901016	12	482	1+2	1	404.3310547	66	575.1953125	30	115	E	1	156
901016	12	482	1+2	0	404.90625	68	1193.359375	30	115	E	1	156
901016	12	482	1+2	0	406.0996094	183	0	30	115	E	1	156
901016	12	482	1+4	1	421.1455078	66	539.0625	31	115	E	1	156
901016	12	482	1+4	0	421.6845703	249	391.6015625	31	115	E	1	143
901016	12	482	1+4	0	422.0761719	240	320.8007813	31	115	E	1	153
901016	12	482	1+4	0	422.3969727	59	428.7109375	31	115	E	1	154
901016	12	482	1+4	0	422.8256836	249	0	31	115	E	1	156
901016	12	482	1+1	1	439.3745117	66	660.15625	32	115	E	1	156
901016	12	482	1+1	0	440.034668	252	0	32	115	E	1	156
901016	12	482	1+4	1	443.0698242	66	646.9726563	33	115	E	1	156
901016	12	482	1+4	0	443.7167969	141	359.8632813	33	115	E	1	155
901016	12	482	1+4	0	444.0766602	162	305.6640625	33	115	E	1	140
901016	12	482	1+4	0	444.3823242	161	291.015625	33	115	E	1	145
901016	12	482	1+4	0	444.6733398	68	0	33	115	E	1	147
901016	12	482	1+1	1	467.1938477	66	678.7109375	34	115	E	1	156
901016	12	482	1+1	0	467.8725586	141	0	34	115	E	1	156
901016	12	482	1+1	1	473.9169922	57	702.1484375	35	115	E	1	156
901016	12	482	1+1	0	474.6191406	141	0	35	115	E	1	156
901016	482	491	34+1	1	482.1617314	66	651.7452117	36	115	R	0	
901016	482	491	34+1	0	482.8134766	141	0	36	115	R	0	
901016	543.4	606	1+9	1	560.2823242	57	433.1054688	37	115	E	1	61
901016	543.4	606	1+9	0	560.7154297	59	267.0898438	37	115	E	1	58
901016	543.4	606	1+9	0	560.9825195	27	235.3515625	37	115	E	1	61
901016	543.4	606	1+9	0	561.2178711	26	228.515625	37	115	E	1	61
901016	543.4	606	1+9	0	561.4463867	55	218.2617188	37	115	E	1	61
901016	543.4	606	1+9	0	561.6646484	55	193.359375	37	115	E	1	61
901016	543.4	606	1+9	0	561.8580078	55	242.6757813	37	115	E	1	59

dog	t1	t2	# beats	paced	time (s)	electrode	interbeat (ms)	ectopic episode	total # episodes	E/R	not registered?	# analyzed beats
901016	543.4	606	1+9	0	562.1006836	55	245.6054688	37	115	E	1	47
901016	543.4	606	1+9	0	562.3462891	27	233.3984375	37	115	E	1	47
901016	543.4	606	1+9	0	562.5796875	54	0	37	115	E	1	46
901016	543.4	606	1+3	1	563.5733398	34	416.9921875	38	115	E	1	61
901016	543.4	606	1+3	0	563.990332	54	262.2070313	38	115	E	1	59
901016	543.4	606	1+3	0	564.2525391	57	247.5585938	38	115	E	1	60
901016	543.4	606	1+3	0	564.5000977	57	0	38	115	E	1	60
901016	543.4	606	1+3	1	566.037207	59	458.984375	39	115	E	1	61
901016	543.4	606	1+3	0	566.4961914	54	264.6484375	39	115	E	1	60
901016	543.4	606	1+3	0	566.7608398	53	237.7929688	39	115	E	1	61
901016	543.4	606	1+3	0	566.9986328	53	0	39	115	E	1	59
901016	543.4	606	1+9	1	568.5420898	57	443.8476563	40	115	E	1	61
901016	543.4	606	1+9	0	568.9859375	57	227.5390625	40	115	E	1	56
901016	543.4	606	1+9	0	569.2134766	54	237.3046875	40	115	E	1	62
901016	543.4	606	1+9	0	569.4507812	58	230.46875	40	115	E	1	61
901016	543.4	606	1+9	0	569.68125	54	208.984375	40	115	E	1	61
901016	543.4	606	1+9	0	569.8902344	54	252.4414063	40	115	E	1	61
901016	543.4	606	1+9	0	570.1426758	54	239.2578125	40	115	E	1	61
901016	543.4	606	1+9	0	570.3819336	53	239.2578125	40	115	E	1	61
901016	543.4	606	1+9	0	570.6211914	54	231.4453125	40	115	E	1	61
901016	543.4	606	1+9	0	570.8526367	54	0	40	115	E	1	61
901016	543.4	606	1+3	1	572.3770508	57	424.3164063	41	115	E	1	57
901016	543.4	606	1+3	0	572.8013672	18	242.1875	41	115	E	1	55
901016	543.4	606	1+3	0	573.0435547	53	304.6875	41	115	E	1	56
901016	543.4	606	1+3	0	573.3482422	53	0	41	115	E	1	57
901016	543.4	606	1+1	1	574.8716797	57	436.5234375	42	115	E	1	60
901016	543.4	606	1+1	0	575.3082031	26	0	42	115	E	1	60
901016	543.4	606	1+1	1	598.5459961	57	1173.339844	43	115	E	1	61
901016	543.4	606	1+1	0	599.7193359	233	0	43	115	E	1	61
901016	543.4	606	1+1	1	602.7657227	59	481.9335938	44	115	E	1	53
901016	543.4	606	1+1	0	603.2476562	54	0	44	115	E	1	53

dog	t1	t2	# beats	paced	time (s)	electrode	interbeat (ms)	ectopic episode	total # episodes	E/R	not registered?	# analyzed beats
901016	543.4	606	1+2	1	604.7808594	57	482.9101563	45	115	E	1	61
901016	543.4	606	1+2	0	605.2637695	39	303.2226563	45	115	E	1	58
901016	543.4	606	1+2	0	605.5669922	39	0	45	115	E	1	62
901016	606	611	14+1	1	606.4796394	65	294.7746777	46	115	R	0	
901016	606	611	14+1	0	606.7744141	65	0	46	115	R	0	
901016	613	631	1+2	1	620.9833984	66	468.2617188	47	115	E	1	150
901016	613	631	1+2	0	621.4516602	57	324.7070313	47	115	E	1	149
901016	613	631	1+2	0	621.7763672	68	0	47	115	E	1	150
901016	613	631	1+1	1	629.2983398	66	480.9570313	48	115	E	1	147
901016	613	631	1+1	0	629.7792969	66	0	48	115	E	1	147
901016	631	635	1+11	1	631.2935693	66	444.2236771	49	115	E	0	
901016	631	635	1+11	0	631.737793	54	238.28125	49	115	E	0	
901016	631	635	1+11	0	631.9760742	54	266.1132813	49	115	E	0	
901016	631	635	1+11	0	632.2421875	54	257.3242188	49	115	E	0	
901016	631	635	1+11	0	632.4995117	54	261.71875	49	115	E	0	
901016	631	635	1+11	0	632.7612305	54	255.859375	49	115	E	0	
901016	631	635	1+11	0	633.0170898	26	270.9960938	49	115	E	0	
901016	631	635	1+11	0	633.2880859	27	247.5585938	49	115	E	0	
901016	631	635	1+11	0	633.5356445	54	236.8164063	49	115	E	0	
901016	631	635	1+11	0	633.7724609	26	255.859375	49	115	E	0	
901016	631	635	1+11	0	634.0283203	26	255.3710938	49	115	E	0	
901016	631	635	1+11	0	634.2836914	26	0	49	115	E	0	
901016	635	640	1+1	1	635.5478516	66	495.6054688	50	115	E	1	161
901016	635	640	1+1	0	636.043457	60	0	50	115	E	1	161
901016	635	640	1+1	1	639.0629883	66	454.5898438	51	115	E	1	161
901016	635	640	1+1	0	639.5175781	66	0	51	115	E	1	161
901016	640	644	1+9	1	641.0377687	66	451.4890995	52	115	E	0	
901016	640	644	1+9	0	641.4892578	54	250.4882813	52	115	E	0	
901016	640	644	1+9	0	641.7397461	54	268.0664063	52	115	E	0	
901016	640	644	1+9	0	642.0078125	54	256.3476563	52	115	E	0	
901016	640	644	1+9	0	642.2641602	27	245.6054688	52	115	E	0	

dog	t1	t2	# beats	paced	time (s)	electrode	interbeat (ms)	ectopic episode	total # episodes	E/R	not registered?	# analyzed beats
901016	640	644	1+9	0	642.5097656	27	234.375	52	115	E	0	
901016	640	644	1+9	0	642.7441406	26	243.6523438	52	115	E	0	
901016	640	644	1+9	0	642.987793	27	270.5078125	52	115	E	0	
901016	640	644	1+9	0	643.2583008	26	265.1367188	52	115	E	0	
901016	640	644	1+9	0	643.5234375	256	0	52	115	E	0	
901016	644	648	1+1	1	645.0478516	66	491.6992188	53	115	E	1	132
901016	644	648	1+1	0	645.5395508	141	0	53	115	E	1	132
901016	648	652	1+8	1	648.5980028	66	424.6901424	54	115	E	0	
901016	648	652	1+8	0	649.0226929	54	283.9477104	54	115	E	0	
901016	648	652	1+8	0	649.3066406	57	244.140625	54	115	E	0	
901016	648	652	1+8	0	649.5507813	57	245.6054688	54	115	E	0	
901016	648	652	1+8	0	649.7963867	27	239.2578125	54	115	E	0	
901016	648	652	1+8	0	650.0356445	54	234.8632813	54	115	E	0	
901016	648	652	1+8	0	650.2705078	27	252.9296875	54	115	E	0	
901016	648	652	1+8	0	650.5234375	26	274.4140625	54	115	E	0	
901016	648	652	1+8	0	650.7978516	26	0	54	115	E	0	
901016	652	677	1+1	1	673.5068359	66	489.2578125	55	115	E	1	146
901016	652	677	1+1	0	673.9960938	54	0	55	115	E	1	146
901016	652	677	1+1	1	675.5263672	66	497.0703125	56	115	E	1	147
901016	652	677	1+1	0	676.0234375	39	0	56	115	E	1	147
901016	677	679	1+3	1	677.5570764	66	481.9860971	57	115	E	0	
901016	677	679	1+3	0	678.0390625	39	279.296875	57	115	E	0	
901016	677	679	1+3	0	678.3183594	39	271.9726563	57	115	E	0	
901016	677	679	1+3	0	678.590332	39	0	57	115	E	0	
901016	679	687	24+1	1	679.901523	66	447.5980469	58	115	R	0	
901016	679	687	24+1	0	680.3491211	65	0	58	115	R	0	
901016	696	700	1+8	1	696.9409931	66	436.3223214	59	115	E	0	
901016	696	700	1+8	0	697.3773154	54	251.2390793	59	115	E	0	
901016	696	700	1+8	0	697.6285545	54	247.422085	59	115	E	0	
901016	696	700	1+8	0	697.8759766	54	273.4375	59	115	E	0	
901016	696	700	1+8	0	698.1494141	54	265.625	59	115	E	0	

dog	t1	t2	# beats	paced	time (s)	electrode	interbeat (ms)	ectopic episode	total # episodes	E/R	not registered?	# analyzed beats
901016	696	700	1+8	0	698.4150391	54	245.6054688	59	115	E	0	
901016	696	700	1+8	0	698.6606445	54	253.90625	59	115	E	0	
901016	696	700	1+8	0	698.9145508	53	250.9765625	59	115	E	0	
901016	696	700	1+8	0	699.1655273	53	0	59	115	E	0	
901016	703	706	1+8	1	703.4308531	66	455.3773942	60	115	E	0	
901016	703	706	1+8	0	703.8862305	66	233.2094254	60	115	E	0	
901016	703	706	1+8	0	704.1194399	54	258.0015121	60	115	E	0	
901016	703	706	1+8	0	704.3774414	54	252.9296875	60	115	E	0	
901016	703	706	1+8	0	704.6303711	54	252.9296875	60	115	E	0	
901016	703	706	1+8	0	704.8833008	54	248.5351563	60	115	E	0	
901016	703	706	1+8	0	705.1318359	54	276.8554688	60	115	E	0	
901016	703	706	1+8	0	705.4086914	53	258.9623236	60	115	E	0	
901016	703	706	1+8	0	705.6676537	54	0	60	115	E	0	
901016	706	710	1+1	1	708.4306641	66	471.1914063	61	115	E	1	150
901016	706	710	1+1	0	708.9018555	66	0	61	115	E	1	150
901016	710	713	1+6	1	710.4158279	66	431.3400616	62	115	E	0	
901016	710	713	1+6	0	710.847168	54	254.3945313	62	115	E	0	
901016	710	713	1+6	0	711.1015625	54	252.4414063	62	115	E	0	
901016	710	713	1+6	0	711.3540039	54	257.8125	62	115	E	0	
901016	710	713	1+6	0	711.6118164	54	250.4882813	62	115	E	0	
901016	710	713	1+6	0	711.8623047	27	244.6289063	62	115	E	0	
901016	710	713	1+6	0	712.1069336	26	0	62	115	E	0	
901016	714	717	1+5	1	714.8806389	66	422.5837954	63	115	E	0	
901016	714	717	1+5	0	715.3032227	54	237.7929688	63	115	E	0	
901016	714	717	1+5	0	715.5410156	54	253.4179688	63	115	E	0	
901016	714	717	1+5	0	715.7944336	54	265.625	63	115	E	0	
901016	714	717	1+5	0	716.0600586	54	254.3945313	63	115	E	0	
901016	714	717	1+5	0	716.3144531	56	0	63	115	E	0	
901016	717	774	1+1	1	717.8349609	66	415.0390625	64	115	E	1	139
901016	717	774	1+1	0	718.25	54	0	64	115	E	1	139
901016	717	774	1+1	1	742.3017578	67	465.8203125	65	115	E	1	139

dog	t1	t2	# beats	paced	time (s)	electrode	interbeat (ms)	ectopic episode	total # episodes	E/R	not registered?	# analyzed beats
901016	717	774	1+1	0	742.7675781	54	0	65	115	E	1	139
901016	717	774	1+1	1	744.2993164	66	490.7226563	66	115	E	1	136
901016	717	774	1+1	0	744.7900391	39	0	66	115	E	1	136
901016	717	774	1+1	1	746.3242188	66	482.9101563	67	115	E	1	134
901016	717	774	1+1	0	746.8071289	39	0	67	115	E	1	134
901016	717	774	1+1	1	748.3442383	66	485.8398438	68	115	E	1	132
901016	717	774	1+1	0	748.8300781	39	0	68	115	E	1	132
901016	717	774	1+1	1	750.3681641	65	480.46875	69	115	E	1	132
901016	717	774	1+1	0	750.8486328	39	0	69	115	E	1	131
901016	717	774	1+2	1	752.3837891	66	484.375	70	115	E	1	138
901016	717	774	1+2	0	752.8681641	39	315.9179688	70	115	E	1	126
901016	717	774	1+2	0	753.184082	158	0	70	115	E	1	138
901016	717	774	1+1	1	754.7460938	67	444.3359375	71	115	E	1	136
901016	717	774	1+1	0	755.1904297	92	0	71	115	E	1	135
901016	717	774	1+1	1	756.7563477	67	482.421875	72	115	E	1	136
901016	717	774	1+1	0	757.2387695	92	0	72	115	E	1	136
901016	717	774	1+1	1	758.7807617	67	511.2304688	73	115	E	1	137
901016	717	774	1+1	0	759.2919922	65	0	73	115	E	1	137
901016	717	774	1+1	1	760.8115234	67	511.2304688	74	115	E	1	137
901016	717	774	1+1	0	761.3227539	65	0	74	115	E	1	137
901016	717	774	1+1	1	765.8383789	66	649.9023438	75	115	E	1	136
901016	717	774	1+1	0	766.4882813	233	0	75	115	E	1	136
901016	717	774	1+1	1	772.5380859	66	538.5742188	76	115	E	1	131
901016	717	774	1+1	0	773.0766602	152	0	76	115	E	1	131
901016	774	778	1+10	1	774.6534337	66	466.6834524	77	115	E	0	
901016	774	778	1+10	0	775.1201172	65	306.9954685	77	115	E	0	
901016	774	778	1+10	0	775.4271127	55	249.8237246	77	115	E	0	
901016	774	778	1+10	0	775.6769364	18	257.0553053	77	115	E	0	
901016	774	778	1+10	0	775.9339917	14	251.0669079	77	115	E	0	
901016	774	778	1+10	0	776.1850586	14	229.4921875	77	115	E	0	
901016	774	778	1+10	0	776.4145508	14	335.9375	77	115	E	0	

dog	t1	t2	# beats	paced	time (s)	electrode	interbeat (ms)	ectopic episode	total # episodes	E/R	not registered?	# analyzed beats
901016	774	778	1+10	0	776.7504883	68	241.2109375	77	115	E	0	
901016	774	778	1+10	0	776.9916992	68	244.140625	77	115	E	0	
901016	774	778	1+10	0	777.2358398	68	259.2773438	77	115	E	0	
901016	774	778	1+10	0	777.4951172	68	0	77	115	E	0	
901016	778	807	1+1	1	778.7602539	67	450.6835938	78	115	E	1	109
901016	778	807	1+1	0	779.2109375	18	0	78	115	E	1	109
901016	778	807	1+1	1	789.8125	66	608.8867188	79	115	E	1	113
901016	778	807	1+1	0	790.4213867	125	0	79	115	E	1	113
901016	778	807	1+1	1	791.9775391	66	490.7226563	80	115	E	1	112
901016	778	807	1+1	0	792.4682617	65	0	80	115	E	1	112
901016	778	807	1+1	1	793.9873047	66	558.1054688	81	115	E	1	113
901016	778	807	1+1	0	794.5454102	60	0	81	115	E	1	113
901016	778	807	1+2	1	796.0625	66	492.1875	82	115	E	1	114
901016	778	807	1+2	0	796.5546875	65	1302.734375	82	115	E	1	112
901016	778	807	1+2	0	797.8574219	95	0	82	115	E	1	114
901016	778	807	1+1	1	799.4272461	66	471.6796875	83	115	E	1	111
901016	778	807	1+1	0	799.8989258	65	0	83	115	E	1	111
901016	778	807	1+1	1	801.4272461	66	498.5351563	84	115	E	1	111
901016	778	807	1+1	0	801.9257813	65	0	84	115	E	1	111
901016	778	807	1+1	1	803.4472656	66	479.4921875	85	115	E	1	110
901016	778	807	1+1	0	803.9267578	65	0	85	115	E	1	110
901016	778	807	1+1	1	805.5322266	66	476.5625	86	115	E	1	110
901016	778	807	1+1	0	806.0087891	65	0	86	115	E	1	110
901016	807	810	1+3	1	807.6173135	66	470.0888357	87	115	E	0	
901016	807	810	1+3	0	808.0874023	65	290.5776681	87	115	E	0	
901016	807	810	1+3	0	808.37798	56	275.8285819	87	115	E	0	
901016	807	810	1+3	0	808.6538086	65	0	87	115	E	0	
901016	810	812	1+1	1	810.2519531	66	468.75	88	115	E	1	166
901016	810	812	1+1	0	810.7207031	18	0	88	115	E	1	166
901016	812	815	1+4	1	812.3270539	66	462.985131	89	115	E	0	
901016	812	815	1+4	0	812.7900391	65	328.125	89	115	E	0	

dog	t1	t2	# beats	paced	time (s)	electrode	interbeat (ms)	ectopic episode	total # episodes	E/R	not registered?	# analyzed beats
901016	812	815	1+4	0	813.1181641	154	215.8203125	89	115	E	0	
901016	812	815	1+4	0	813.3339844	152	224.609375	89	115	E	0	
901016	812	815	1+4	0	813.5585938	152	0	89	115	E	0	
901016	815	837	1+1	1	816.5019531	66	542.4804688	90	115	E	1	164
901016	815	837	1+1	0	817.0444336	152	0	90	115	E	1	164
901016	815	837	1+1	1	820.121582	66	546.875	91	115	E	1	165
901016	815	837	1+1	0	820.668457	152	0	91	115	E	1	165
901016	815	837	1+1	1	822.246582	66	541.9921875	92	115	E	1	165
901016	815	837	1+1	0	822.7885742	152	0	92	115	E	1	165
901016	815	837	1+1	1	824.3662109	66	542.96875	93	115	E	1	165
901016	815	837	1+1	0	824.9091797	152	0	93	115	E	1	165
901016	815	837	1+2	1	830.9863281	66	502.9296875	94	115	E	1	166
901016	815	837	1+2	0	831.4892578	65	789.0625	94	115	E	1	165
901016	815	837	1+2	0	832.2783203	129	0	94	115	E	1	166
901016	815	837	1+1	1	835.3393555	66	494.140625	95	115	E	1	165
901016	815	837	1+1	0	835.8334961	65	0	95	115	E	1	165
901016	837	848	46+1	1	837.3564345	66	474.1319531	96	115	R	0	
901016	837	848	46+1	0	837.8305664	65	0	96	115	R	0	
901016	1007.3	1074	1+1	1	1012.956738	59	1308.59375	97	115	E	1	27
901016	1007.3	1074	1+1	0	1014.265332	18	0	97	115	E	1	27
901016	1007.3	1074	1+1	1	1057.783398	66	470.703125	98	115	E	1	104
901016	1007.3	1074	1+1	0	1058.254102	26	0	98	115	E	1	104
901016	1007.3	1074	1+5	1	1059.783398	66	490.7226563	99	115	E	1	105
901016	1007.3	1074	1+5	0	1060.274121	39	788.0859375	99	115	E	1	105
901016	1007.3	1074	1+5	0	1061.062207	130	664.0625	99	115	E	1	105
901016	1007.3	1074	1+5	0	1061.72627	130	941.8945313	99	115	E	1	105
901016	1007.3	1074	1+5	0	1062.668164	130	498.046875	99	115	E	1	105
901016	1007.3	1074	1+5	0	1063.166211	60	0	99	115	E	1	105
901016	1007.3	1074	1+1	1	1064.683301	66	476.0742188	100	115	E	1	105
901016	1007.3	1074	1+1	0	1065.159375	142	0	100	115	E	1	105
901016	1007.3	1074	1+1	1	1068.233105	66	490.234375	101	115	E	1	104

dog	t1	t2	# beats	paced	time (s)	electrode	interbeat (ms)	ectopic episode	total # episodes	E/R	not registered?	# analyzed beats
901016	1007.3	1074	1+1	0	1068.72334	142	0	101	115	E	1	104
901016	1007.3	1074	1+1	1	1070.307813	66	500	102	115	E	1	105
901016	1007.3	1074	1+1	0	1070.807813	165	0	102	115	E	1	105
901016	1007.3	1074	1+1	1	1072.342969	66	520.9960938	103	115	E	1	105
901016	1007.3	1074	1+1	0	1072.863965	141	0	103	115	E	1	105
901016	1074	1080	20+1	1	1074.130098	67	493.4369106	104	115	R	0	
901016	1074	1080	20+1	0	1074.623535	142	0	104	115	R	0	
901016	1080	1106	1+1	1	1104.661621	66	487.7929688	105	115	E	1	151
901016	1080	1106	1+1	0	1105.149414	142	0	105	115	E	1	151
901016	1106	1108	1+3	1	1106.676952	66	462.2080813	106	115	E	0	
901016	1106	1108	1+3	0	1107.13916	59	271.484375	106	115	E	0	
901016	1106	1108	1+3	0	1107.410645	58	234.375	106	115	E	0	
901016	1106	1108	1+3	0	1107.64502	59	0	106	115	E	0	
901016	1108	1117	36+1	1	1109.18166	66	453.1054975	107	115	R	0	
901016	1108	1117	36+1	0	1109.634766	54	0	107	115	R	0	
901016	1271.3	1335.6	1+1	1	1276.470898	66	410.15625	108	115	E	1	113
901016	1271.3	1335.6	1+1	0	1276.881055	141	0	108	115	E	1	113
901016	1271.3	1335.6	1+1	1	1277.670605	66	418.4570313	109	115	E	1	113
901016	1271.3	1335.6	1+1	0	1278.089063	141	0	109	115	E	1	113
901016	1271.3	1335.6	1+1	1	1278.880566	66	422.3632813	110	115	E	1	113
901016	1271.3	1335.6	1+1	0	1279.30293	141	0	110	115	E	1	113
901016	1271.3	1335.6	1+1	1	1296.59541	66	413.5742188	111	115	E	1	113
901016	1271.3	1335.6	1+1	0	1297.008984	141	0	111	115	E	1	113
901016	1271.3	1335.6	1+1	1	1300.05	66	417.4804688	112	115	E	1	113
901016	1271.3	1335.6	1+1	0	1300.46748	141	0	112	115	E	1	113
901016	1271.3	1335.6	1+1	1	1301.259961	66	417.4804688	113	115	E	1	113
901016	1271.3	1335.6	1+1	0	1301.677441	141	0	113	115	E	1	113
901016	1271.3	1335.6	1+1	1	1302.469922	66	422.8515625	114	115	E	1	113
901016	1271.3	1335.6	1+1	0	1302.892773	141	0	114	115	E	1	113